ORBITS CONTAINING ARCS OF MINIMUM ALTITUDE VARIATION

THESIS

Christina L. Cain
Captain, USAF

AFIT/GA/ENY/89J-1

DEPARTMENT OF THE AIR FORCE
AIR UNIVERSITY
AIR FORCE INSTITUTE OF TECHNOLOGY
Wright-Patterson Air Force Base, Ohio

AFIT/GA/ENY/89J-1

ORBITS CONTAINING ARCS OF MINIMUM ALTITUDE VARIATION

THESIS

Christina L. Cain
Captain, USAF

AFIT/GA/ENY/89J-1

AFIT/GA/ENY/89J-1

ORBITS CONTAINING ARCS OF MINIMUM ALTITUDE VARIATION

THESIS

Presented to the Faculty of the School of Engineering

of the Air Force Institute of Technology

Air University

In Partial Fulfillment of the

Requirements for the Degree of

Master of Science in Astronautical Engineering

Christina L. Cain, B.S.

Captain, USAF

June 1989

Acknowledgements

Many thanks to both my advisor, Capt Bain, and everyone in the Environmental Control Branch of the Flight Dynamics Laboratory.

C. L. Cain

Table of Contents

List of Figures

List of Figures

List of Figures

List of Figures

List of Tables

Notation

a	semi-major axis
C_D	coefficient of drag
$C_{\ell,m}, S_{\ell,m}$	spherical harmonic coefficients
D	acceleration due to drag
e	eccentricity
E	eccentric anomaly
f	ellipticity
h	ellipsoidal altitude
i	inclination
JD	Julian Day
J_k	zonal harmonics of the geopotential
m	mass
M	mean anomaly
n	mean motion
r	radius
R	radius of a planet as a function of latitude
R_e	equatorial radius of planet
R'	disturbing potential function due to a third body
S	angle between position vector of third body and satellite (for third body calculations)
	cross-sectional area (for drag problems)
t	time
T	time in Julian centuries
$T_k(x)$	Chebyshev polynomial
V	geopotential function
	velocity
z	ellipsoidal altitude used for density calculations

β	ballistic coefficient
Δa	secular change in semi-major axis over one period
Δe	secular change in eccentricity over one period
Δh	change in ellipsoidal altitude during an arc
Δe	secular change in eccentricity over one period
Δi	secular change in inclination axis over one period
$\Delta\omega$	secular change in argument of periapsis over one period
$\Delta\Omega$	secular change in longitude of the ascending node over one period
μ	product of universal gravitational constant and mass
$\overline{\rho}$	vector between the third body and satellite
ρ	density
ω	argument of periapsis
ν	true anomaly
Ω	longitude of the ascending node
Ω'	right ascension
ϕ	latitude
Φ'	declination

Abstract

This thesis identifies the mean orbital elements which produce arcs of minimum altitude variation over an oblate planet with an axi-symmetric gravitational field. Such orbits are useful for surveillance or scientific study missions using optics with fixed focal lengths.

Both Earth and Mars are considered and the optimum eccentricity is found as a function of argument of periapsis and inclination for two values of semi-major axis for each planet. The results are curve fit to develop a single equation which identifies the eccentricity needed to produce an arc of minimum altitude variation given the argument of periapsis, inclination, semi-major axis, ellipticity of the planet, equatorial radius, and the zonal J_2.

Once arcs with minimum altitude variations are identified, the properties of the arcs are considered. The mid-latitude, altitude, duration, and latitude range of the arcs are found as a function of argument of periapsis and inclination for various planet and semi-major axis combinations.

The secular change in mean orbital elements is considered to determine the most stable orbits. Secular changes in orbital elements due to the geopotential, drag, and third body effects are considered. The velocity impulse needed to return the satellite to the original orbit from the perturbed orbit is found and used to determine stability. Identifying orbits which require minimum station keeping fuel allows planners to select orbits permitting longer useful operational life.

ORBITS CONTAINING ARCS OF MINIMUM ALTITUDE VARIATION

I. Introduction

Background

Mean orbital elements may be determined to produce orbits about an oblate planet which contains arcs of constant altitude[6]. The arcs of constant altitude may be positioned over specified latitude ranges -- this ability is useful for surveillance or scientific study missions using optics with fixed focal lengths. This thesis focuses on finding orbits with arcs of constant ellipsoidal altitude for axi-symmetric planets (only zonal harmonics are considered in the geopotential). Because of these restrictions, the longitude of the ascending node is not considered as a variable. Given the required orbit, arcs of nearly constant altitude may be identified. The eccentricity becomes a function of the required inclination, argument of periapsis, semi-major axis, and planet parameters (ellipticity, equatorial radius, and geopotential). The independent variables are also functions of the desired altitude and latitude of the arc.

Mean orbital elements which produce stable orbits need to be considered. Missions requiring these types of orbits will typically have low altitudes, so drag needs to be addressed. Kalil [6] presents a first order analysis neglecting drag. Drag primarily affects eccentricity and semi-major axis; consequently, it can't be neglected for missions longer than one orbital period. The change in semi-major axis due to drag will act to reduce the altitude of the arc of constant altitude in a few orbits. Eventually, reducing the semi-major axis will result in an orbit which no longer contains an arc of constant altitude;

however, the orbit is much more sensitive to a change in eccentricity, inclination, or argument of periapsis -- as the drag reduces the eccentricity, the resulting orbit will no longer contain an arc of constant altitude.

Definition of Constant Altitude Arc

A constant altitude arc is defined for the purpose of this thesis as a portion of an orbit during which the ellipsoidal altitude of the satellite changes only slightly with time.

$$0 \simeq \Delta h = \int_{t_1}^{t_2} \frac{dh}{dt}\, dt$$

Objective

Mean orbital elements of orbits containing constant altitude arcs are identified for both Earth and Mars. The planets' ellipticity, zonal harmonics up to the third order, atmospheric drag, and third body effects are considered. For a given planet, the required orbital elements are identified to achieve a desired altitude at a given latitude. Secular changes in the mean orbital elements are then considered in order to locate the most stable orbits.

Approach

A search method is employed to determine the eccentricity, as a function of argument of periapsis and inclination for several cases (varying the following parameters: planet, semi-major axis, and the perturbative accelerations considered). First, the two-body problem is considered and an empirical relationship is developed which determines eccentricity as a function of argument of periapsis and a non-dimensional grouping of ellipticity, equatorial radius, inclination,

and semi-major axis. Next, additional perturbative accelerations are addressed [1,2,8,13,17]. For the short term considered (one period), the J_2 term of the geopotential causes the most significant change. An empirical relationship to predict the change in eccentricity from the two-body results is determined as a function of argument of periapsis and a non-dimensional grouping of J_2, inclination, semi-major axis, and the equatorial radius.

The choice of ω, i, and a which minimizes secular variations is then considered. Secular perturbations due to third bodies[7], zonal harmonics up to sixth order[12], and atmospheric drag (including a rotating atmosphere[16]) are addressed. The sum of the velocity impulses needed to correct the secular changes in the orbit caused by perturbations is calculated and used in identifying the most stable orbits.

II. Theory

Satellite Motion

In order to determine orbital elements of orbits which contain arcs of minimum altitude variation, the motion of the satellite must be know. Kepler identified satellite position and velocity under the influence of a central body modeled as a point mass. This two-body solution identifies the position of the satellite using the six classical orbital elements (semi-major axis (a), eccentricity (e), inclination (i), argument of periapsis (ω), longitude of the ascending node (Ω), and true anomaly (ν)) . Perturbations from two-body motion due to small accelerations may be calculated. Averaging the change in orbital elements over one period eliminates periodic short term variations [15]. The secular changes in orbital elements identify changes which must be corrected to return the satellite to the original orbit. This section will present two-body motion and perturbations from the two-body motion due to non-spherical gravitational fields, third bodies, and atmospheric drag. The secular changes in classical orbital elements will be presented for each perturbing acceleration considered.

The equations of motion presented in this section will be evaluated with various combinations of classical orbital elements to identify combinations of elements which produce orbits with minimum altitude variation arcs.

The secular variations of classical orbital elements presented in this section will be evaluated for orbits containing arcs of minimum altitude variation and will be used to determine the velocity impulse required to maintain the satellite in the desired orbit.

Equation (1) may be solved to determine the position and velocity of a satellite

$$\ddot{\bar{r}} = -\nabla V = \bar{a} \tag{1}$$

where $\bar{a}$ is the sum of accelerations acting on the satellite and V is the potential function. The two-body solution and perturbations from two-body motion due to a non-spherical gravitational field, third body, and drag will now be presented.

Two-Body Motion. For two-body motion, equation (1) may be rewritten by recognizing $\nabla V = \mu/r^2$

$$\ddot{\bar{r}} + \frac{\mu \bar{r}}{r^3} = 0 \tag{2}$$

where $\bar{r}$ is the position of the satellite, and μ is the product of the universal gravitational constant and the mass of the planet. Equation (2) may be solved to provide the satellite's distance from the center of the planet. Equation (3) presents Kepler's equation:

$$r = a(1 - e^2)/[1 + e \cos(\nu)] \tag{3}$$

Where *r* is the distance from the center of the planet, *a* is the semi-major axis of the orbit, *e* is the eccentricity, and ν is the true anomaly.

Geopotential. The geopotential function for a spherical gravitational field is $-\mu/r$. The geopotential function for a non-spherical gravitational field is presented in equation (4) [1]

$$V = \sum_{\ell=0}^{\infty} \sum_{m=0}^{\infty} V_{\ell m} \tag{4}$$

$$V_{\ell m} = - \frac{\mu R^{\ell}}{r^{\ell+1}} \sum_{p=0}^{\ell} F_{\ell mp}(i) \begin{cases} C_{\ell m} \cos H + S_{\ell m} \sin H & \ell\text{-m even} \\ -S_{\ell m} \cos H + C_{\ell m} \sin H & \ell\text{-m odd} \end{cases} \tag{5}$$

where

$$F_{\ell mp}(i) = \sum_{t=0}^{tmax} \frac{(2\ell-2t)!}{t!\ (\ell-t)!\ (\ell-m-2t)!\ 2^{2(\ell-t)}} \sin^{\ell-m-2t} i$$

$$X \sum_{s=0}^{m} \binom{m}{s} \cos^{s} i \sum_{g=g_1}^{g_u} (-1)^{g-k} \binom{\ell-m-2t+s}{g} \binom{m-s}{p-t-g} \tag{6}$$

$$g_1 = \max[0, p-t-m-s]$$

$$g_u = \min[\ell-m-2t+s, p-t]$$

$$H = (1-2p)(\omega+\nu) + m(\Omega+\theta_g)$$

$$tmax = \begin{cases} p\ , & p \le k \\ k\ , & p > k \end{cases}$$

$$k = \left[\frac{\ell-m}{2}\right]$$

By considering only zonal harmonics, equation (6) may be simplified:

$$V = \sum_{\ell=0}^{\infty} V_{\ell 0} \tag{7}$$

$$V_{\ell 0} = - \frac{\mu R_e^{\ell}}{r^{\ell+1}} C_{\ell 0} \sum_{t=0}^{k} \frac{(2\ell-2t)!}{t!\ (\ell-t)!\ (\ell-2t)!\ 2^{2(\ell-t)}} \sin^{\ell-2t} i$$

$$X \sum_{c=0}^{\ell-2t} \binom{\ell-2t}{c} (-1)^{k+c} \begin{bmatrix} \cos(\ell-2t-2c)(\omega+\nu) & \ell \text{ even} \\ \sin(\ell-2t-2c)(\omega+\nu) & \ell \text{ odd} \end{bmatrix} \quad (8)$$

where

$$k = \left[\frac{\ell}{2}\right]$$

Recognizing

$$\binom{n}{m} = \binom{n}{n-m}$$

$$\cos x = \cos -x$$

$$-\sin x = \sin -x$$

and defining J_ℓ as $-C_{\ell 0}$ results in further simplification of equation (8).

$$V_{\ell 0} = \frac{\mu R_e^{\ell}}{r^{\ell+1}} J_\ell \sum_{t=0}^{k} \frac{(2\ell-2t)!}{t!\ (\ell-t)!\ (\ell-2t)!\ 2^{2(\ell-t)}} \sin^{\ell-2t} i$$

$$X \left[\begin{matrix} \binom{2p}{p} (-1)^t \\ 2\binom{2p+1}{p} (-1)^t \sin(\omega+\nu) \end{matrix} + 2 \sum_{c=0}^{p} \binom{2p}{c} (-1)^{k+c} \begin{matrix} \cos[(2p-2c\ \ )(\omega+\nu)] \\ \sin[(2p-2c+1)(\omega+\nu)] \end{matrix} \right] \quad (9)$$

where the top choices in equation (9) are used when ℓ is even, bottom choices are used when ℓ is odd, and $p = k-t$.

Merson [12] has averaged the perturbations due to zonal harmonics over one period, his results are presented in equations (10) and (11). The equations for change in argument of periapsis (ω) and longitude of ascending node (Ω) are not valid if the inclination (i) is zero; also, the equation for change in argument of periapsis is not valid if the eccentricity (e) is zero.

For semi-major axis:

$$\Delta a = -(18/4)\pi J_2^{\,2} R^4 a^{-3}(1-e^2)^{-5} e\sin\omega(1+e\cos\omega)^2(4-5\sin^2 i) \qquad (10)$$

Changes in the other orbital elements are described by equation (11) where Δx represents either Δe, Δi, $\Delta\omega$, or $\Delta\Omega$; x_k represents e_k, i_k, ω_k, or Ω_k ($k = 2,3,4,5,6$); and x_{22} represents e_{22}, i_{22}, ω_{22}, or Ω_{22}. For example, to calculate the secular change in eccentricity over one period, replace Δx with Δe, x_k with e_k, and x_{22} with e_{22} in equation (11). The equations used to calculate the variables in equation (11) are presented below for each orbital element.

$$\Delta x = 2\pi[\sum J_k (R/p)^k x_k + J_2^{\,2}(R/p)^4 x_{22}] \qquad (11)$$

For eccentricity:

$$e_2 = 0$$

$$e_3 = -\frac{3}{8}(1-e^2)\sin i\cos\omega\,(4-5\sin^2 i)$$

$$e_4 = -\frac{45}{96}(1-e^2)(6-7\sin^2 i)\sin^2 i\; e\sin 2\omega$$

$$e_5 = \frac{15}{256}(1-e^2)\sin i[(8-24\sin^2 i+21\sin^4 i)(8+6e^2)\cos\omega + 7(8-9\sin^2 i)\sin^2 i\; e^2\cos 3\omega]$$

$$e_6 = \frac{525}{5120}(1-e^2)\sin^2 i[(16-48\sin^2 i+33\sin^4 i)(10+5e^2)\sin 2\omega + 3(10-11\sin^2 i)\sin^2 i\; e^3\sin 4\omega]$$

$$e_{22} = \frac{3}{16}\sin\omega[6(4-5\sin^2 i)(1+e\cos\omega)^2 - \sin^2 i(1-e^2)\{(16-20\sin^2 i)-(14-15\sin^2 i)\}e\cos\omega]$$

For inclination:

$$i_2 = 0$$

$$i_3 = -\frac{3}{8} e \cos i \cos\omega (4-5\sin^2 i)$$

$$i_4 = -\frac{45}{192} e^2(6-7\sin^2 i)\sin^2 i \sin 2\omega$$

$$i_5 = -\frac{15}{256} e \cos i[(8-24\sin^2 i+21\sin^4 i)(8+6e^2)\cos\omega + 7(8-9\sin^2 i)\sin^2 i\, e^2 \cos 3\omega]$$

$$i_6 = -\frac{525}{5120} e \sin 2i\, [(16-48\sin^2 i+33\sin^4 i)(10+5e^2)\sin 2\omega + 3(10-11\sin^2 i)\sin^2 i\, e^3 \sin 4\omega]$$

$$i_{22} = \frac{3}{64} \sin 2i\, [(32-40\sin^2 i)e \sin\omega) + (-14+15\sin^2 i)e^2 \sin 2\omega]$$

For longitude of the ascending node ($i \neq 0$):

$$\Omega_2 = -(3/2)\cos i$$

$$\Omega_3 = (3/8)(4-15 \sin^2 i)\, e \sin\omega \cot i$$

$$\Omega_4 = \frac{15}{96} \cos i[(4-7\sin^2 i)(6+9e^2)-3(6-14\sin^2 i)e^2\cos 2\omega]$$

$$\Omega_5 = \frac{15}{256} \cot i[(8-84\sin^2 i+33\sin^4 i)(8+6e^2)e \sin\omega + 7(8-15\sin^2 i)e^3 \sin 3\omega]$$

$$\Omega_6 = -\frac{105}{10,240} \cos i[10(8-36\sin^2 i+33\sin^4 i)(8+40e^2+15e^4) - 25(16-96\sin^2 i+99\sin^4 i)(4+2e^2)e^2\cos 2\omega - 15(20-33\sin^2 i)\sin^2 i\, e^4 \cos 4\omega]$$

$$\Omega_{22} = (3/32)\cos i[(12-80\sin^2 i) + 16(4-10\sin^2 i)e\cos\omega + (-4-5\sin^2 i)e^2 + 2(-7+15\sin^2 i)e^2\cos 2\omega]$$

For the argument of periapsis ($i \neq 0$, $e \neq 0$):

$$\omega_2 = (3/4)(4-5\sin^2 i)$$

$$\omega_3 = (3/8)e^{-1}\sin\omega\sin i[(4-5\sin^2 i) + (35\cos^2 i - 4\mathrm{cosec}^2 i)e^2]$$

$$\omega_4 = -\frac{15}{32}[(16-62\sin^2 i+49\sin^4 i) + (6\sin^2 i-7\sin^4 i)\cos 2\omega$$

$$+ (18 - 63\sin^2 i + \frac{189}{4}\sin^4 i)e^2$$

$$+ (-6 + 35\sin^2 i - \frac{63}{2}\sin^4 i)e^2\cos 2\omega]$$

$$\omega_5 = \frac{105}{16}e^{-1}\sin\omega\,\mathrm{cosec}\, i\left[\left(-\frac{4}{7} + 2\sin^2 i - \frac{3}{2}\sin^4 i\right)\sin^2 i\right.$$

$$+ \left(\frac{4}{7} - \frac{87}{7}\sin^2 i + \frac{67}{2}\sin^4 i - \frac{357}{16}\sin^6 i\right)e^2$$

$$+ \left(-1 + \frac{9}{8}\sin^2 i\right)\sin^4 i\; e^2\cos 2\omega$$

$$+ \left(\frac{3}{7} - 7\sin^2 i + \frac{267}{16}\sin^4 i - \frac{165}{16}\sin^6 i\right)e^4$$

$$+ \left.\left(1 - \frac{39}{8}\sin^2 i + \frac{33}{8}\sin^4 i\right)\sin^2 i\; e^2\cos 2\omega\right]$$

$$\omega_6 = \frac{525}{64}\left[\frac{8}{5}\left(1 - 8\sin^2 i + \frac{129}{8}\sin^4 i - \frac{297}{32}\sin^6 i\right)\right.$$

$$+ \left(2 - 6\sin^2 i + \frac{33}{8}\sin^4 i\,\sin^2 i\,\cos 2\omega\right)$$

$$+ 6\left(1 - \frac{43}{6}\sin^2 i + \frac{109}{8}\sin^4 i - \frac{121}{8}\sin^6 i\right)e^2$$

$$+ \left(-2 + 25\sin^2 i - \frac{459}{8}\sin^4 i + \frac{561}{16}\sin^6 i\right)e^2\cos 2\omega$$

$$+ \frac{3}{8}\left(1 - \frac{11}{10}\sin^2 i\right)\sin^4 i\; e^2\cos 4\omega$$

$$+ 2\left(-\frac{27}{2}\sin^2 i + \frac{99}{4}\sin^4 i - \frac{429}{32}\sin^6 i\right)e^4$$

$$+ \left(-1 + \frac{21}{2}\sin^2 i - \frac{363}{16}\sin^4 i + \frac{429}{32}\sin^6 i\right)e^4\cos 2\omega$$

$$+ \left.\frac{3}{8}\left(-1 + \frac{22}{5}\sin^2 i - \frac{143}{40}\sin^4 i\right)\sin^2 i\; e^4\cos 4\omega\right]$$

$$\omega_{22} = \frac{9}{4}\left[\left(-2 + \frac{23}{6}\sin^2 i - \frac{5}{3}\sin^4 i\right)e^{-1}\cos\omega\right.$$
$$+ \left(\frac{95}{12}\sin^2 i - \frac{445}{48}\sin^4 i\right) + \left(-2 + \frac{23}{12}\sin^2 i + \frac{5}{8}\sin^4 i\right)\cos 2\omega$$
$$+ \left(-\frac{25}{6} + \frac{461}{24}\sin^2 i - \frac{50}{3}\sin^4 i\right)e\cos\omega + \left(-\frac{1}{2} + \frac{5}{8}\sin^2 i\right)e\cos 3\omega$$
$$\left. + \left(\frac{7}{12} - \frac{3}{8}\sin^2 i - \frac{15}{32}\sin^4 i\right)e^2 + \left(\frac{7}{12} - \frac{79}{24}\sin^2 i + \frac{45}{16}\sin^4 i\right)e^2\cos 2\omega\right]$$

These equations will be used to determine the secular changes in orbital elements due to perturbations caused by the geopotential. The changes will be combined with secular changes due to third bodies and atmospheric drag to determine the velocity impulse required to keep a satellite in the desired orbit which contains a constant altitude arc.

Third Body. For Martian cases, perturbations due to the Sun will be evaluated, while perturbations due to both the Sun and Moon will be evaluated for Earth orbits. The analysis presented below is applicable to any third body. Figure 1 demonstrates the relationship between the central body, the satellite, and the third body.

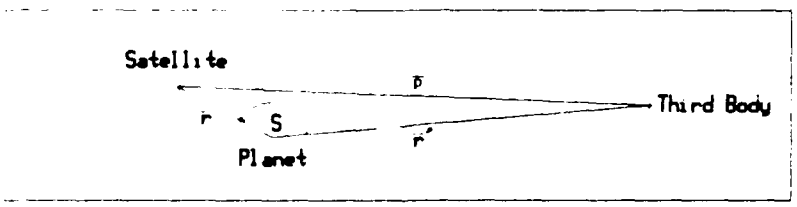

Figure 1. Geometry for Third-Body Perturbations

The position of the satellite with respect to the central body is $\bar{r}$, $\bar{r}'$ is the position of the third body with respect to the central body, and $\bar{\rho}$ is the position of the third body with respect to the satellite. The angle between $\bar{r}'$ and $\bar{r}$ is S, and $\bar{\rho} = \bar{r}' - \bar{r}$.

Equation (12) presents the disturbing function due to a third body where the perturbing accelerations due to the third body are $\nabla R'$.

$$R' = \mu_3\left[\frac{1}{\rho} - \frac{\bar{r}'\cdot\bar{r}}{\bar{r}'^3}\right] \tag{12}$$

Recognizing

$$\rho = (\bar{r}'\cdot\bar{r})^{.5}$$
$$= r'[1 + (r/r')^2 - 2(r/r')\cos S]^{1/2}$$

and

$$\bar{r}'\cdot\bar{r} = r'r\cos S$$

results in equation (13), an expansion of equation (12)

$$R' = \frac{\mu_3}{r'}\left[\left(1 + \frac{r^2}{r'^2} - \frac{2r}{r'}\cos S\right)^{-.5} - \frac{r\cos S}{r'}\right] \tag{13}$$

The binomial expansion is employed to expand the first term in equation (13)

$$[1 + (r/r')^2 - 2(r/r')\cos S]^{-.5} = \sum_{n=0}^{\infty}\binom{n-.5}{n}(-1)^n[(r/r')^2 - 2(r/r')\cos S]^n$$

Neglecting terms of (r/r') equal to or greater than third order results in an approximation to equation (12). For the case of Earth's moon, if the satellite orbit remains within six Earth radii, $(r/r')^3 < .001$. For perturbations due to the Sun this term will be much less than unity for both Earth and Mars. Equation (14) incorporates these approximations to equation (12)

$$R' \simeq \frac{\mu_3}{r'} + \frac{\mu_3 r^2}{2r'^3}(3\cos^2 S - 1) \qquad (14)$$

Substituting $\mu_3 = n'^2 a'^3$ in equation (14) and observing $\nabla(\mu_3/r')=0$ results in a simplified potential equation for a third body

$$R' = (a^2 n'^2/2)(r/a)^2(a'/r')^3(3\cos^2 S - 1) \qquad (15)$$

Kaufman [7] has developed the secular change in orbital elements due to third body perturbations. Equations (16) - (20) are the averaged change in orbital elements for one period. Equations (18) and (19) are not applicable when the inclination is zero.

$$\Delta a = 0 \qquad (16)$$

$$\Delta e = (-15\pi)\,(1-e^2)^{.5}\,(n'/n)^2\,e\alpha\beta(a'/r')^3 \qquad (17)$$

$$\Delta i = -6\pi\,(n'/n)^2\,(1-e^2)^{-.5}\,(\sin i)^{-1}\,(a'/r')^3 \times [\alpha\delta(1+4e^2) + \beta\epsilon(1-e^2) - 5\alpha\beta e^2\cos i] \qquad (18)$$

$$\Delta\Omega = 6\pi\,(n'/n)^2\,(1-e^2)^{-.5}\,(\sin i)^{-1}\,(a'/r')^3 \times [\alpha\gamma(1+4e^2)\sin\omega + \beta\gamma(1-e^2)\cos\omega] \qquad (19)$$

$$\Delta\omega = 6\pi\,(n'/n)^2\,(a'/r')^3\,(1-e^2)^{.5} \times \{(4\alpha^2-\beta^2-1) - (\gamma\cos i/\sin i)(1-e^2)[\alpha(1+4e^2)\sin\omega + \beta(1-e^2)\cos\omega]\} \qquad (20)$$

where:

$$\bar{r}'^{,o} = \begin{bmatrix} \cos\Omega'\cos\Phi' \\ \sin\Omega'\cos\Phi' \\ \sin\Omega'\cos\Phi' \end{bmatrix}$$

$$\bar{P} = \begin{bmatrix} \cos\Omega\cos\omega - \sin\Omega\sin\omega\cos i \\ \sin\Omega\cos\omega + \cos\Omega\sin\omega\cos i \\ \sin i\cos\omega \end{bmatrix}$$

$$\bar{Q} = \begin{bmatrix} -\cos\Omega\cos\omega - \sin\Omega\sin\omega\cos i \\ -\sin\Omega\cos\omega + \cos\Omega\sin\omega\cos i \\ \sin i\cos\omega \end{bmatrix}$$

$$\bar{R} = \begin{bmatrix} \sin\Omega\sin i \\ -\cos\Omega\sin i \\ \cos i \end{bmatrix}$$

$$\bar{P}' = \begin{bmatrix} -\sin\Omega\cos\omega - \cos\Omega\sin\omega\cos i \\ \cos\Omega\cos\omega - \sin\Omega\sin\omega\cos i \\ 0 \end{bmatrix}$$

$$\bar{Q}' = \begin{bmatrix} \sin\Omega\cos\omega - \cos\Omega\sin\omega\cos i \\ -\cos\Omega\cos\omega - \sin\Omega\sin\omega\cos i \\ 0 \end{bmatrix}$$

$$\alpha = \bar{r}'^{o} \cdot \bar{P}$$

$$\beta = \bar{r}'^{o} \cdot \bar{Q}$$

$$\gamma = \bar{r}'^{o} \cdot \bar{R}$$

$$\delta = \bar{r}'^{o} \cdot \bar{P}'$$

$$\epsilon = \bar{r}'^{o} \cdot \bar{Q}'$$

Equations (16) through (20) will be used to calculate the average change in orbital elements over one period due a third body.

Atmospheric Drag. The acceleration due to drag acts in the opposite direction from the velocity of the satellite with respect to the atmosphere and is modeled by equation (21):

$$D = V_s^2 \rho\beta \tag{21}$$

where

$$\beta = C_D S/2m$$

and C_D is the drag coefficient, S is the cross-sectional area of the satellite normal to the velocity of the satellite with respect to the atmosphere, m is the satellite mass, ρ is the atmospheric density, and V_s is the velocity of the satellite relative to the velocity of the atmosphere.

The atmospheric density at a given location doesn't remain constant, but changes due to the time of day, solar activity, and season. Consequently, modeling the atmosphere accurately is extremely

difficult and the best results are obtained by employing models or tabulated mean values which vary with time. However, the atmospheric density may be approximated as decreasing exponentially with increasing altitude (see equation (22)).

$$\rho = \rho_0 e^{-z/H} \tag{22}$$

where ρ_0 is atmospheric density at some reference height above the surface of the planet, z is the actual altitude minus the reference altitude, and H is the scale height of the atmosphere.

The velocity term in equation (21) is the velocity of the satellite with respect to the atmosphere. A technique to approximate the velocity in terms of orbital parameters is presented [19:275-276]. Let

$$\bar{V} = \bar{V}_s + \bar{V}_a$$

where $\bar{V}$ is the velocity of the satellite with respect to an inertial reference frame with its origin at the center of the planet, $\bar{V}_s$ is the velocity of the satellite relative to the velocity of the atmosphere, and $\bar{V}_a$ is the velocity of the atmosphere with respect to an inertial reference frame with its origin at the center of the planet.

Assuming the angular velocity of the atmosphere (ω_a) is uniform about the north-south axis results in an atmospheric velocity in terms of the geocentric latitude (ϕ) and satellite radius (r).

$$V_a = r\omega_a \cos\phi \tag{24}$$

If ψ' is the angle between $\bar{V}$ and $\bar{V}_s$ then

$$V_s^2 = V^2 + V_a^2 - 2VV_a\cos\psi' \qquad (25)$$

The atmospheric velocity vector is in the local horizontal plane and the satellite's velocity vector is almost in the local horizontal plane. The angle between the two vectors (ψ') may be approximated by the angle between the projection of the satellite's velocity vector onto the local horizontal and the atmospheric velocity vector (ψ)[9]. Consequently, using the law of cosines from spherical trigonometry,

$$\cos\psi\ \cos\phi = \cos i$$

$$V_a\ \cos\psi' \simeq V_a\ \cos\psi = r\omega_a\ \cos i \qquad (27)$$

The satellite's velocity relative to the atmosphere may be approximated in terms of its velocity with respect to an inertial reference frame, orbital elements, and angular velocity of the atmosphere.

$$\begin{aligned} V_s^2 &\simeq V^2 + V_a^2 - 2VV_a\cos\psi \\ &= V^2 + r^2\omega_a{}^2\cos^2\phi - 2Vr\omega_a\cos i \\ &= V^2[1 - (r\omega_a/V)\cos i]^2 + r^2\omega_a{}^2(\cos^2\phi - \cos^2 i) \end{aligned}$$

V_s^2 may be further approximated by recognizing $r^2\omega_a{}^2 < .005\ V^2$ [9]:

$$V_s^2 \simeq V^2[1 - (r\omega_a/V)\cos i]^2 \qquad (28)$$

Consequently,

$$D = \rho\beta V^2[1 - (r\omega_a/V)\cos i]^2 \qquad (29)$$

Sterne [16] has considered secular changes in the classical orbital elements due to a rotating atmosphere about an oblate planet. Equations

(30) - (34) present the secular changes in orbital elements over one period.

$$\Delta a = -\,2\beta a^2 \int_0^{2\pi} \rho \,\frac{E_2^{3/2}}{E_1^{1/2}} \left(1 - d\frac{E_1}{E_2}\right)^2 dE \tag{30}$$

$$\Delta e = -\,2(1-e^2)\beta a \int_0^{2\pi} \rho \,\frac{E_2^{1/2}}{E_1^{1/2}} \left(1 - d\frac{E_1}{E_2}\right) \times [\cos E - .5d(E_1)(2\cos E - e - e\cos^2 E)/(1-e^2)]\, dE \tag{31}$$

$$\Delta i = -\,.5(\omega_a/n)\beta a \sin i (1-e^2)^{-.5} \int_0^{2\pi} \rho\, E_1^{5/2}\, E_2^{1/2} \left(1 - d\frac{E_1}{E_2}\right) \times (1 + \cos 2\omega E_1^{-2}[(2-e^2\cos^2 E - 1 + 2e^2 - 2e\cos E])\, dE \tag{32}$$

$$\Delta\Omega = -\,.5(\omega_a/n)\beta a \sin 2\omega (1-e^2)^{-.5} \int_0^{2\pi} \rho\, (1-e^2\cos^2 E) \left(1 - d\frac{E_1}{E_2}\right) \times [2e^2 - 1 - 2e\cos E + (2-e^2)\cos^2 E]\, dE \tag{33}$$

$$\Delta\omega = -\cos i\, \Delta\Omega \tag{34}$$

where

$$E_1 = (1 - e\cos E)$$

$$E_2 = (1 + e\cos E)$$

$$d = (\omega_a/n)\cos i (1-e^2)^{1/2}$$

$$n = (\mu/a^3)^{1/2}$$

Equations (30) through (34) will be numerically integrated to determine the average change in orbital elements over one period due to drag. Secular changes in orbital elements due to all the perturbations considered will be combined to determine the total change in orbital elements over one period. For orbits about Earth and Mars perturbations due to the geopotential, atmospheric drag, and the Sun will be

calculated. For Earth orbits, the secular changes in mean orbital elements due to the Moon will also be calculated.

Planet Geometry

In this section, the radius of an oblate planet is found as a function of latitude. The radius is needed to calculate the ellipsoidal altitude which is the difference between the radius of the orbit and the radius of the planet.

Consider an axi-symmetric planet with semi-major axis (a), semi-minor axis (b), and radius (R) as a function of latitude (ϕ). The ellipticity (f) of the planet is defined in terms of the semi-major (a) and semi-minor (b) axes as

$$f = 1 - b/a$$

or in terms of the planet's eccentricity (e)

$$f = 1 - (1 - e^2)^{.5}$$

A relationship to determine the planet's eccentricity is presented below,

$$1 - e^2 = (1 - f)^2$$

Equation (36) may be employed to approximate the planet's radius given the latitude and the ellipticity:

$$R = a[1 - f \sin^2\phi + O(f^2)] \qquad (36)$$

The reasoning employed to achieve this result is presented. Consider an ellipse circumscribed by a circle (see Figure 2). The geometry of the ellipse dictates the relationship between the semi-major and semi-minor axes, the eccentricity, and any point on the perimeter of the ellipse.

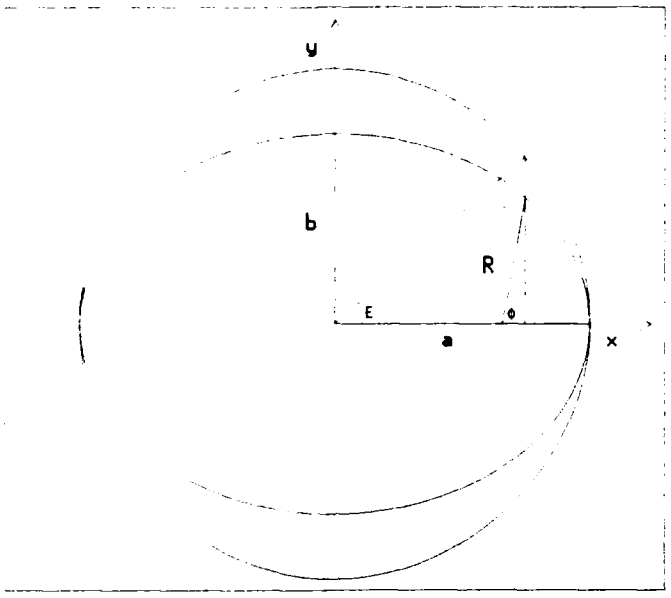

Figure 2. Geometry of Planet

$$1 = (x/a)^2 + (y/b)^2$$
$$ae = (a^2 - b^2)^{.5}$$

Eventually, an expression for R/a as a function of ϕ must be found. First, $(R/a)^2$ is found as a function of E.

$$\begin{aligned} R^2 &= x^2 + y^2 \\ &= [a \cos E]^2 + [b \sin E]^2 \\ &= [a \cos E]^2 + [a (1 - e^2)^{.5} \sin E]^2 \\ &= a^2 [\cos^2 E + \sin^2 E - e^2 \sin^2 E] \\ (R/a)^2 &= 1 - e^2 \sin^2 E \end{aligned}$$

Sin$E$ is found as a function of ϕ and length y may be expressed in terms of the semi-major axis, eccentricity, and sin$E$:

$$\begin{aligned} y &= R \sin\phi \\ &= b \sin E \\ &= a\,(1 - e^2)^{.5} \sin E \end{aligned}$$

These relationships are used to solve for sin$E$.

$$\sin E = (R/a)[\sin\phi/(1 - e^2)^{.5}]$$

Consequently,

$$(R/a)^2 = [1 + F \sin^2\phi]^{-1}$$

where

$$F = e^2/(1 - e^2) = [(1-f)^{-2} - 1]$$

Equation (37) presents a relationship to evaluate the radius given the eccentricity and latitude.

$$R = a \left[\frac{(1-e)^2}{1 + e^2\cos^2\phi} \right]^{.5} \qquad (37)$$

Equation (37) will be approximated by a truncated series expansion. The series will be developed by expanding (R/a) and F using the binomial expansion. Equation (38) presents the expansion of F.

$$F = -1 + \sum_{n=0}^{\infty} \binom{-2}{n} (-f)^n$$

$$F = \sum_{n=1}^{\infty} (n+1)\ f^n \tag{38}$$

Equation (39) presents the expansion of (R/a):

$$R/a = \sum_{n=0}^{\infty} \binom{-1/2}{n} [F \sin^2\phi]^n \tag{39}$$

Combining equations (38) and (39) results in equation (40) which determines the radius of the planet as a function of latitude, ellipticity, and equatorial radius.

$$R = R_e \sum_{n=0}^{\infty} \binom{-1/2}{n} \left[\sum_{m=1}^{\infty} (m+1)\ f^m \right]^n [\sin^{2n}\phi] \tag{40}$$

Truncating third order terms and higher from equation (40) results in an approximation of the radius as a function of latitude, ellipticity, and equatorial radius:

$$R \simeq R_e\ [1 - f \sin^2\phi + 1.5\ f^2\ (\sin^4\phi - \sin^2\phi) + O(f^3)] \tag{41}$$

Consider the term $(\sin^4\phi - \sin^2\phi)$ in equation (41). Taking the derivative with respect to ϕ indicates optimums will occur at 0°, $\pm 45^\circ$, and $\pm 90^\circ$. The maximum error due to the second order terms will occur at a latitude of $\pm 45^\circ$. Consequently, ΔR_{max} is the maximum error which will be caused by truncating second order terms:

$$\Delta R_{max} = - (3/8)\ R_e\ f^2$$

For Earth (R_e=6378 km, f=.003352[11]) the maximum magnitude of error due to second order terms is 27 m. For Mars (R_e=3393 km, f=.005185[11]) the maximum magnitude error due to second order terms is 34 m.

Ellipsoidal Altitude

In this section, the ellipsoidal altitude (which is the difference between the satellite's radius and the planet's radius) will be developed in terms of the classical orbital elements. The radius of the satellite is know in terms of the classical orbital elements and the radius of the planet is expressed in terms of the latitude. Equation (42) presents the equation for the ellipsoidal altitude

$$h = r - R \tag{42}$$

where r is the satellite radius, and R is the radius of the planet. For accurate evaluation equation (37) will be employed to determine R and r will be determine by numerically integrating the satellite's equations of motion.

First Order Approximation. An approximation to the ellipsoidal altitude may be found by considering two-body motion (equation (3)) and using only first order terms of equation (41).

$$h = a(1 - e^2)/(1 + e\cos\nu) - R_e(1 - f\sin^2\phi) \tag{43}$$

It's much more convenient to know the ellipsoidal altitude as a function of orbital elements instead of latitude; consequently, the $\sin^2\phi$ term will be rewritten in terms of classical orbital elements. Consider the orbit presented in Figure 3 with inclination (i), argument of periapsis (ω), and true anomaly (ν). Using the law of sines from spherical

trigonometry, results in an expression for latitude in terms of inclination, argument of periapsis, and true anomaly.

$$\sin\phi/\sin i = \sin(\omega+\nu)/\sin 90$$

$$\sin\phi = \sin i \sin(\omega+\nu)$$

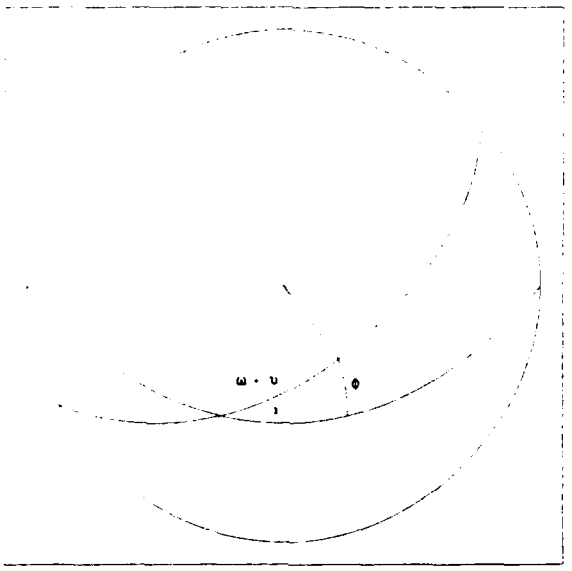

Figure 3. Relationship between Latitude and Orbital Elements

The ellipsoidal altitude may now be written in terms of orbital elements.

$$h = [a(1-e^2)/(1 - e\cos\nu)] - R_e[1 - f \sin^2 i \sin^2(\omega+\nu)] \quad (44)$$

Change in Ellipsoidal Altitude

The derivative of ellipsoidal altitude will be zero for the duration of the constant altitude arc. In this section the derivative of the ellipsoidal altitude is calculated with respect to true anomaly.

Differentiating Equation (44) with respect to the true anomaly and employing

$$\sin 2a = 2 \cos a \sin a$$

results in an expression for the change in ellipsoidal altitude.

$$dh/d\nu = a\ e\ (1 - e^2)\ \sin\nu/(1 + e\ \cos\nu)^2 + R_e\ f\ \sin^2 i\ \sin[2(\omega+\nu)] \tag{45}$$

An arc of constant altitude would occur between ν_1 and ν_2 when

$$0 \simeq \Delta h = \int_{\nu_1}^{\nu_2} \frac{dh}{d\nu}\, d\nu$$

It is clear the altitude will remain constant throughout the entire orbit if i=e=0. Also, as long as the orbital elements remain constant, the semi-major axis only changes the altitude (not the position or length of the arc of constant altitude). The argument of periapsis and inclination will cause the position of the constant arc to move while the eccentricity must be matched with the argument of periapsis and inclination to produce an arc of constant altitude.

Relationship between Mean and Osculating Orbital Elements

All orbital elements presented are mean values with respect to short term variations caused by J_2. When the equations of motion are numerically integrated, the osculating elements are output at each time step [18]. To determine the secular change in orbital elements, the mean orbital elements are needed instead of the osculating elements. The method Kwok [11], employs to transform from mean to osculating elements is presented:

$$X_i = X_i' + \delta X_i(X_i') \tag{46}$$

X_i' are six mean orbital elements describing two-body motion and δX_i are the variations in orbital elements due to J_2. X_i are the osculating elements. Recalling $r = p/(1+e\cos\nu)$,and $p=a(1-e^2)$ the change in orbital elements may be calculated as functions of the mean orbital elements.

$$\delta i = (3/4)J_2(R_e/p')^2 \sin i' \cos i'$$
$$\times [\cos 2(\nu'+\omega') + e'\cos(\nu'+2\omega') + (e'/3)\cos(3\nu'+2\omega')]$$

$$\delta p = 2\, p' \tan i' \, \delta i$$

$$\delta\Omega = -(3/2)J_2(R_e/p')^2 \cos i' \, [\omega' - M' + e'\sin\nu' - (1/2)\sin 2(\nu'+\omega')$$
$$- (e'/2)\sin(\nu'+3\omega') - (e'/6)\sin(3\nu'+5\omega')]$$

$$\delta r = -(p'/4)J_2(R_e/p')^2 \{(3\cos^2 i'-1)$$
$$\times [2r'(1-e^2)/p' + e'\cos\nu'/(1+(1-e'^2)) + 1] - \sin^2 i' \cos 2(\nu'+\omega')\}$$

$$\delta\dot{r} = -(p'/4)\, J_2(R_e/p')^2\{(3\cos^2 i'-1)e'\sin\omega'$$
$$\times [(1-e'^2)^{1/2} + (p'/r')^2/(1 + (1-e'^2)^{1/2}]$$
$$- 2\sin^2 i'(1 + e'\cos\nu')^2\sin 2(\nu'+\omega')\}$$

Let $F' = (1-3\cos^2 i')/[1 + (1-e'^2)^{1/2}]$

$$\delta(\nu+\omega) = (J_2/8)(R_e/p')^2[6(1-5\cos^2 i')(\nu'-M')$$
$$+ 4e'\sin\nu'(1-6\cos^2 i' + F') + F'e'^2\sin 2\nu'$$
$$+ 2(5\cos^2 i'-2)e'\sin(\nu'+2\omega') + (7\cos^2 i'-1)\sin 2(\nu'+\omega')$$
$$+ 2\cos^2 i'e'\sin(3\nu'+2\omega')]$$

$$p = p' + \delta p'$$

$$r = r' + \delta r'$$

$$\dot{r} = \dot{r}' + \delta \dot{r}'$$

$$(\nu+\omega) = (\nu'+\omega') + \delta(\nu'+\omega')$$

$$A = (p/r) - 1$$

$$B = (p/\mu)^{.5}\, r$$

The osculating elements may now be calculated:

$$i = i' + \delta i'$$

$$\Omega = \Omega' + \delta \Omega'$$

$$e = (A^2 + B^2)^{1/2}$$

$$\nu = \tan^{-1}(B/A)$$

$$a = p/(1-e^2)$$

$$\omega = (\omega+\nu) - \nu$$

Transformation from osculating to mean orbital elements requires iteration. First calculate the variations as a function of the osculating elements then solve for the mean elements. Use these new mean elements to calculate the variations. Continue iterating until a group of mean elements is found which satisfy equation (46) by producing the original osculating elements.

Impulsive Velocity Changes Needed to Correct Orbit

Once an orbit with a constant altitude arc which covers the correct latitude range is chosen for a mission, secular changes to the orbital elements will cause the location, duration, and altitude of the arc to change. Consequently, the velocity impulse needed to negate the effects

of the changes in orbital elements is presented. Figure 4 demonstrates the two possible cases where the change in semi-major axis is either positive or negative. Also shown on the figure is the change in argument of periapsis. In practice, the optimum starting and ending true anomalies and eccentricity of the transfer ellipse between two elliptical orbits must be chosen to minimize the impulsive velocity change[3:67-71]. In a Hohmann transfer, the initial and final orbits are circular and the transfer ellipse ranges from apoapsis to periapsis. In view of the fact that the orbits being considered are nearly circular, the portion of the transfer ellipse used in this analysis will arbitrarily be fixed to range from apoapsis to periapsis. When the ratio of larger semi-major axis to smaller semi-major axis of the initial and final orbits being considered is between 0 and 11.94 [3:62], the Hohmann transfer is the transfer requiring a minimum velocity impulse. The cases to correct for secular changes in orbital elements result in a ratio of semi-major axes of about unity, with nearly circular initial and final orbits. As a result, the impulsive velocity change calculated should be near the minimum required velocity change. The method used to determine the required velocity impulse is presented. From conservation of energy in an elliptical orbit, the magnitude of the velocity at any point on the ellipse may be determined by equation (47):

$$V = (\mu(2/r - 1/a))^{1/2} \tag{47}$$

Also for an elliptical orbit, equation (48) may be employed to calculate the angle (γ) [14:83]. Angle γ is measured from the radius vector to the velocity vector.

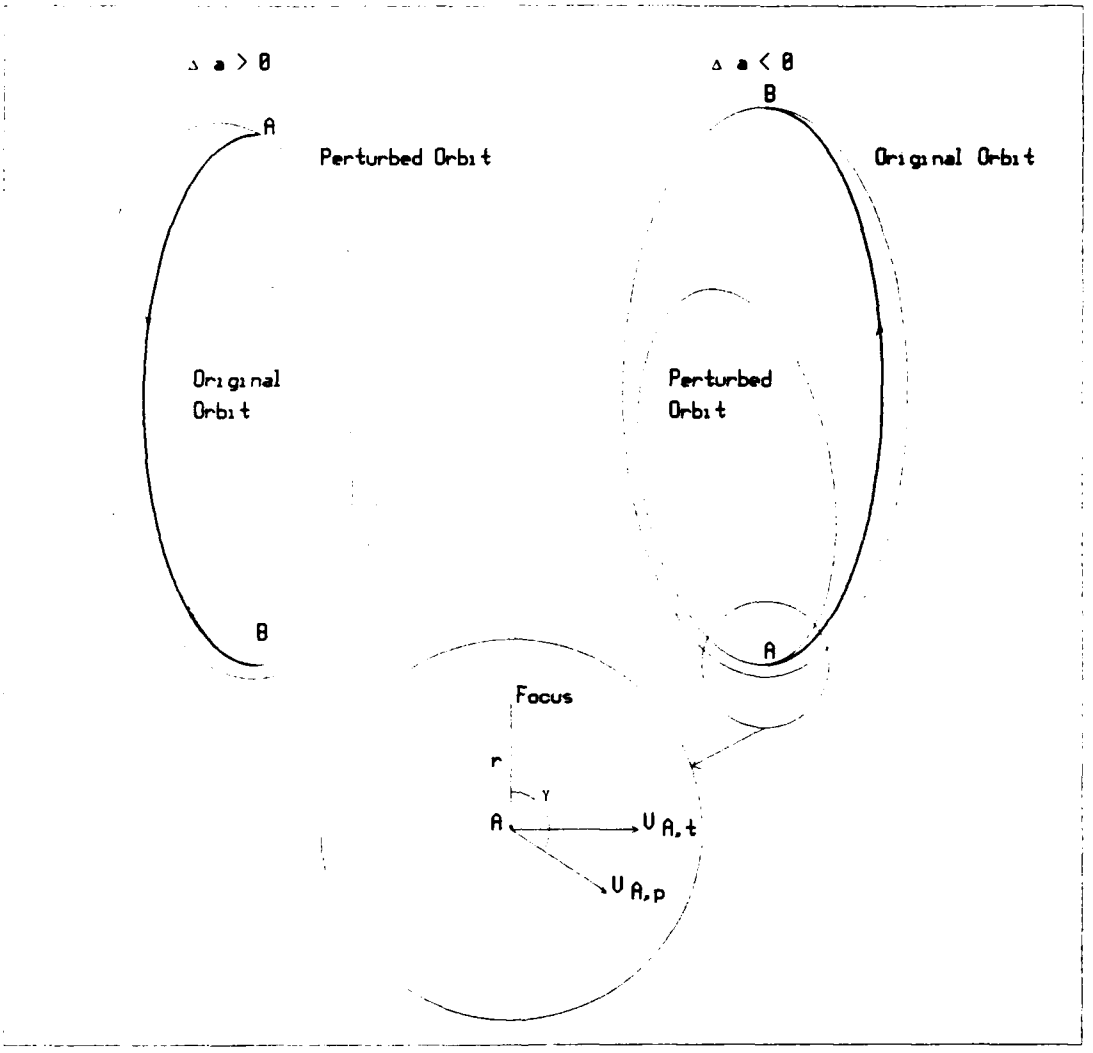

Figure 4. Geometry of Transfer Orbits

$$\sin\gamma = (1+e\cos\nu)/(1 + e^2 + 2e\cos\nu)^{1/2} \qquad (48)$$

$$\cos\gamma = -e\sin\nu/(1 + e^2 + 2e\cos\nu)^{1/2}$$

Considering Figure 4, point "A" represents the point where the perturbed orbit is initially changed to follow the transfer orbit, and point "B"

is the point where the transfer orbit is changed to achieve the original orbit. The semi-major axis of the perturbed orbit is the semi-major axis of the original orbit (a) plus the secular change in the semi-major axis over one period (Δa) and similarly the eccentricity of the initial and final orbits are e and $e+\Delta e$ respectively.

First, the velocity impulse needed at "A" is considered. Equation (3) is employed to calculate the radius of the perturbed orbit at "A" ($r_{A,p}$) where the true anomaly at point "A" is $\Delta\omega$ when $\Delta a<0$, and $180^{\circ}+\Delta\omega$ when $\Delta a>0$. Knowing $r_{A,p}$, the velocity at "A" on the perturbed orbit ($V_{A,p}$) may be evaluated by applying equation (47).

Considering point "B", the radius of the initial orbit at "B" ($r_{B,i}$) is calculated by employing equation (3) where the true anomaly is 180° when $\Delta a<0$ and 0° when $\Delta a>0$; the velocity of the initial orbit at point "B" is calculated by employing equation (47) with the original semi-major axis.

The transfer semi-major axis is found in terms of the radius of the perturbed orbit at point "A" and the radius of the original orbit at point "B",

$$a_t = (r_{A,p} + r_{B,i})/2$$

The velocity on the transfer ellipse may be determined at points "A" and "B" by applying equation (47), with a_t and $r_{A,p}$ (for $V_{A,t}$) and $r_{B,i}$ (for $V_{B,t}$). The transfer ellipse velocity and the initial ellipse velocity at point "B" are colinear. As a result, the magnitude of the velocity impulse required at point "B" is simply the difference between the desired velocity ($V_{B,i}$) and the velocity of the satellite on the transfer ellipse ($V_{B,t}$).

$$\Delta V_B = | V_{B,t} - V_{B,i} |$$

The velocities at point "A" are not colinear due to the change in argument of periapsis -- the angle between $V_{A,t}$ and $V_{A,p}$ is $|90^{o}-\gamma|$ = γ'. Consequently,

$$\Delta V_A = [\ (V_{A,t} - V_{A,p}\cos\gamma')^2 + (V_{A,p}\sin\gamma')^2\ ]^{1/2}$$

$$= [\ V_{A,t}^{\ 2} - 2V_{A,t}V_{A,p}\sin\gamma + V_{A,p}^{\ 2}\ ]^{1/2}$$

where equation (48) is employed to calculate $\sin\gamma$ as a function of the true anomaly of the perturbed orbit at point A.

The velocity impulse needed to change the plane of the orbit to correct for the secular change in inclination (Δi) is now considered. The velocity impulse required for this maneuver is directly proportional to the magnitude of the velocity of the satellite; consequently, the maneuver should be accomplished at apoapsis of the largest orbit.

If $\Delta a<0$

$$\Delta V_{\Delta i} = 2V_{B,i}|\sin(\Delta i/2)|$$

and if $\Delta a>0$

$$\Delta V_{\Delta i} = 2V_{A,p}|\sin(\Delta i/2)|$$

The total change in velocity due to secular changes in semi-major axis, argument of periapsis, eccentricity, and inclination is the sum of the velocity impulses required at points "A" and "B", and the impulse required to change the plane of the orbit.

$$\Delta V = \Delta V_A + \Delta V_B + \Delta V_{\Delta i} \qquad (49)$$

Correcting secular changes due to the change in the longitude of the ascending node was not considered. The eccentricity needed to produce an orbit with a constant altitude arc is a function of inclination, semi-major axis, argument of periapsis, J_2, ellipticity, and equatorial radius (see equation (52)). The longitude of the ascending node (Ω) doesn't affect the orbital elements needed to accomplish an orbit which contains an arc of constant altitude.

III Numerical Methods

Search Method

Identify Orbits with Arcs of Constant Altitude. In order to map the combinations of mean orbital elements which produce orbits with arcs of constant ellipsoidal altitude, the semi-major axis (a), argument of periapsis (ω), inclination (i), and planet were chosen as independent variables. Several cases were considered where the planet, semi-major axis, and perturbing accelerations were fixed. The eccentricity (e) which produced arcs of constant ellipsoidal altitude was found as a function of argument of periapsis and inclination. The following matrix of independent variables was considered for each case:

$$\omega = j(10) \quad 0 \leq j \leq 18$$

$$i = k(10) \quad 0 \leq k \leq 9$$

The method employed to find values of eccentricity required an input of the ellipsoidal altitude as a function of an independent variable (time or true anomaly) over one period. The change in altitude with time (or true anomaly) was calculated at each time step. The longest group of points where $dh/dt \leq \epsilon$ was found; where ϵ is the tolerance used to sort the derivatives. A function (F) indicating the shape of this group of points was employed to evaluate the orbit and iterated to find the optimum eccentricity

$$F = [\Delta h_{max} + n^{-1}] \prod_{j=0}^{m} S_j \qquad n \neq 0$$

$$F = [\Delta h_{max} + 1] \prod_{j=0}^{m} S_j \qquad n = 0$$

where Δh_{max} is the difference between the maximum and minimum altitudes attained in the range, n is the number of points with $dh/dt = 0$, S_o is the sign of the derivative at the first point on the range and m is the number of times dh/dt changes sign. The combination of orbital elements which forced F to be zero were found (see Appendix A for a flow chart of the method).

Figures 5 and 6 demonstrate changing the eccentricity changes the satellite's altitude above the Earth. For both cases inclination is 63.44° and semi-major axis is 7000 km; however, Figure 5 has an argument of perigee of 0° while Figure 6 has an argument of perigee of 135°.

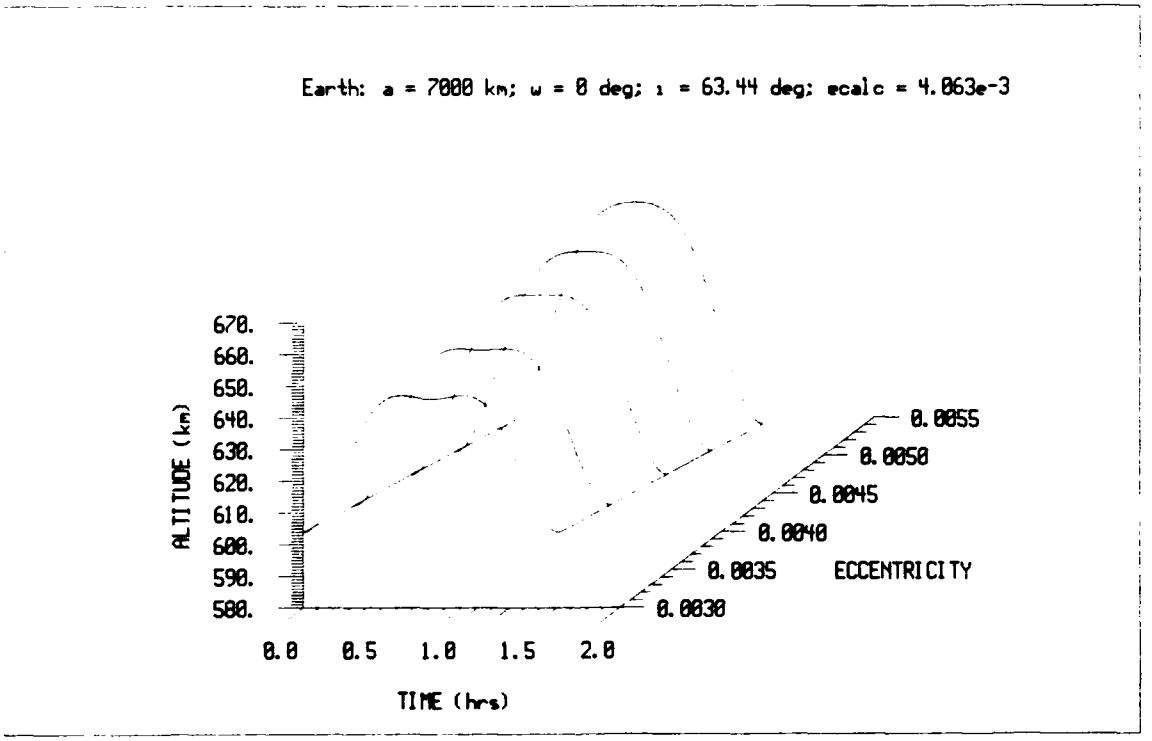

Figure 5. Satellite Altitude as a Function of Eccentricity ($\omega = 0^{\circ}$)

To get an indication of the sensitivity of the arc of constant altitude to eccentricity, a Martian case with a large eccentricity is also presented. Figure 7 demonstrates the changing altitude of a Martian

satellite as a function of eccentricity. The parameters which were held constant follow: a = 3600 km, $\omega = 0^{o}$, and $i = 90^{o}$.

Figures 5, 6, and 7, indicate the eccentricity may differ from the optimum by as much as $.1x10^{-3}$ and still produce a reasonably constant arc.

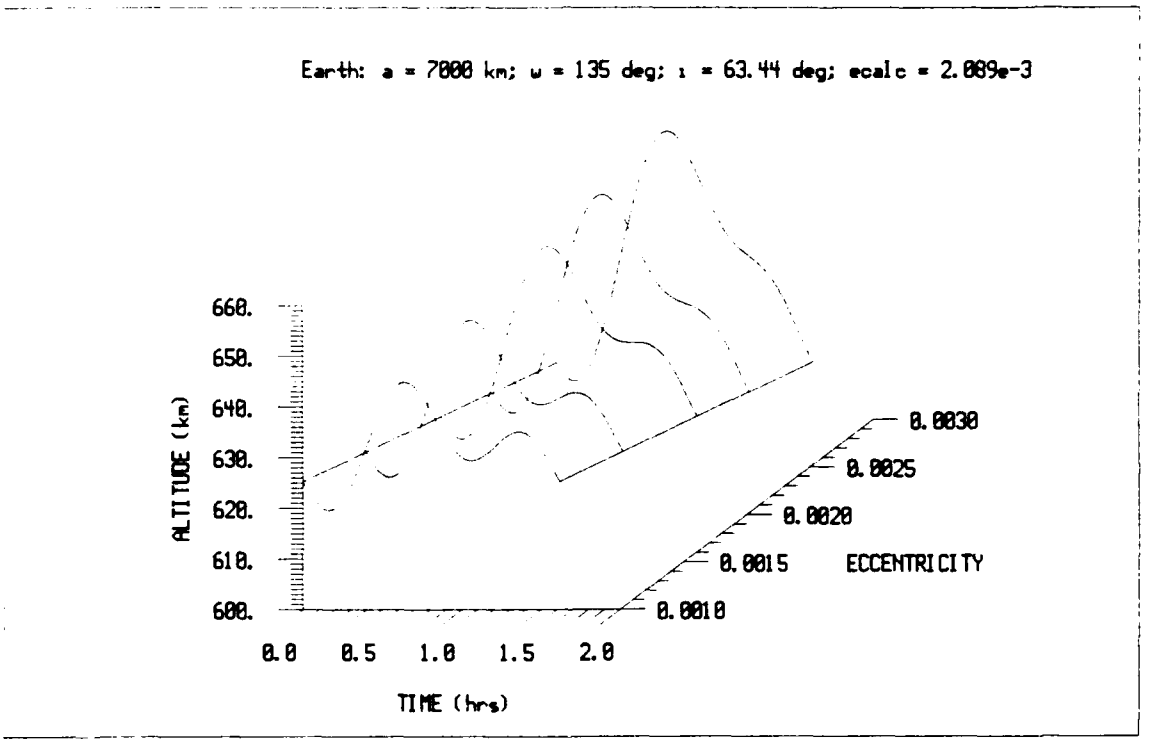

Figure 6. Satellite Altitude as a Function of Eccentricity ($\omega = 135^{o}$)

The eccentricity required to produce an arc of constant altitude was identified to $\pm .001 \times 10^{-3}$. The largest deviation from the fitted data due to the curve fit was on the order of $\pm.01 \times 10^{-3}$ (see Appendix F) and most calculated curve fit points were within $\pm .003 \times 10^{-3}$ of the data. The largest deviations occurred at larger eccentricities where larger deviations from the optimum eccentricity may be tolerated and still produce a constant altitude arc.

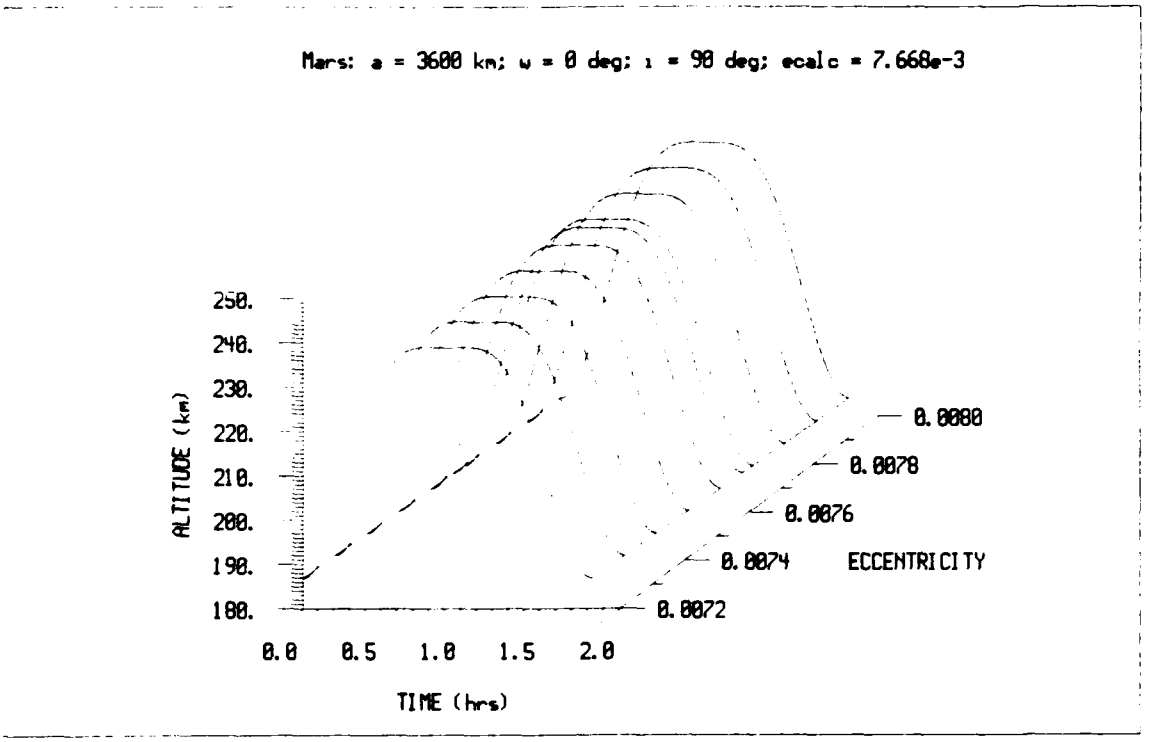

Figure 7. Sensitivity of Altitude due to Eccentricity

Two methods were used to produce the values of ellipsoidal altitude over one period. For the two-body case, equations (44) and (45) were simply evaluated at each time step. When perturbative effects were considered, ASAP [11] was used to numerically integrate the equations of motion and provide values of ellipsoidal altitude as a function of time. A central differences scheme was then used to estimate the derivatives as a function of time.

Curve Fit. A polynomial fit was employed to curve fit both the two-body results and the change in eccentricity due to J_2. The general curve fit method is presented here -- independent variables which were employed and the coefficients which resulted are presented in Section IV.

$$F = \sum_{k=0}^{kx} \sum_{\ell=0}^{\ell y} C\, A_{k,\ell}\, T_k(\bar{X})\, T_\ell(\bar{Y})$$

where

$$C = \begin{cases} 1. & k\neq 0 \text{ and } \ell\neq 0 \\ 0.5 & k=0 \text{ or } \ell=0 \\ 0.25 & k=0 \text{ and } \ell=0 \end{cases}$$

kx = order of the polynomial in x

ℓy = order of the polynomial in y

$$\bar{X} = \frac{2x - (x_{max}+x_{min})}{x_{max}-x_{min}}$$

$$\bar{Y} = \frac{2y - (y_{max}+y_{min})}{y_{max}-y_{min}}$$

The fit may only be used for interpolation, and not extrapolation; consequently,

$$x_{min} \leq x \leq x_{max}$$

$$y_{min} \leq y \leq y_{max}$$

The standard recurrence relationship utilized to calculate the Chebyshev polynomials is presented below

$$T_0(x) = 1$$

$$T_1(x) = x$$

$$T_n(x) = 2xT_{n-1}(x) - T_{n-2}(x)$$

Choice of Independent Variables. The independent variables were selected so a single empirical equation (good for either planet, and all the semi-major axis and inclination combinations considered) could be developed to predict the eccentricity which produces orbits with arcs of constant altitude. The rational employed to choose the non-dimensional groupings of independent variables for the curve fits is now presented.

First, the first order equation for ellipsoidal altitude was considered. Equation (44) was rewritten in a non-dimensional form:

$$\frac{h + R_e}{R_e f \sin^2 i} = \frac{a}{R_e f \sin^2 i}\left[\frac{(1-e^2)}{(1+e\cos\nu)}\right] + \sin^2(\omega+\nu) \qquad i \neq 0$$

$$h + R_e = a \qquad i = 0$$

It is clear from this arrangement that for a given inclination and planet, the value of eccentricity which produces an arc of constant altitude will depend on ω and $(R_e f \sin^2 i/a)$, while the position of the arc will depend on ν. Consequently, ω and $(R_e f \sin^2 i/a)$ were chosen as the independent variables used to curve fit the two-body results from all the cases. In this term, $R_e f$ describes the planet, while $\sin^2 i/a$ describes the orbit. The change in the optimum eccentricity from two-body motion due to the J_2 term of the geopotential must also be curve fit. The perturbing potential caused by the J_2 term of the geopotential was used to select the portion of the independent variable dependent on planet properties. V_{20} is presented below for completeness.

$$V_{20} = -\frac{J_2 R_e^2 \mu}{r^3}(3\sin^2 i \sin^2(\omega+\nu) - 1)$$

The second zonal harmonic and equatorial radius were chosen to represent the planet $(J_2 R_e^2)$, and in order to make the variable non-dimensional, the term $(\sin i/a)^2$ was used to describe the orbit. The value used as the independent variable was $J_2(R_e \sin i/a)^2$. Again, this term and ω were used as independent variables to curve fit all the results for the change in eccentricity from the two-body cases. A correction for J_3 was not included. For the Earth cases considered, the change in e caused by J_3 was insignificant (on the order of $.001 \times 10^{-3}$). The

largest deviation from the J_2 results due to J_3 occurred for Mars (a=3600km, i=90°) where the change due to the J_3 term was $-.026 \times 10^{-3}$. As Figure 7 indicates, a change of this magnitude is not enough to significantly change the results.

Cases. Table 1 presents the cases which were considered. In each case, the eccentricity was found which produced an orbit with an arc of constant altitude for the following values of argument of periapsis and inclination: $\omega = j(10) \quad 0 \leq j \leq 18$, and $i = k(10) \quad 0 \leq k \leq 9$.

Without a specific application to determine spacecraft geometry and attitude, choosing a drag coefficient, area, and mass become arbitrary. For the cases in Table 1 which considered drag, $S/m = .02 \times 10^{-6}$ km^2/kg, and $C_D = 2.0$ [11] were chosen resulting in $\beta = .02 \times 10^{-6}$ km^2/kg. This is a realistic estimate of β as typical area to mass ratios of satellites (not including balloons), are between $.002 \times 10^{-6}$ and $.02 \times 10^{-6}$ km^2/kg [8:xiii].

Table 1. Cases Considered to Determine $e(\omega,i)$ which Produce Constant Altitude Arcs

Case	Planet	Semi-Major Axis (km)	Model
1 2 3	Earth	6700 7000 7500	Two-Body
4 5 6 7		6700	J2 J3 J2 + Drag J3 + Drag
8 9 10 11		7500	J2 J3 J2 + Moon J3 + Moon
12 13	Mars	3600 4000	Two-Body
14 15		3600 4000	J2

Secular Considerations

Calculate Secular Changes in Mean Orbital Elements over One Period. Once the orbital elements which produce arcs of constant altitude were identified, the secular changes in semi-major axis, argument of periapsis, inclination, eccentricity and longitude of the ascending node were determined for several cases by varying the semi-major axis, ballistic coefficient, and planet. The start time was not varied, consequently, cases for the various positions of the third body were not considered. Perturbations due to zonal harmonics up to the sixth order, drag, and third bodies (Earth: Moon and Sun; Mars: Sun) were considered. For perturbations due to the geopotential, equations (10) and (11) were employed. The orbits are circular at i=0, and equations (10) and (11) are not valid for eccentricities or inclinations of zero; consequently, the comparisons considered only the inclination range from 15^{o} to 90^{o}. For perturbations due to drag, equations (30) through (34) were numerically integrated while employing equation (22) to calculate the density. The altitude of the satellite was calculated by applying equation (36), and the rotation rate of the atmosphere was assumed to be the same as the planet. Values employed to calculate secular changes in orbital elements due to drag and geopotential are presented in Table 2. For third body effects, equations (16) through (20) were employed. This model requires the position of the third body be provided with respect to an inertial reference frame centered on the planet with the *x* axis aligned with the vernal equinox. The position of the third body was calculated once per orbit. The position was found as a function of time (in Julian centuries since epoch (T)). The time used to define the position of the third body was a start time (input variable) plus half the period calculated using the original mean orbital elements.

Table 2. Values used to Calculate Secular Changes in Orbital Elements

Parameter	Earth	Mars	Reference
J_2	1.082627×10^{-3}	1.960454×10^{-3}	Earth: [20]
J_3	-2.542×10^{-6}	-3.144926×10^{-5}	GEM-6 Model
J_4	-1.609×10^{-6}	-1.889437×10^{-5}	
J_5	-2.192×10^{-6}	2.669249×10^{-6}	Mars: [3]
J_6	5.23×10^{-7}	-1.340757×10^{-6}	
H (km)	78.4	9.98	Earth: [11]
ρ_0 (kg/m^3)	5.215×10^{-13}	1.72×10^{-7}	Mars : [10]
z_0 (km)	500	100	
ω_a (rad/s)	7.292×10^{-5}	7.088×10^{-5}	[11]

The positions which were used are presented.

Position of the Sun with respect to the Earth (ref JD: 2415020.)[5]:

$$a_s = 1.496 \times 10^8 \text{ km}$$

$$e_s = 1.675104e\text{-}2 - 1.1444e\text{-}5T - 9.4e\text{-}9T^2$$

$$i_s = .4093197474 - 6.217910e\text{-}5T - 2.1468e\text{-}9T^2 + 1.7977e\text{-}10T^3 \text{ rad}$$

$$\Omega_s = 0 \text{ rad}$$

$$\omega_s = 4.908229653 + 8.24149855e\text{-}7T + 5.9167e\text{-}7T^2 + 1.22e\text{-}9T^3 \text{ rad}$$

$$M_s = 6.25658 + 172.0197T - 1.9548T^2 - 1.22e\text{-}9T^2 \text{ rad}$$

Position of the Moon with respect to the ecliptic -- all angles are in radians. (ref JD: 2415020.)

$$a_m = 384.4 \times 10^{-3} \text{ km}$$

$$e_m = .054900489$$

$$i_m' = 8.980411e\text{-}2$$

$$\Omega_m' = 4.523601514 - 9.242202945T + 2.7174776e\text{-}6T^2 + 8.7266e\text{-}10T^3$$

$$\omega_m' = 5.8351515 + 19.44368005T - 1.35071e\text{-}5T^2 - 4.53786e\text{-}9T^3 - \Omega_m'$$

$$M_m' = 4.71997 + 2299.715T - 1.4835e\text{-}6T^2 + 6.81e\text{-}10T^3 - \Omega_m' - \omega_m'$$

The position of the Moon with respect to the Earth is required. Transformations to determine the position of the Moon with respect to the Earth instead of the ecliptic are completed using spherical trigonometry and are presented below. Figure 8 demonstrates the geometry of the orbits[5:107-109]. To find i_m use spherical trigonometry to find α,

$$\cos\alpha = -\cos i_s \cos i_m + \sin i_s \sin i_m' \cos\Omega_m$$

where α is in the second quadrant. Now i_m may be found,

$$i_m = \pi - \alpha$$

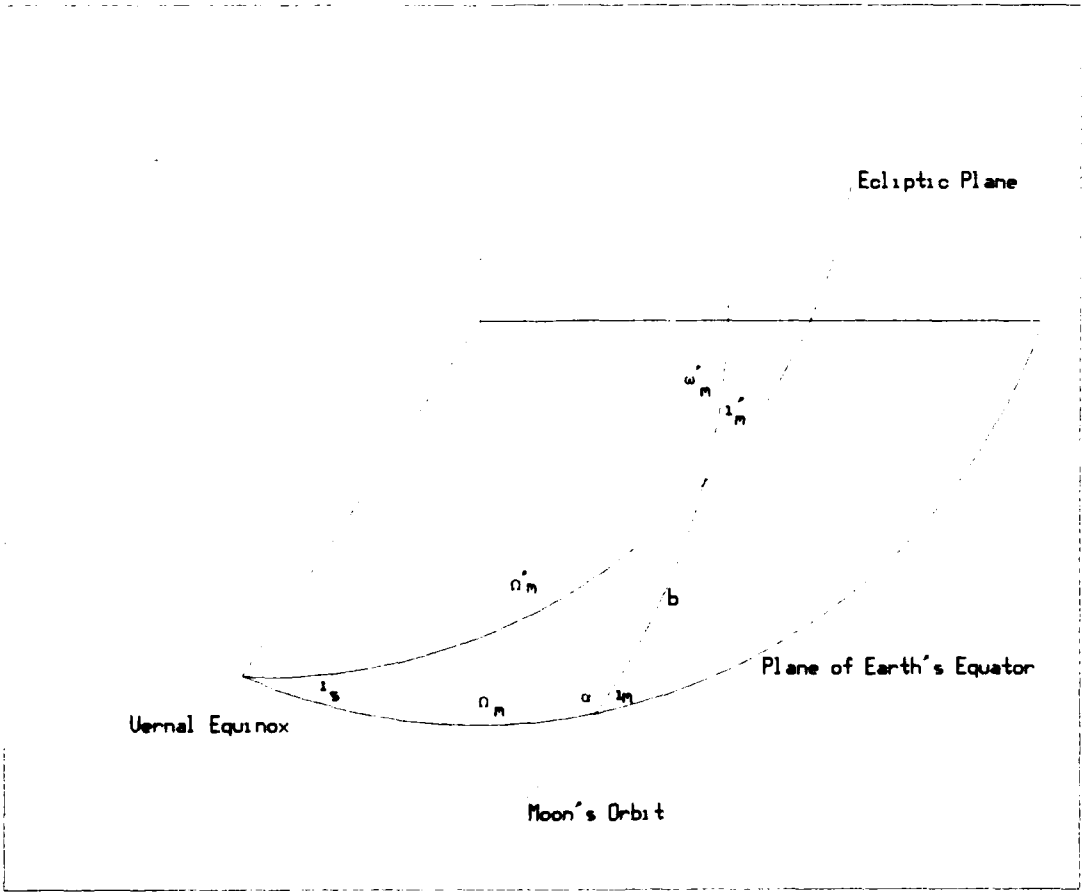

Figure 8. Geometry of Lunar Orbit with Respect to Ecliptic and Earth

In order to find ω_m, solve for "b" using the law of cosines for angles and ensure "b" lies in the same hemisphere as Ω_m'

$$\cos b = (\cos i_s + \cos\alpha \cos i_m')/(\sin\alpha \sin i_m')$$

$$\omega_m = \omega_m' + b$$

Finally, solve for Ω_m using the law of cosines for sides and ensure Ω_m is in the same hemisphere as Ω_m'.

$$\cos\Omega_m = \cos\Omega_m' \cos b + \sin\Omega_m' \sin b \cos i_m'$$

Position of the Sun with respect to Mars (reference Julian date 2448400.5)[11]

$a_s = 227.941 \times 10^6$ km

$e_s = .933969 \times 10^{-2}$

$i_s = 25.191153$ deg

$\Omega_s = 0.$ deg

$\omega_s = -109.05076$ deg

$M_s = -171.60476$ deg

The equations defining perturbations due to the third body require the semi-major axis, radius, right ascension, declination and mean motion of the third body. The methods which were employed to find these values are presented. The radius is calculated using equation (3) where ν is approximated by an expansion in mean anomaly and eccentricity[15]

$$\nu \simeq M + (2e - e^3/4)\sin M + (5e^2/4 + 11e^4/24)\sin 2M + (13/12)e^3\sin 3M + (103/96)e^4\sin 4M \qquad (50)$$

The mean motion is found using the semi-major axis and mass of the third body:

$$n = (\mu/a^3)^{1/2}$$

The declination (Φ') and right ascension (Ω') are calculated using relationships from spherical trigonometry. The range of inclinations of the third bodies considered in this thesis were only in the first quadrant; consequently, declination is in the same hemisphere as $(\omega+\nu)$. The right ascension is the sum of the longitude of the ascending node (Ω) and "b". Equation (51) is employed to calculate "b" which must be in the same quadrant as $(\omega+\nu)$.

$$\Phi' = \sin^{-1}[\sin i \sin(\omega+\nu)]$$
$$\tan b = \cos i \tan\Phi' \qquad (51)$$

Determine Orbit Stability. Finally, in order to compare the various orbits to determine which was the most stable, the change in velocity needed to transfer the satellite from the perturbed orbit back to the original orbit was considered. Equation (49) was used to determine the change in velocity.

Cases. Table 3 presents the cases consider to determine secular changes in orbital elements.

Table 3. Cases Considered to Determine Secular Changes in Orbital Elements and Velocity Change as a Function of ω and i

Case	Planet	Semi-Major Axis (km)	β (km^2/kg)
1	Earth	6700	.01e-6
2			.02e-6
3			.04e-6
4		7500	.01e-6
5			.02e-6
6			.04e-6
7	Mars	3600	.01e-6
8			.02e-6
9			.04e-6
10		4500	.01e-6
11			.02e-6
12			.04e-6

IV Results

Two-Body Solutions

First, the eccentricity which produces constant altitude arcs was found as a function of argument of periapsis and inclination while holding the semi-major axis and planet fixed. Figures B-1 and B-2 present the results for Earth with semi-major axes of 6700 km and 7500 km respectively. Figures B-3 and B-4 present the results for Mars with semi-major axes of 3600 km and 4000 km.

The eccentricities identified are all quite small and the orbits are almost circular. As may be seen in all the figures, $\delta e/\delta\omega$ is greatest at argument of periapses of 0^{o} and 180^{0} and a minimum at 45^{o}, and 135^{o}; and $\delta i/\delta\omega$ is smallest for inclinations of 0^{o} and 90^{o}. As would be expected from equation (44), the eccentricity increases as the inclination increases, and is zero when the inclination is zero. Comparing Figures B-1 and B-2, and Figures B-3 and B-4, indicates the eccentricity decreases as the semi-major axis increases.

Perturbed Solution

Figures B-5 though B-8 present the change in eccentricity due to J_2. Although all the perturbations listed in Table 1 were considered, it became apparent for a single period, the only significant effect on the eccentricity required to achieve an arc of constant altitude was due to the J_2 term of the geopotential. For Earth, the difference between the eccentricity found considering J_3, drag, and the Moon and the eccentricity found considering J_2 was on the order of $.001 \times 10^{-3}$. For Mars, the largest change in eccentricity due to J_3 was on the order of $.01 \times 10^{-3}$. Changes due to drag weren't considered for Martian cases. The Martian atmosphere is much less dense than the Earth's and

short term perturbations due to drag shouldn't significantly affect the choice of eccentricity.

The change in eccentricity presented in Figures B-5 through B-8 is subtracted from the eccentricity predicted using the two-body motion to give the required eccentricity. Figures B-5 and B-6 present the results for Earth with semi-major axes of 6700 km and 7500 km respectively. Figures B-7 and B-8 present the results for Mars with semi-major axes of 3600 km and 4000 km.

Once the optimum eccentricity was found which produced constant altitude arcs, the location, duration, and latitude range covered by the arcs were found. The mid-latitude presented is the average of the maximum and minimum latitudes covered by the constant altitude arcs, while the latitude range presented is the difference between the maximum and minimum latitudes covered. Both the duration of the arc and the latitude range of the arc are presented for a maximum change in altitude of 100 m and 1 km. The change in altitude is the difference between the maximum and minimum altitudes attained by the arc. Figures C-1 through C-12 present the results for Earth where Figures C-1 through C-6 are for the 6700 km semi-major axis orbits and Figures C-7 through C-12 are for the 7500 km orbits. Figures C-13 through C-24 are the results for the Martian cases where Figures C-13 through C-18 present the 3600 km results and Figures C-19 through C-24 are for the 4000 km semi-major axis case.

Mid-Latitude of Arcs. Figures C-1, C-7, C-13, and C-19 present the mid-latitude as a function of argument of periapsis and inclination. There are a large number of combinations which produce arcs with a given mid-latitude. The arcs are positioned over the northern hemisphere when the argument of periapsis is between 0^{o} and 180^{o} and are positioned over

the southern hemisphere when the argument of periapsis is between 180° and 360°. As inclination increases, the magnitude of the mid-latitude of the arc increases. Of course, the inclination must be at least as large as the sum of the mid-latitude and half the desired latitude range. The mid-latitude was calculated by taking the difference between the maximum and minimum latitudes achieved by the arc; consequently, the mid-latitude of polar orbits with the arc positioned over the poles (ω = 90° and 270°) is less than 90°.

Altitude of Arc. Figures C-2, C-8, C-14, and C-20 present the altitude of the arcs as a function of argument of periapsis and inclination. The altitude is dependent on the mid-latitude of the arc, the argument of periapsis, and the true anomaly range covered by the arc. At argument of periapses of 0° and 180°, the constant altitude arc occurs at apoapsis, while the arc occurs at periapsis when the argument of periapses are 90° and 270°.

Duration of Arc. Figures C-3, C-9, C-15, and C-21 present the duration of the arcs where the maximum change in altitude is less than 100 m. When i=e=0, the arc lasts the entire orbital period; however, the latitude range covered is zero. The duration of the arc is reasonably constant for inclinations larger than 20° and for a given argument of periapsis the duration decreases as the inclination increases. Longer duration arcs may be produced when the argument of periapsis is an integer multiple of 90° with the largest duration arcs occurring at $\omega = 0^{\circ}$ or 180°. When the argument of periapsis is 0° or 180°, the mid-latitude of the constant altitude arc is positioned at 0° latitude. For these orbits, the symmetry of the orbit and planet are aligned causing a longer constant altitude arc. Figures C-4, C-10, C-16, and C-22 present the duration of the arcs when the change in

altitude is less than 1 km. As the allowable altitude variation of the arc is increased, the duration increases.

Latitude Range of the Arc. Figures C-5, C-11, C-17, and C-23 present the latitude range of the arcs as a function of argument of periapsis and inclination when the altitude variation is less than 100 m. Figures C-6, C-12, C-18, and C-24 present the latitude range when the altitude variation is less than 1 km. In all cases, the largest latitude coverage occurs when the argument of periapsis is 0^{o} or 180^{o}. Again, this is due to the matched symmetry of the orbit and planet, and coincides with the longest duration arcs. Also, at a given argument of periapsis, the latitude coverage increases with increasing inclination. The latitude range presented for an inclination of 90^{o} at argument of periapses of 90^{o} and 270^{o} is low due to the method used to calculated the latitude range. An orbit with these parameters will have the constant altitude arc positioned over the poles and when the difference between the maximum and minimum latitudes achieved is calculated, the resulting latitude range will be less than the range reported if the arc was not positioned over a pole. A latitude range of about 50^{o} is possible while maintaining an altitude variation of less than 100 m and a latitude range of up to 90^{o} can be achieved if an altitude variation of less than 1 km is acceptable.

Non-dimensionalized Results

The results from the previous cases were combined. Figure 9 presents a plot of eccentricity as a function of ω and $R_e f \sin^2 i/a$ for the two-body cases, while Figure 10 presents the change in eccentricity from the two-body cases as a function of ω, and $J_2(R_e \sin i/a)^2$.

The results presented in Figures 9 and 10 were curve fit producing a single empirical equation. Equation (52) may be used with the

coefficients presented in Tables 4 and 5 to determine the eccentricity required to produce an arc of constant altitude given the semi-major axis, argument of periapsis, inclination, ellipticity, and the J_2 zonal harmonic of the geopotential.

$$e = e_{2B} - \Delta e \qquad i \neq 0 \tag{52}$$
$$e = 0 \qquad i = 0$$

where

$$e_{2B} = \sum_{k=0}^{8} \sum_{\ell=0}^{2} C\, A_{k,\ell}\, T_k(\bar{\Omega})\, T_\ell(\bar{I}_{2B}) \tag{53}$$

$$\Delta e = \sum_{k=0}^{8} \sum_{\ell=0}^{5} C\, B_{k,\ell}\, T_k(\bar{\Omega})\, T_\ell(\bar{I}_{J2}) \tag{54}$$

$$C = \begin{cases} 1. & k \neq 0 \text{ and } \ell \neq 0 \\ 0.5 & k=0 \text{ or } \ell=0 \\ 0.25 & k=0 \text{ and } \ell=0 \end{cases}$$

The argument of periapses is the same for both e_{2B} and Δe.

$$\bar{\Omega} = \bar{\omega}/45.0 - 1.0$$

$$\bar{\omega} = \begin{cases} \omega & 0. \leq \omega \leq 90. \\ 180. - \omega & 90. < \omega \leq 180. \\ \omega + 180. & 180. < \omega \leq 360. \end{cases}$$

The inclination is combined with planet properties and differs for e_{2B} and Δe. For e_{2B}, $\bar{I}_{2B}$ is a function of semi-major axis, inclination, ellipticity, and equatorial radius

$$\bar{I}_{2B} = 2i_{2B}/i_{2B(max)} - 1.0$$

$$i_{2B} = (f\ R_e/a)\ \sin^2 i$$

$$0 \leq i_{2B} \leq .48874383 \times 10^{-2} = i_{2B(max)}$$

For Δe, $\bar{I}_{J2}$ is a function of semi-major axis, inclination, ellipticity, and J_2

$$\bar{I}_{J2} = 2i_{J2}/i_{J2(max)} - 1.0$$

$$i_{J2} = J_2\ (R_e/a)^2\ \sin^2 i$$

$$0 \leq i_{J2} \leq .17418950 \times 10^{-2} = i_{J2(max)}$$

Table 4. Coefficients for e

$A_{k,\ell}$			
ℓ	0	1	2
k			
0	1.3382318E-2	6.6831547E-3	-8.8992362E-6
1	5.9572268E-5	3.9537390E-5	9.6394148E-6
2	2.2556540E-3	1.1263017E-3	-2.0021737E-6
3	4.6696319E-5	3.0815889E-5	7.3419897E-6
4	5.9702036E-4	3.0177004E-4	3.1364165E-6
5	2.6463970E-5	1.7652256E-5	4.3897306E-6
6	1.8920545E-3	9.6492837E-5	2.2358554E-6
7	8.4988295E-6	5.9054707E-6	1.6974386E-6
8	4.2832099E-5	2.2063680E-5	1.2341417E-6

Table 5. Coefficients for Δe

$B_{k,\ell}$			
ℓ	0	1	2
k			
0	2.4192677E-3	1.2121056E-3	1.0566496E-5
1	2.2288511E-5	1.4267904E-5	2.9502728E-6
2	4.6494823E-4	2.2535319E-4	5.4081346E-6
3	1.7652175E-5	1.1116183E-5	2.2108308E-6
4	1.7222103E-4	8.6194009E-5	6.6663719E-6
5	9.8102319E-6	6.3723936E-6	1.3617805E-6
6	6.7878651E-5	3.4179548E-5	3.6139002E-6
7	2.9070219E-6	2.1377139E-6	5.7416986E-7
8	1.8819281E-5	8.8447405E-6	9.3013404E-7
ℓ	3	4	5
k			
0	1.3977998E-5	4.5367581E-8	-2.4362035E-6
1	2.0193706E-8	1.5042158E-7	-1.5487548E-7
2	1.2653309E-5	-3.2310241E-7	9.7169557E-7
3	1.9007614E-7	8.1730486E-8	-4.1539688E-7
4	7.1543029E-6	1.7824329E-6	2.3768136E-6
5	-7.8643838E-8	8.5013670E-8	7.9025722E-8
6	3.1601894E-6	1.0169085E-6	2.2980839E-6
7	-2.5954531E-7	7.5947404E-8	4.2068010E-7
8	1.0599178E-6	-2.6786479E-7	1.4068201E-6

Figures 11 and 12 are plots of equations (53) and (54). Comparing Figures 11 and 12 with Figures 9 and 10 indicates the curve fit is sufficiently accurate. Tabulated comparisons of the data points and eccentricities calculated using equation (52) are presented in Appendix F. A discussion of the required accuracy in predicting eccentricity is presented in Section III.

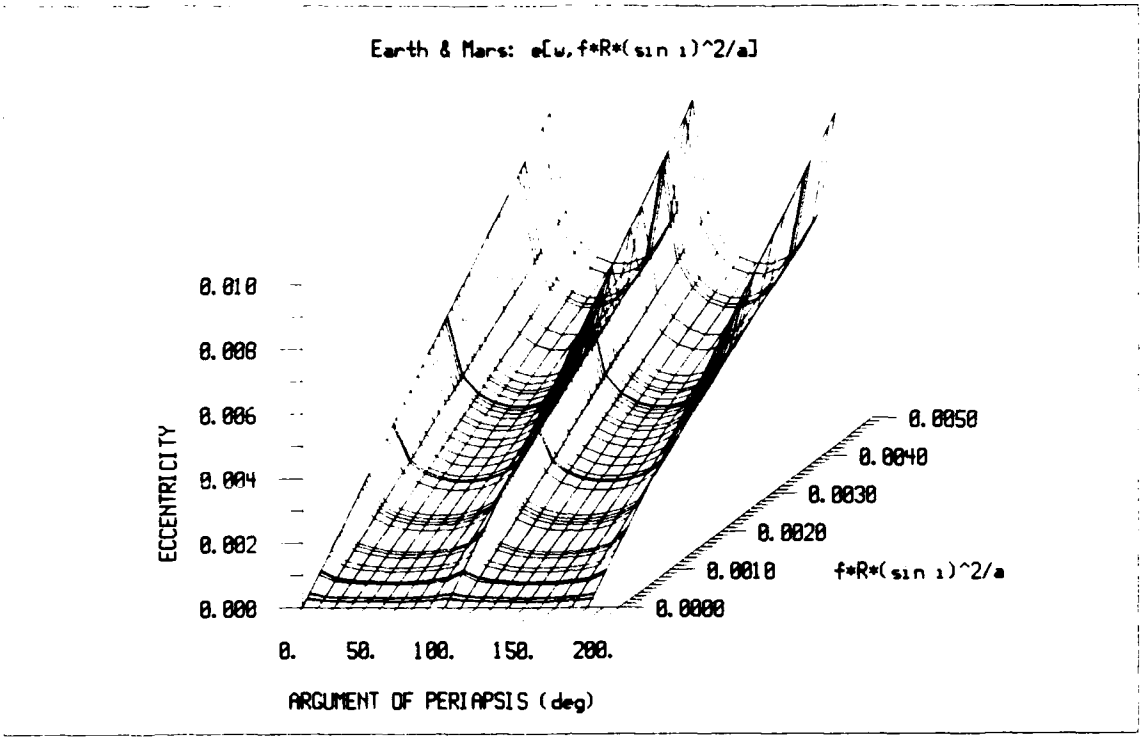

Figure 9. Non-dimensional Presentation of Two-Body Solutions

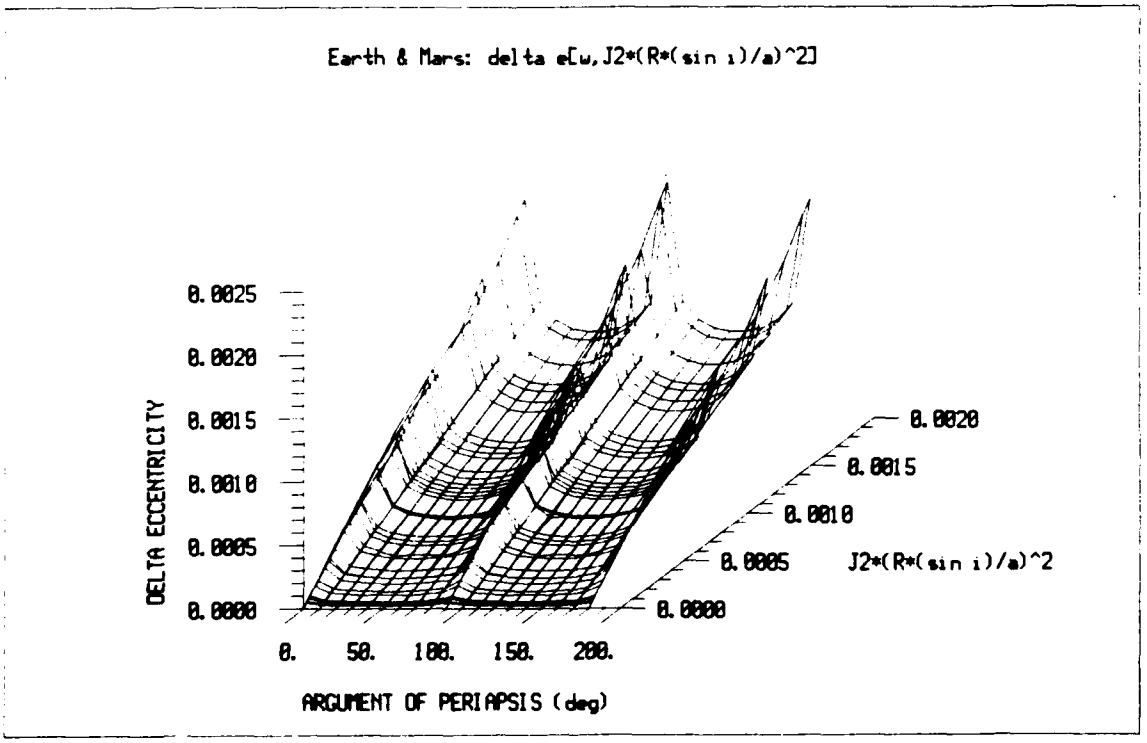

Figure 10. Non-dimensional Presentation of Change Due to J_2

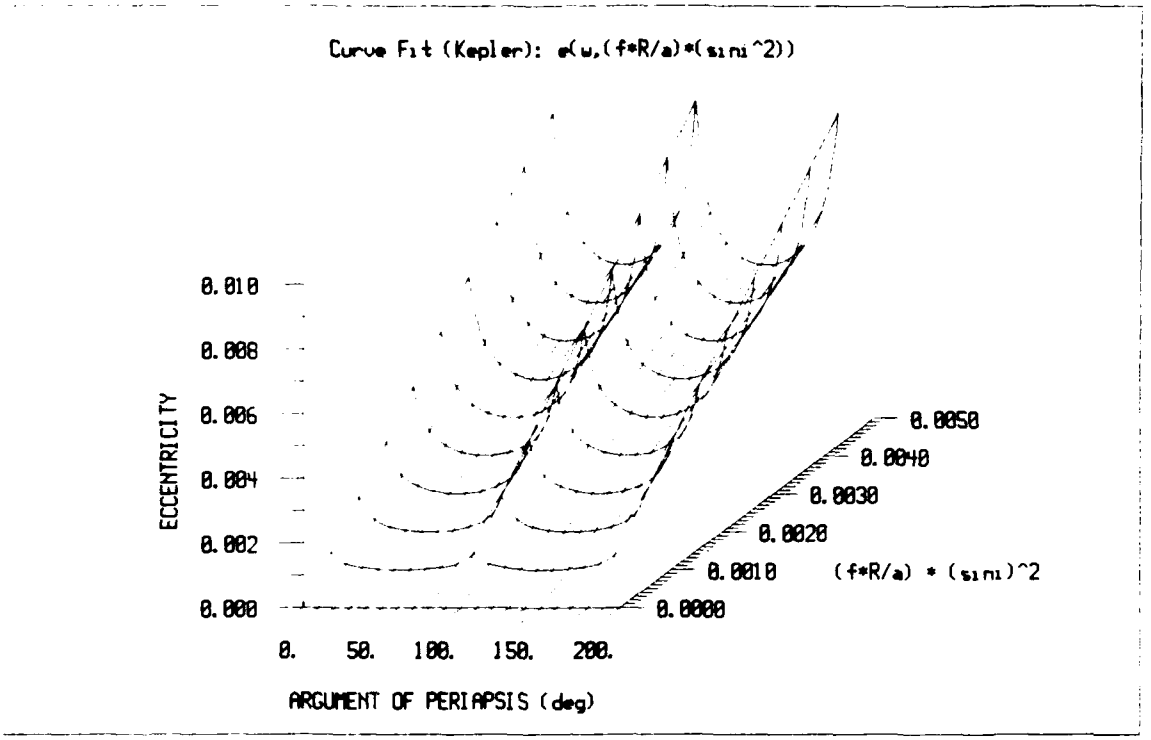

Figure 11. Curve Fit of Two-Body Solutions

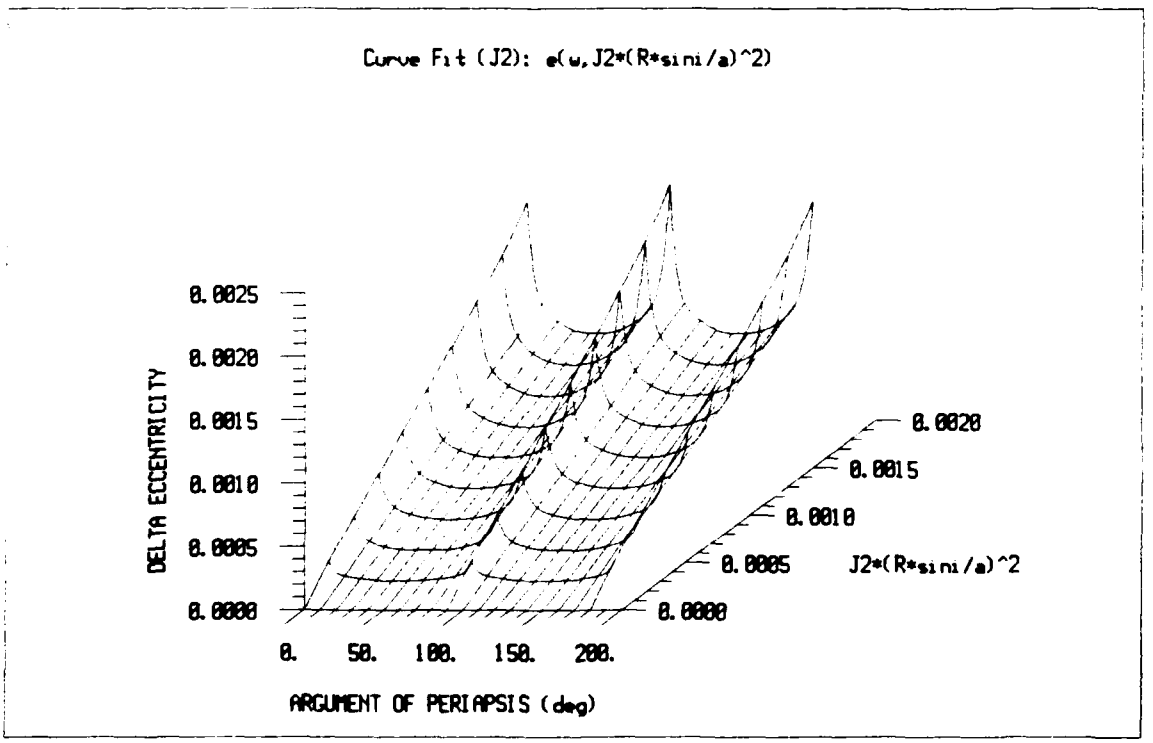

Figure 12. Curve Fit of Change Due to J_2

Secular Considerations

The secular changes in orbital elements were calculated using the mean orbital elements which produce orbits with arcs of constant altitude. Perturbations due to the geopotential, drag, and third bodies were considered. The secular changes in a, e, i, ω, and Ω are presented as a function of the initial argument of periapsis and inclination. In all cases, the initial longitude of ascending node was set to 0°.

Secular Change in Semi-Major Axis over One Period. Figures D-1 through D-6 present the results for the secular change in semi-major axis. Figures D-1 and D-2 present the results for Earth with a semi-major axis of 6700 km and ballistic coefficients of $.01 \times 10^{-6}$ km^2/kg and $.04 \times 10^{-6}$ km^2/kg respectively while Figures D-3 and D-4 present the same results for Mars with a semi-major axis of 3600 km. In order to consider cases in which drag doesn't play an important role, Figures D-5 and D-6 present the results for Earth (a = 7500 km) and Mars (a = 4500 km) with a ballistic coefficient of $.04 \times 10^{-6}$ km^2/kg. Comparing Figures D-1 and D-2 and Figures D 3 and D-4 indicate increasing the ballistic coefficient increases the change in semi-major axis for low orbits. Equation (30) is directly proportional to the ballistic coefficient and the square of the semi-major axis, and supports this observation. For both Earth and Mars, the minimum change in semi-major axis due to atmospheric drag occurs at an argument of periapsis of 45° or 225° and an inclination of 63°. In Figures D-5 and D-6, the geopotential caused the most significant change in semi-major axis. Equation (10) indicates the change in semi-major axis due to the geopotential will be zero when ω is 0° or 180° or i is 63.44°. These areas where semi-major axis doesn't change are clearly presented by Figures D-5 and D-6. The small negative offset of Figure D-5 is due to atmospheric drag.

Secular Change in Inclination over One Period. Figures D-7 through D-12 present the results for the change in inclination. Again, Figures D-7 and D-8 are for Earth (a=6700km) and Figures D-9 and D-10 are for Mars (a=3600km), where the first figure for each planet presents the data for β=.01x10^{-6} km^2/kg and the second figure presents data for β=.04x10^{-6}km^2/kg. Figures D-11 and D-12 present results for Earth (a=7500km) and Mars (a=4500km) with β=.04x10^{-6} km^2/kg. For Earth the largest change in inclination was caused by the Moon in Figures D-7 and D-11 and drag in Figure D-8. For Mars the largest change in inclination was caused by the geopotential and Sun in Figure D-9, drag in Figure D-10, and geopotential at low inclinations and the Sun at high inclinations in Figure D-12. Comparing Figures D-7 and D-8 and Figures D-9 and D-10, indicates at low altitude, high inclination and argument of periapsis, drag significantly affects the change in inclination by reducing the inclination. The secular change in inclination due to drag is calculated using equation (32) which is zero when the inclination is zero. If all other parameters remain constant equation (32) will have the largest magnitude when the inclination is 90^{o}.

Secular Change in Argument of Periapsis over One Period. Figures D-13 through D-18 present the results for the secular change in argument of periapsis. Figures D-13 and D-14 are for Earth (a=6700km) and Figures D-15 and D-16 are for Mars (a=3600km) -- for each planet, β = .01x10^{-6} km^2/kg is presented first while β = .04x10^{-6} km^2/kg is presented second. Figures D-17 and D-18 present results for Earth (a=7500km) and Mars (a=4500km) with β = .04x10^{-6} km^2/kg. In all cases considered, the largest secular change in the argument of periapsis was caused by the geopotential. By comparing the figures, it may be

concluded that the change in argument of periapsis is not significantly affected by drag. The large magnitudes at low inclinations were from the ω_3, ω_5, and ω_{22} components of equation (11). The change in argument of periapsis is zero at an inclination of 63.4° when the argument of periapsis is zero. Mars and Earth have the opposite sign on the change in argument of periapsis at high inclinations -- this is due to the difference in signs of the J_5 terms of their respective geopotentials.

Secular Change in Eccentricity over One Period. Figures D-19 through D-24 present the results for the change in eccentricity. The cases presented are in the same order as previously mentioned. In the cases with the smallest semi-major axes and largest ballistic coefficient for both Earth and Mars (Figures D-20 and D-22), the change in eccentricity was due primarily to drag. For all the other cases considered, the change in eccentricity was primarily due to the geopotential. Drag increases the reduction is eccentricity -- Figure D-20 has been shifted down relative to Figure D-19, and similarly Figure D-22 has been shifted down relative to Figure D-21.

Secular Change in Longitude of the Ascending Node over One Period. Figures D-25 through D-30 present the changes in longitude of the ascending node. The change in longitude of the ascending node was primarily due to the geopotential in all the cases considered. All the figures indicate, the minimum change occurs at an inclination of 90° and the largest magnitude change occurs at an inclination of 0°. The Ω_2 term of equation (11) is a multiple of cos*i*, and consequently indicates the secular change in longitude of the ascending node will be largest when the inclination is 0° and zero when the inclination is 90°.

Velocity Impulse Required to Counteract Secular Changes. Figures E-1 through E-6 present the velocity impulses needed to move the satellite from the perturbed orbit to the original orbit. For all the cases considered, the change in velocity was driven by the required plane change to correct inclination. As a result, station keeping fuel can be minimized by choosing an orbit which minimizes the change in inclination.

V Conclusions

In this thesis an equation was developed to empirically determine the mean orbital elements which produce arcs of minimum altitude variation about an oblate planet. These orbits are useful for surveillance or scientific missions using optics with fixed focal lengths. The resulting orbits were considered and the characteristics of minimum variation arcs were identified. The secular changes to the mean orbital elements due to geopotential, drag, and third body perturbations were found and the velocity impulse needed to maintain the desired orbit was also calculated.

Conclusions

1. Orbits which contain arcs of minimum altitude variation were identified.

2. An empirical relationship was developed to identify combinations of the mean orbital elements which produce arcs of constant altitude. The equation determines eccentricity as a function of semi-major axis, inclination, argument of periapsis, the J_2 zonal harmonic, and the planet's ellipticity and equatorial radius.

$$\begin{aligned} e &= e_{2B} - \Delta e \qquad i \neq 0 \\ e &= 0 \qquad\qquad\quad i = 0 \end{aligned} \tag{52}$$

where

$$e_{2B} = \sum_{k=0}^{8} \sum_{\ell=0}^{2} C\, A_{k,\ell}\, T_k(\bar{\Omega})\, T_\ell(\bar{I}_{2B}) \tag{53}$$

$$\Delta e = \sum_{k=0}^{8} \sum_{\ell=0}^{5} C\ B_{k,\ell}\ T_k(\bar{\Omega})\ T_\ell(\bar{I}_{J2}) \qquad (54)$$

The coefficients for the equation are presented in Tables 4 and 5, and the independent variables are defined in Section IV. This curve fit is valid for inclinations from 0° to 90° for Earth orbits with semi-major axes greater than one Earth radius and Martian orbits with semi-major axes greater than 3600 km. For smaller Martian semi-major axes, the inclination range becomes limited. For Martian orbits with semi-major axes of one planet radius, the equation is valid for an inclination range of 0° to 70°. The valid inclination range increases as the semi-major axis increases until the full range of 0° to 90° is achieved for semi-major axes greater than or equal to 3600 km.

3. All the orbits with arcs of minimum altitude variation were nearly circular. The orbits became more eccentric for smaller semi-major axes and larger inclinations.

4. The velocity impulse required to counteract secular changes to the mean orbital elements due to a non-spherical gravitational field, drag, and third bodies was calculated. In all cases, the magnitude of the required impulse was driven by the plane change to correct the inclination. Consequently, in order to minimize station keeping fuel, an orbit with the minimum change in inclination should be chosen.

Recommendations

1. Further work should be done to identify orbits with arcs of minimum altitude variation over specific latitude and longitude ranges.

2. Third body perturbations of orbits with large semi-major axes should be considered for different third body positions.

Appendix A

Flow Chart of Method Used to Identify Orbital Elements which Produce Minimum Altitude Variation Arcs

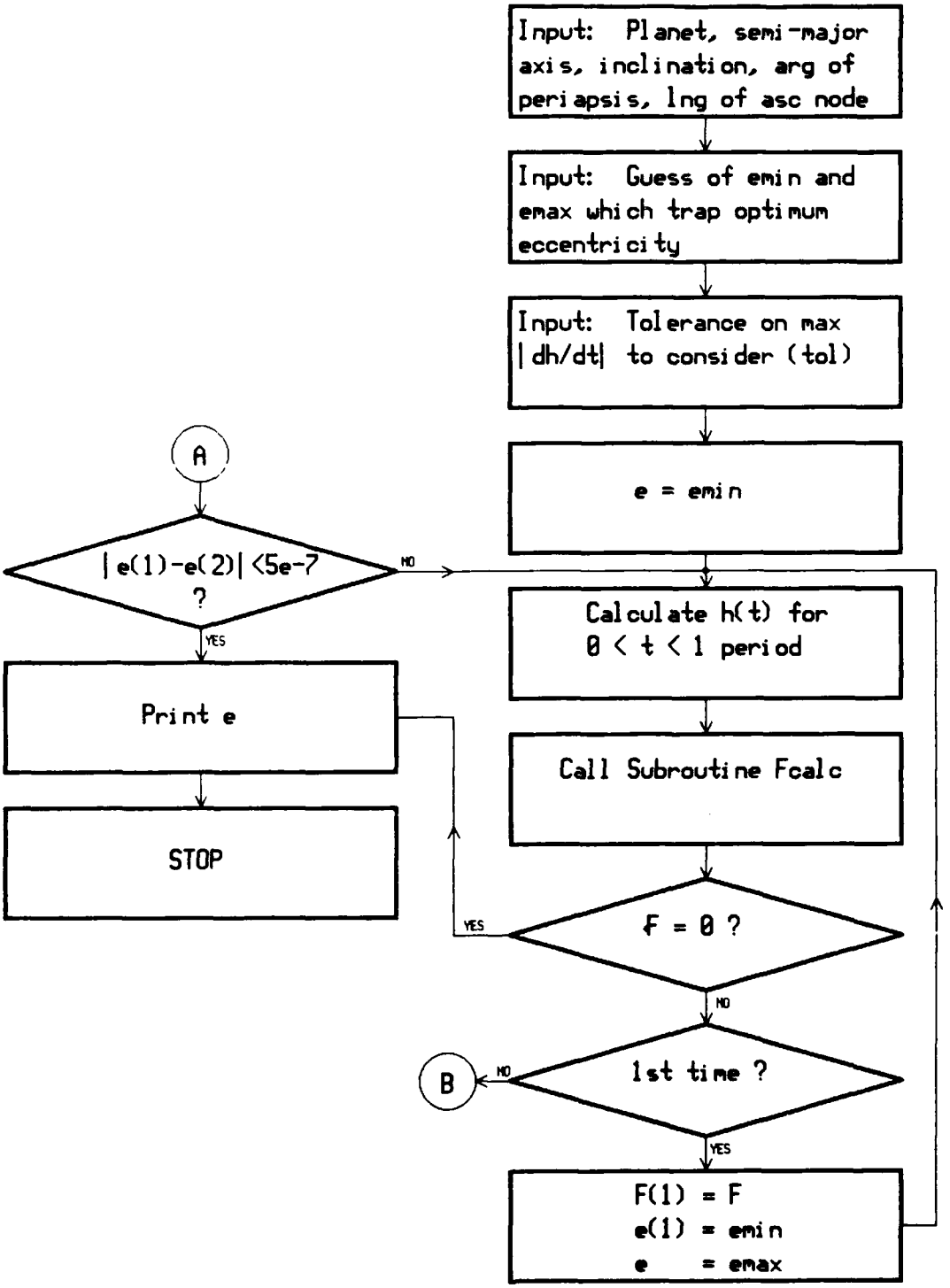

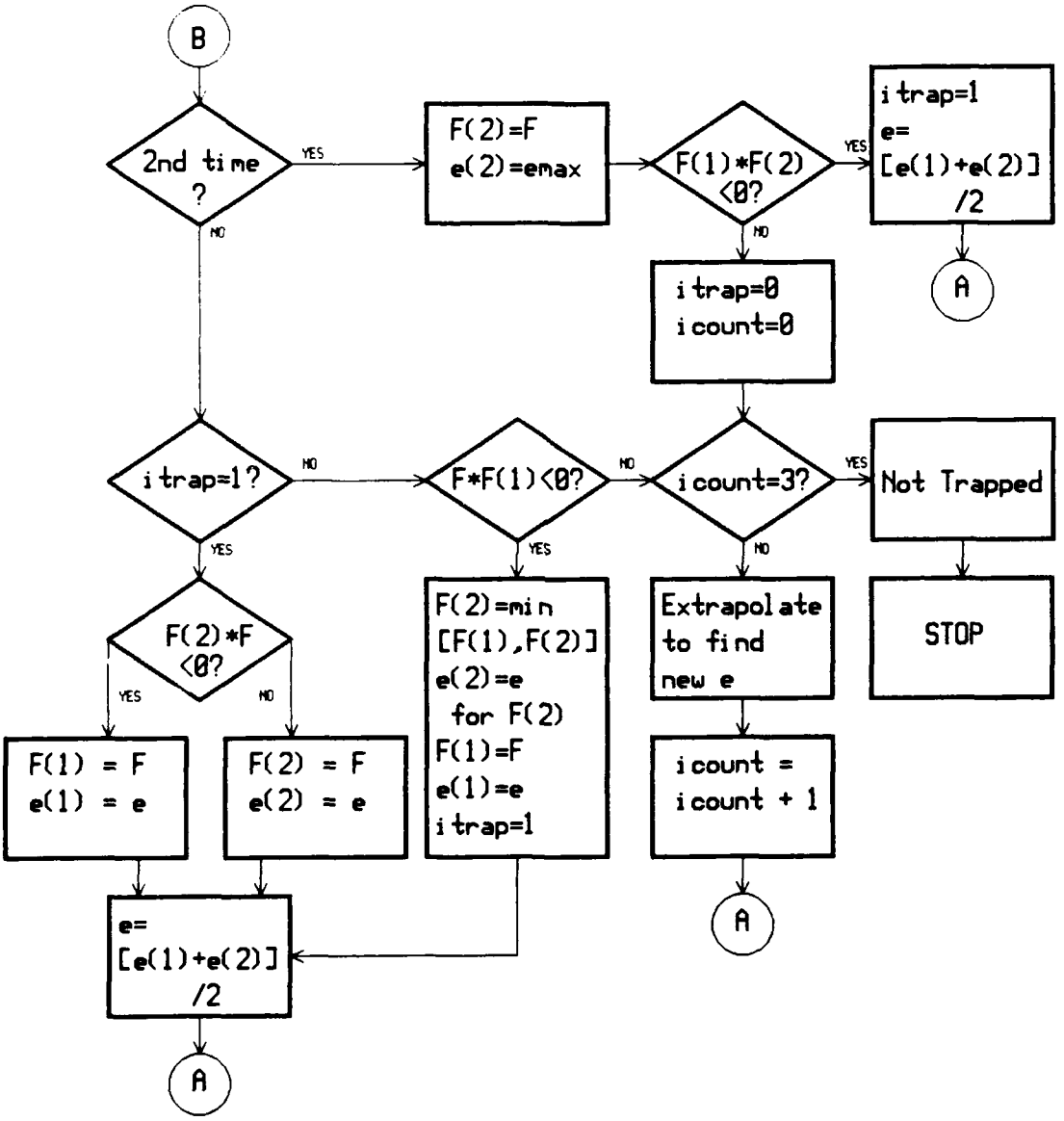
B
2nd time ?
YES
NO
F(2)=F
e(2)=emax
F(1)*F(2) <0?
YES
NO
itrap=1
e=
[e(1)+e(2)]
/2
A
itrap=0
icount=0
itrap=1?
NO
YES
F*F(1)<0?
NO
YES
icount=3?
YES
NO
Not Trapped
STOP
F(2)*F <0?
YES
NO
F(2)=min [F(1),F(2)]
e(2)=e for F(2)
F(1)=F
e(1)=e
itrap=1
Extrapolate to find new e
icount = icount + 1
A
F(1) = F
e(1) = e
F(2) = F
e(2) = e
e=
[e(1)+e(2)]
/2
A

SUBROUTINE FCALC

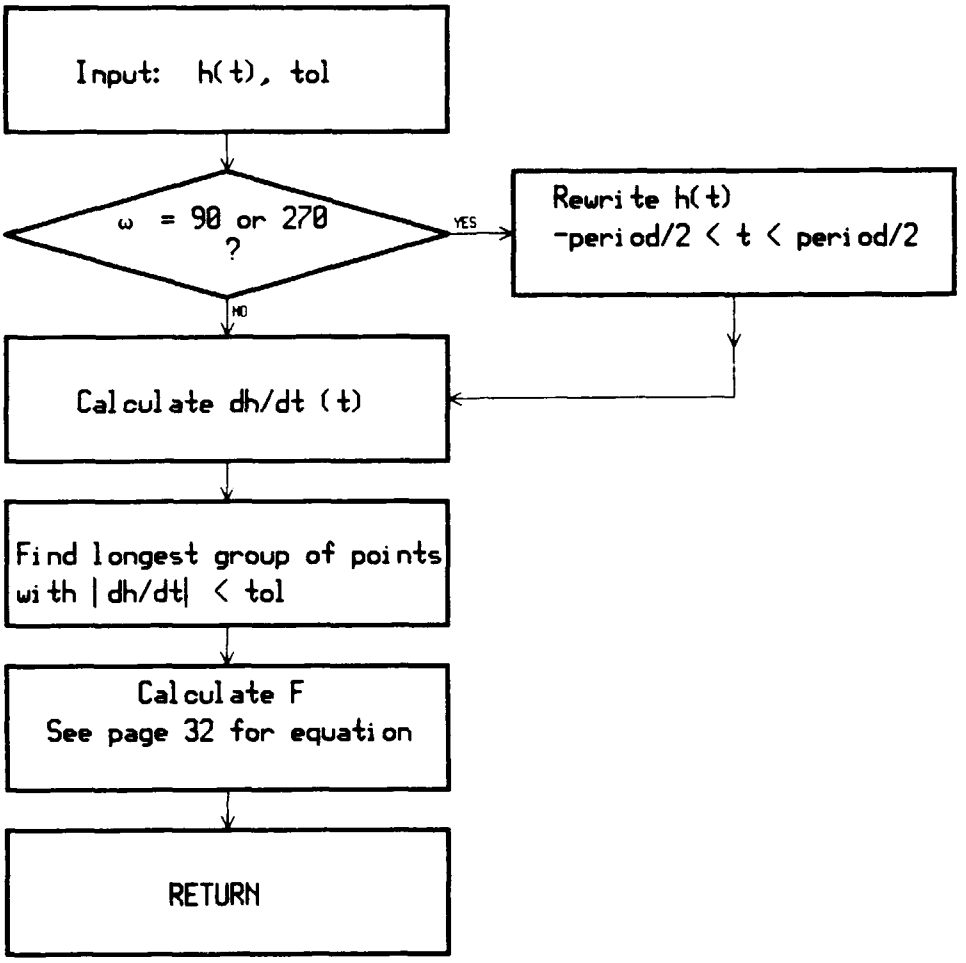

Appendix B

Eccentricity Required to Produce an Arc of Minimum Altitude Variation

Figures B-1 through B-8 present the optimum eccentricity to produce arcs of minimum altitude variation.

Figures B-1 and B-5 present results for Earth orbits with a semi-major axis of 6700 km; Figures B-2 and B-6 present results for Earth orbits with 7500 km semi-major axes; Figures B-3 and B-7 present Martian orbits with 3600 km semi-major axes; and Figures B-4 and B-8 are Martian results with semi-major axes of 4000 km.

Figures B-1 through B-4 present solutions to the two-body problem, while Figures B-5 through B-8 present the change in optimum eccentricity caused by perturbations due to J_2. The optimum eccentricity for a given argument of periapsis and inclination is found by subtracting the change due to J_2 from the two-body solution.

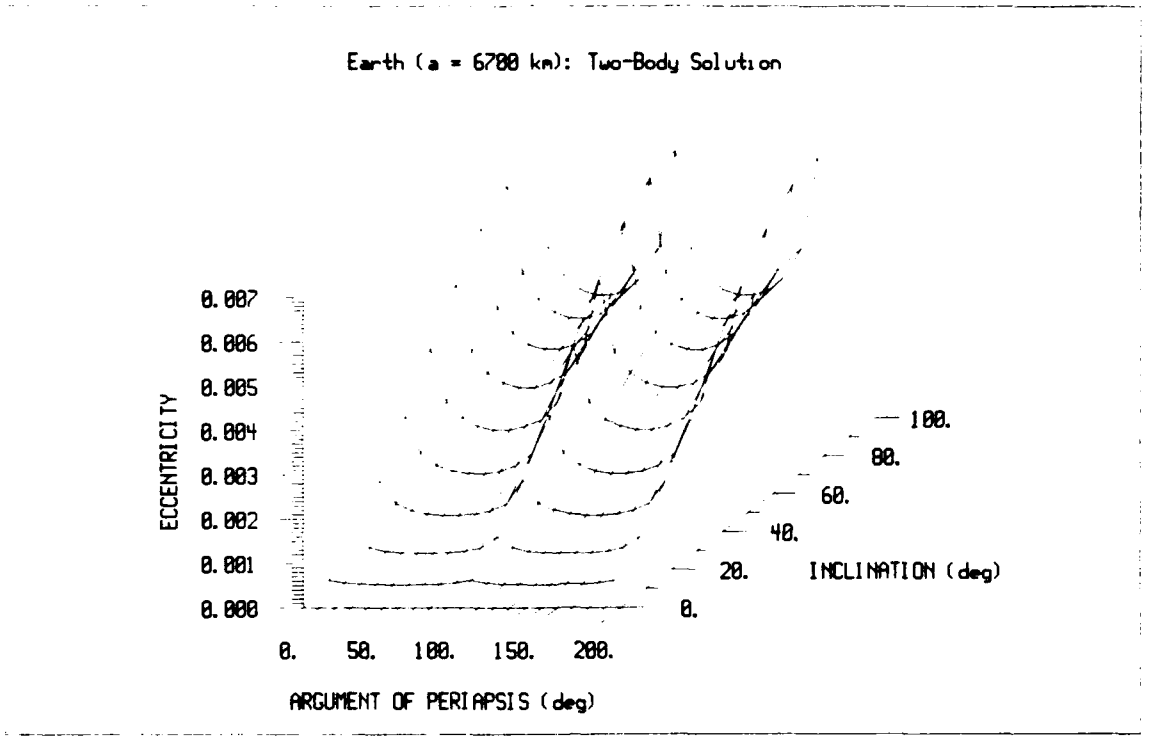

Figure B-1. Earth (a=6700 km): Eccentricity to Produce a Constant Arc

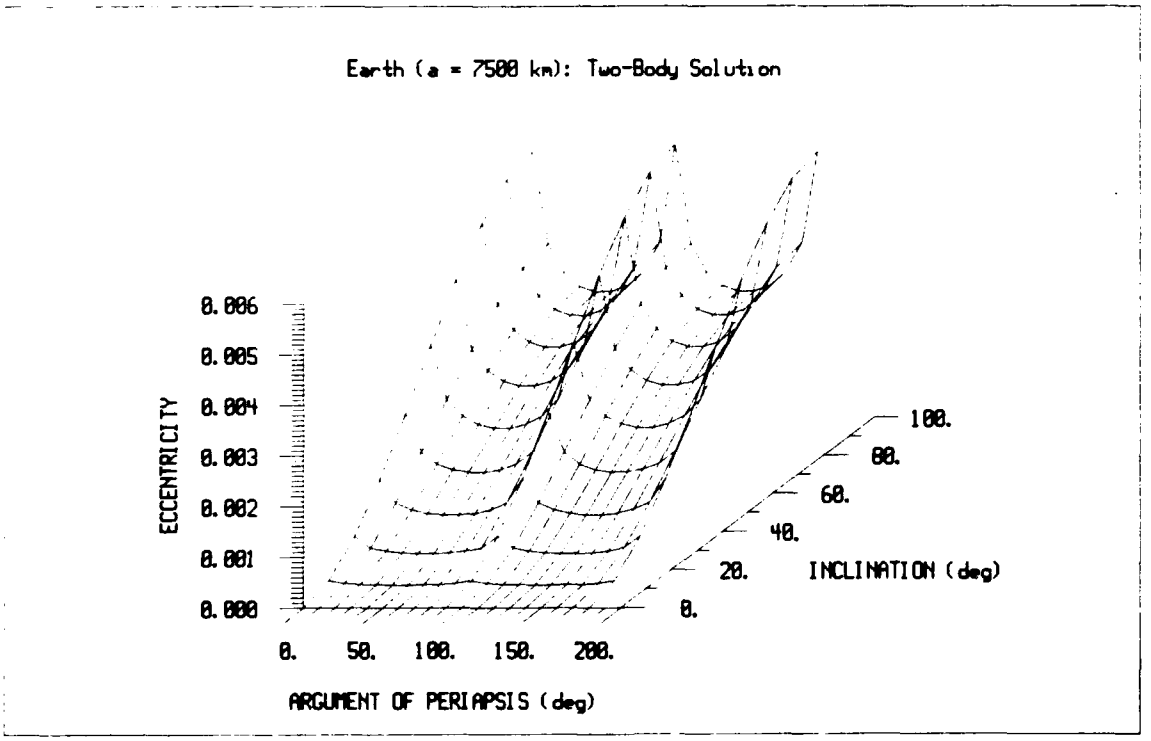

Figure B-2. Earth (a=7500 km): Eccentricity to Produce a Constant Arc

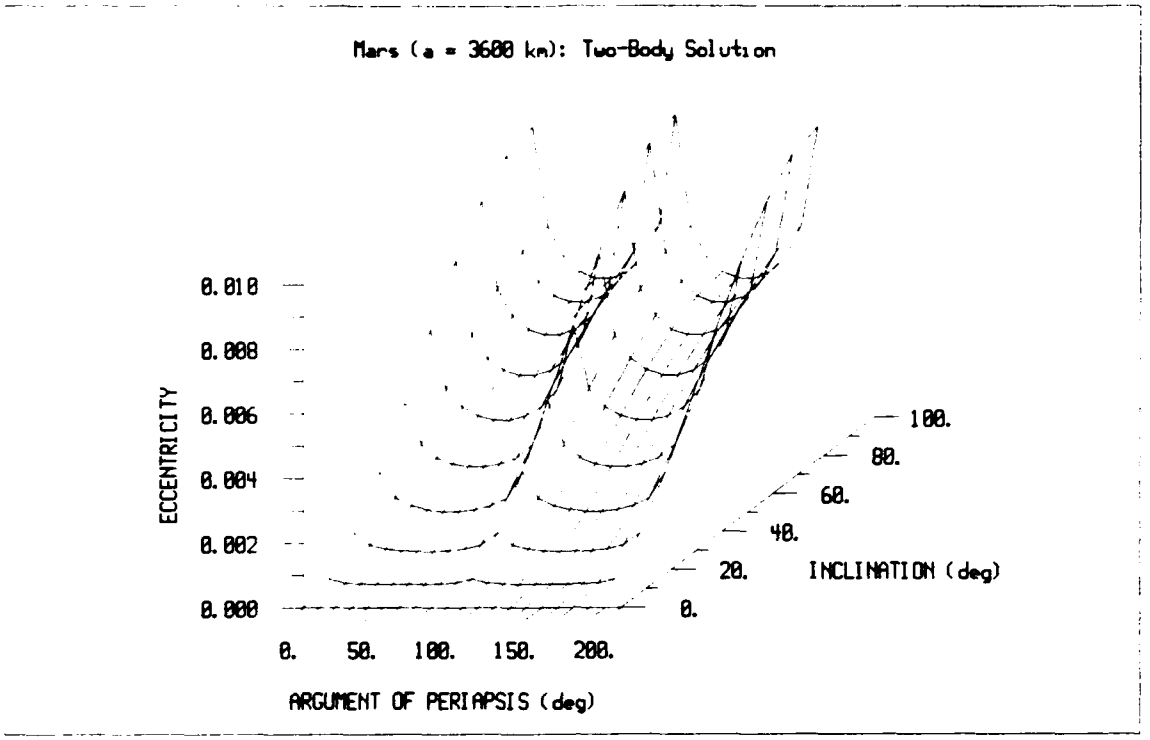

Figure B-3. Mars (a=3600 km): Eccentricity to Produce a Constant Arc

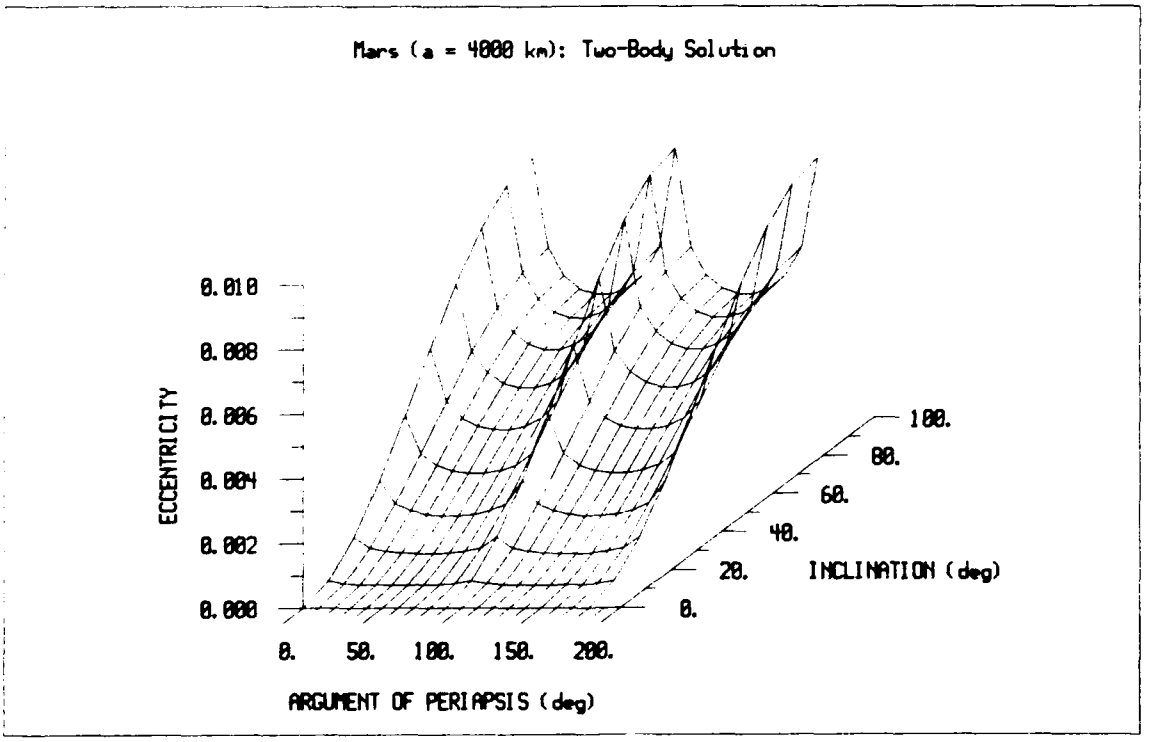

Figure B-4. Mars (a=4000 km): Eccentricity to Produce a Constant Arc

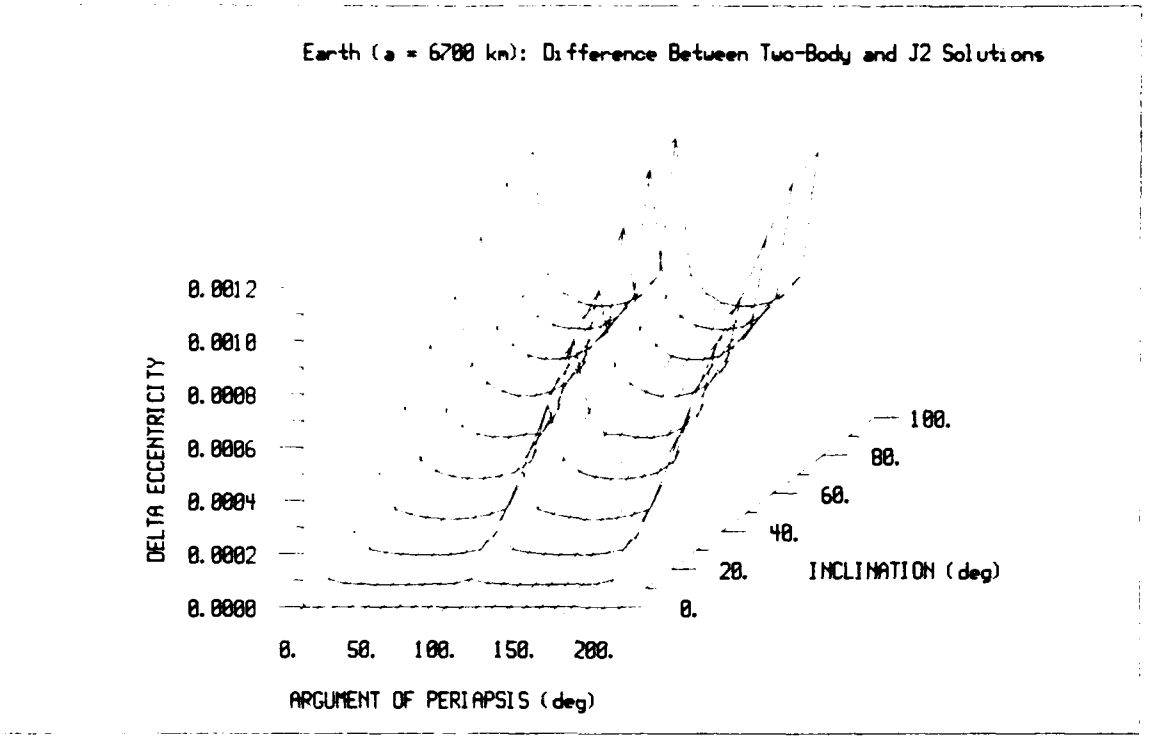

Figure B-5. Earth (a=6700 km): Change in Eccentricity due to J_2

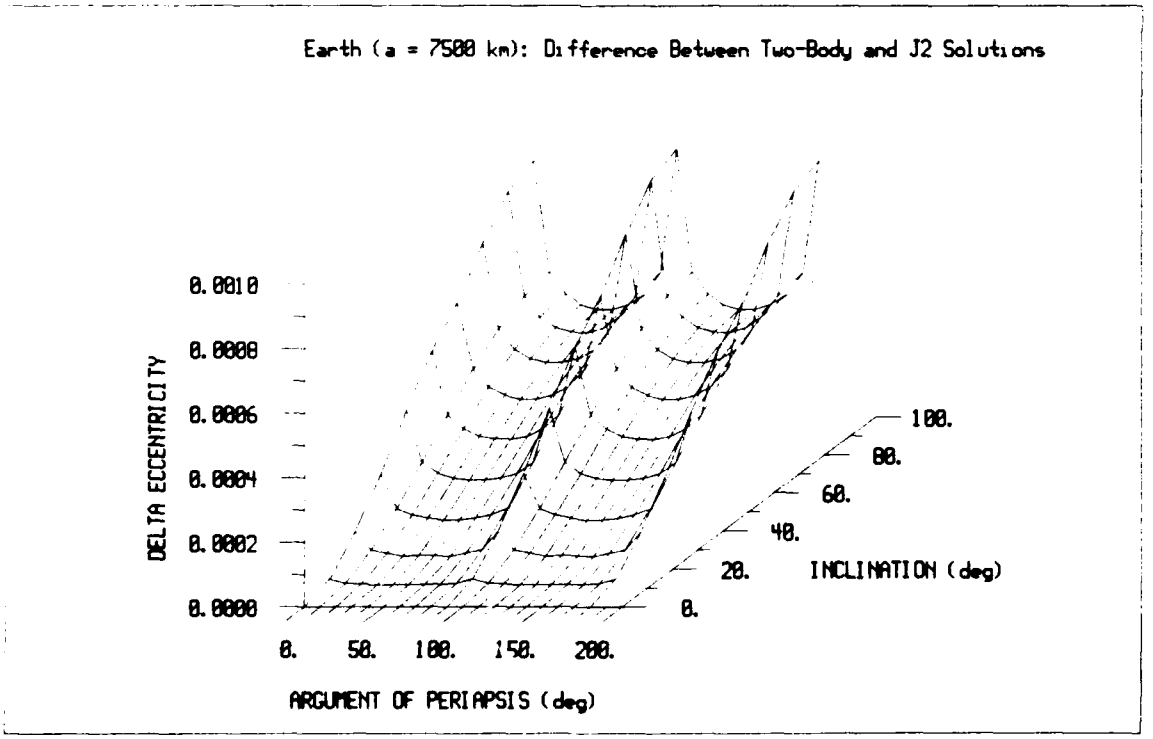

Figure B-6. Earth (a=7500 km): Change in Eccentricity due to J_2

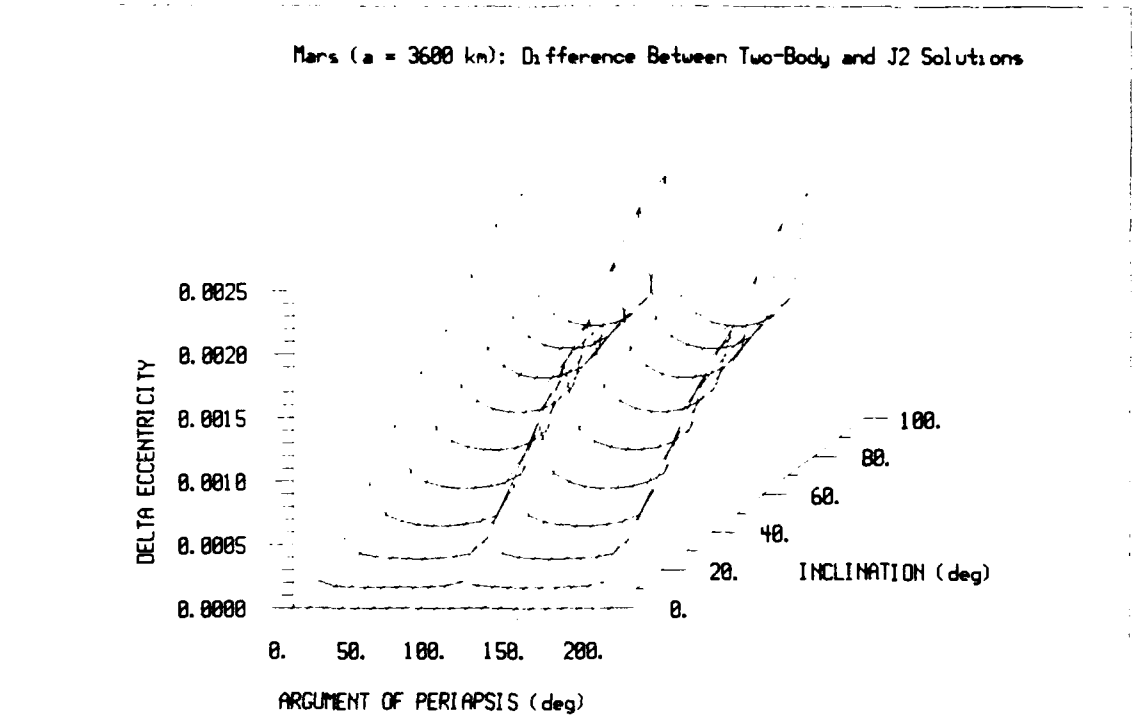

Figure B-7. Mars (a=3600 km): Change in Eccentricity due to J_2

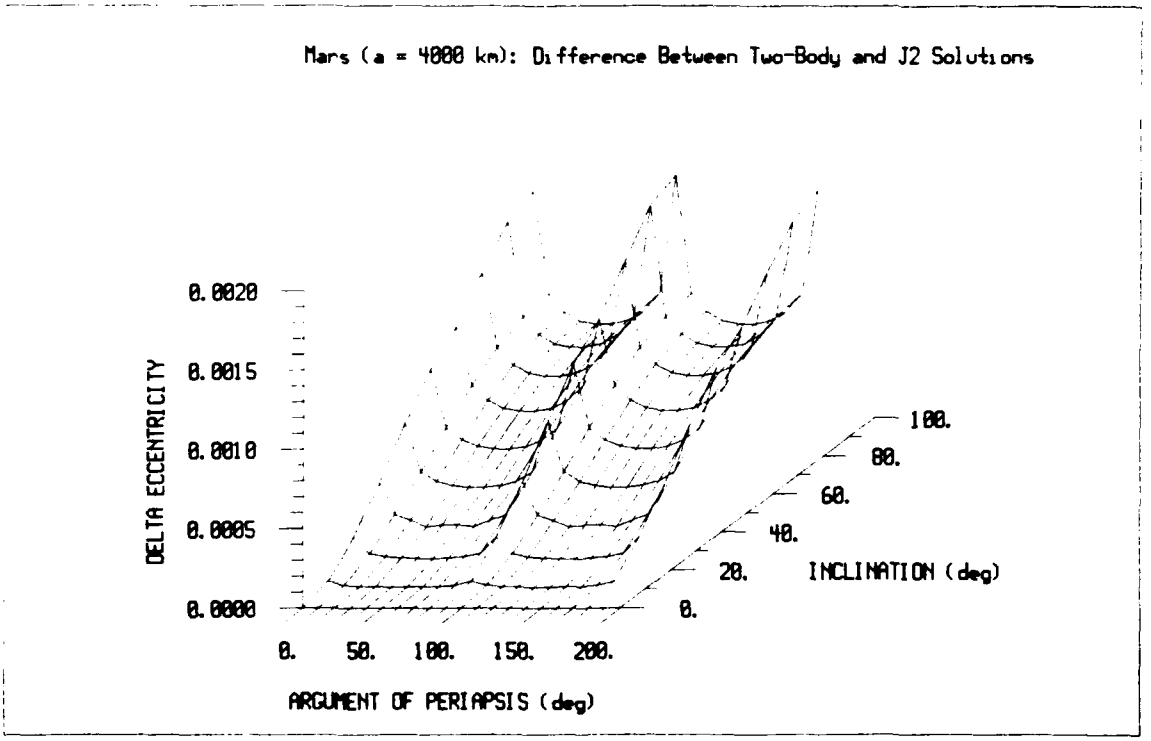

Figure B-8. Mars (a=4000 km): Change in Eccentricity due to J_2

Appendix C

Characteristics of Arcs of Minimum Altitude Variation

Figures C-1 through C-24 present the characteristics of the arcs of minimum altitude variation.

Figures C-1 through C-6 present the results for Earth with a semi-major axis of 6700 km. Figures C-7 through C-12 present results for Earth with a semi-major axis of 7500 km. Figures C-13 through C-18 present results for Mars with a semi-major axis of 3600 km while Figures C-19 through C-24 are for Martian orbits with 4000 km semi-major axes.

For each of the cases considered, the first figure presents the mid-latitude of the constant altitude arc, and the second figure presents the altitude of the arc. The third and fourth figures present the duration of the arc for a change in altitude less than 100 m and 1 km respectively. Finally, the last two figures present the latitude range of the arc for a change in altitude of less than 100 m and 1 km.

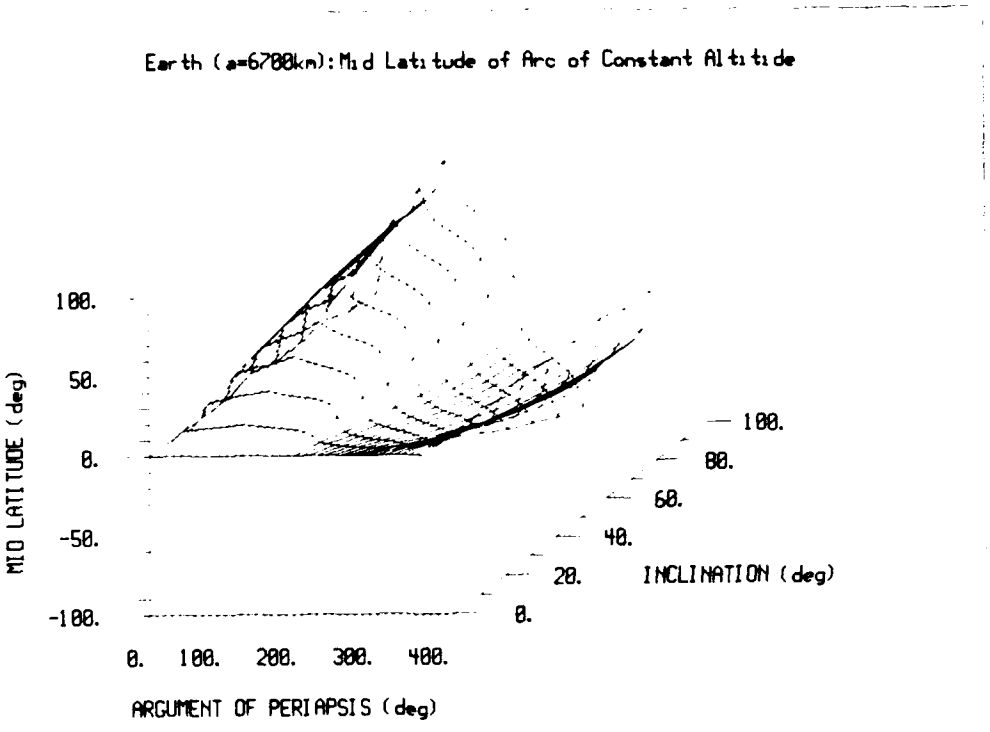

Figure C-1. Earth (a=6700 km): Mid-Latitude of Arc

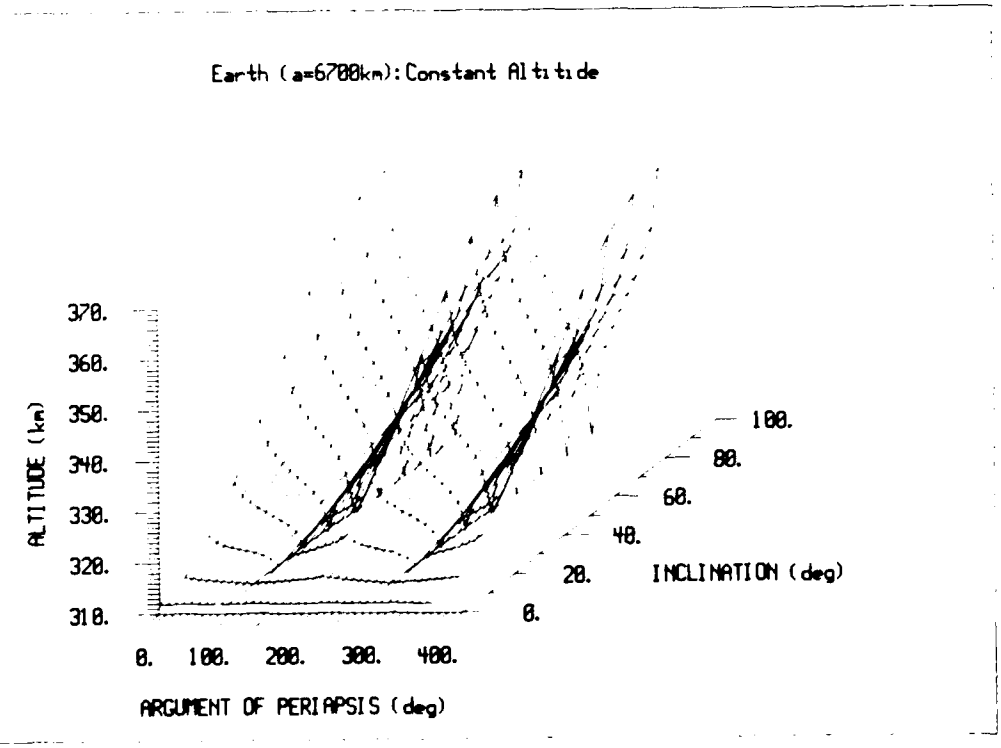

Figure C-2. Earth (a=6700 km): Altitude of Arc

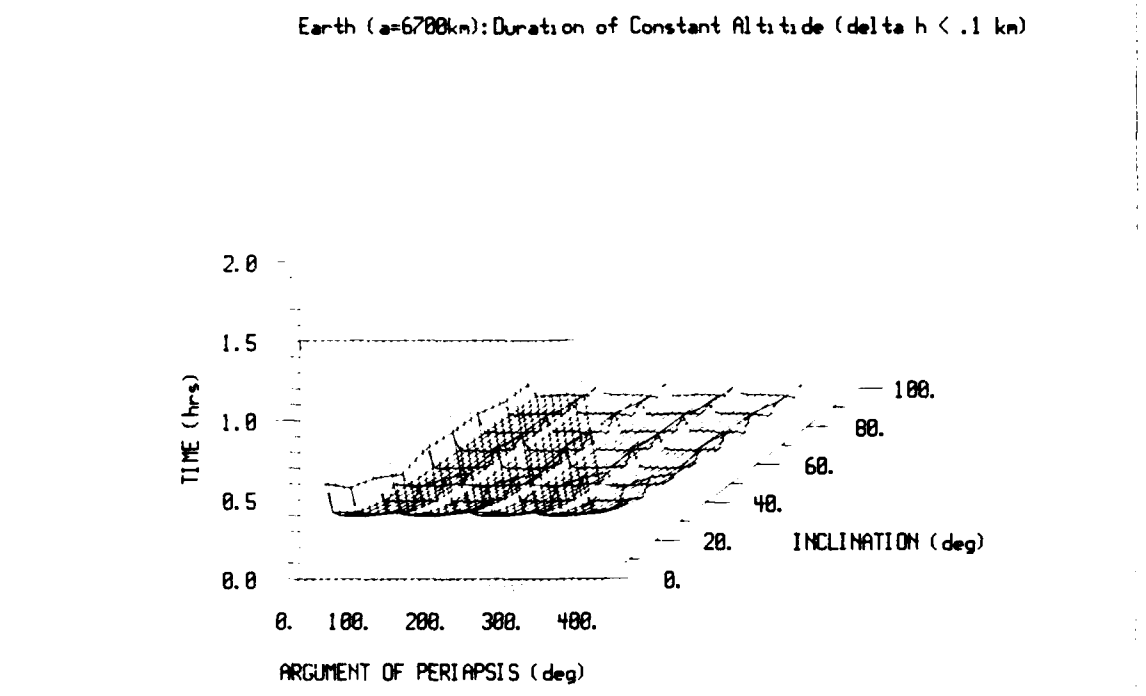

Figure C-3. Earth (a=6700 km): Duration of Arc $\Delta h < .1$ km

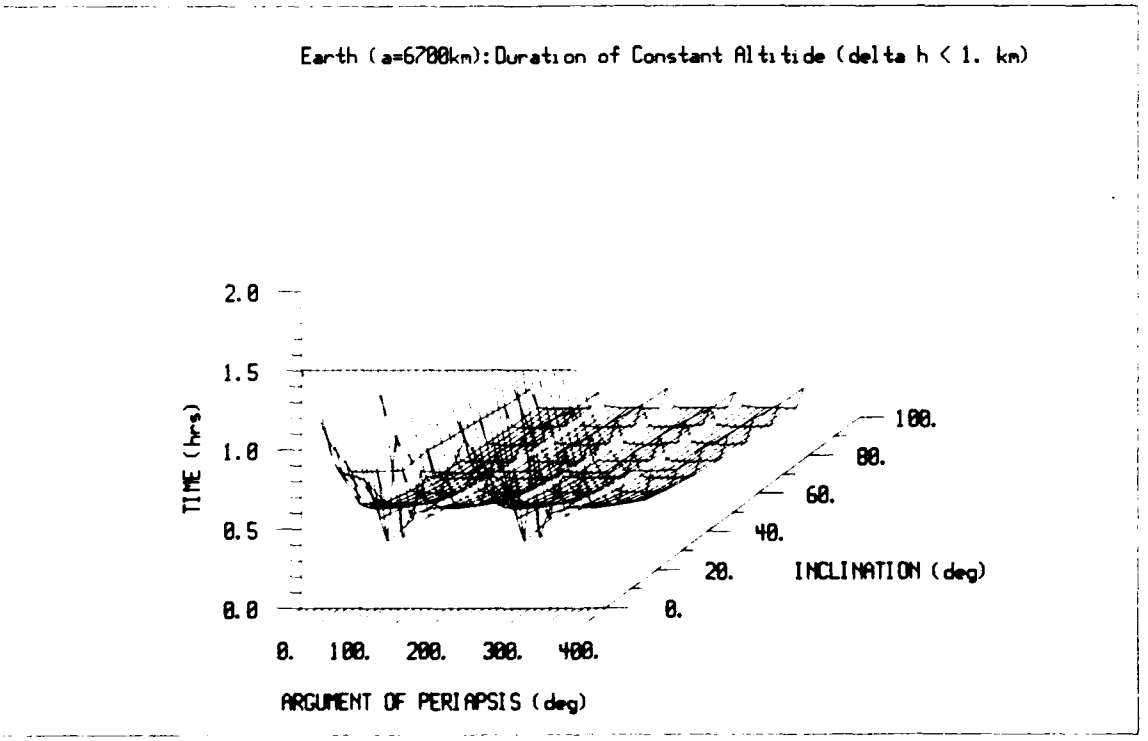

Figure C-4. Earth (a=6700 km): Duration of Arc $\Delta h < 1$km

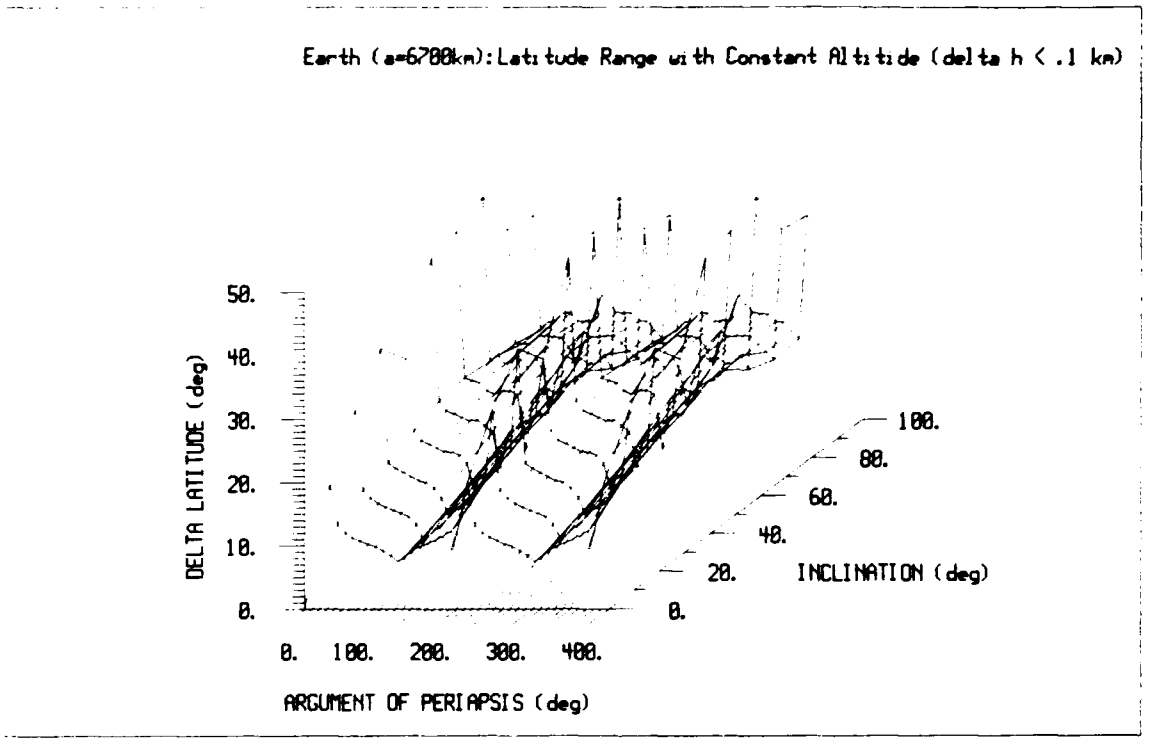

Figure C-5. Earth (a=6700 km): Latitude Range of Arc $\Delta h < .1$ km

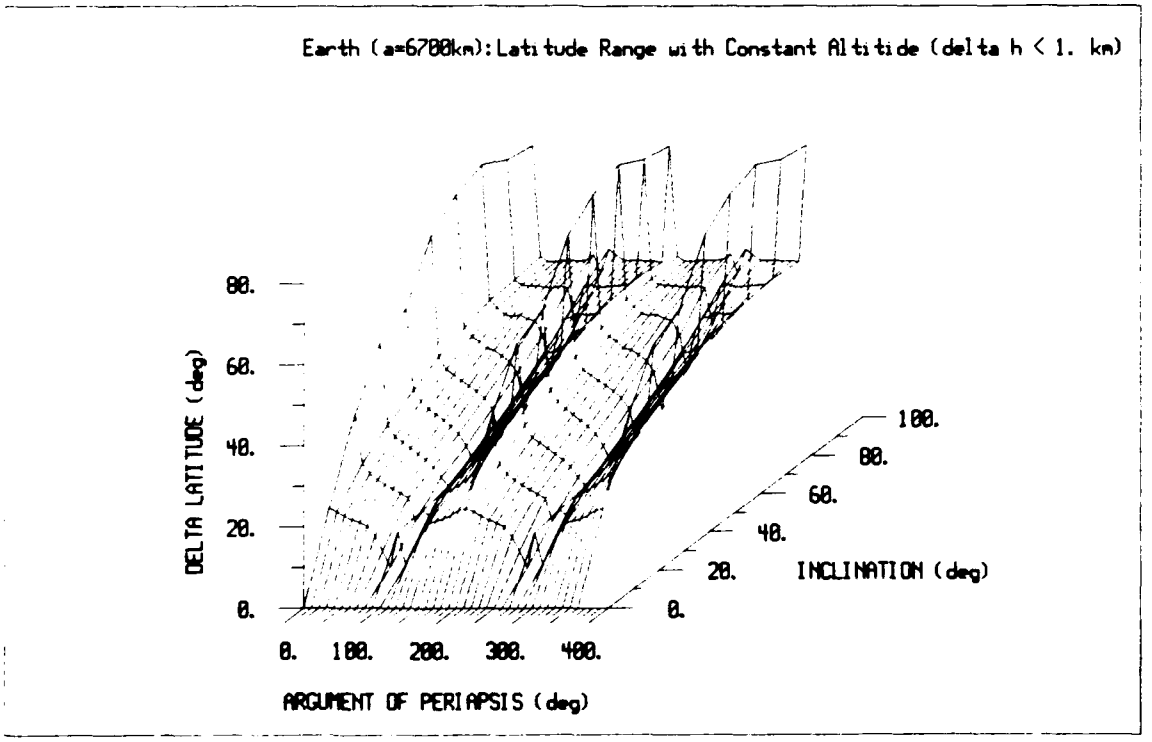

Figure C-6. Earth (a=6700 km): Latitude Range of Arc $\Delta h < 1$km

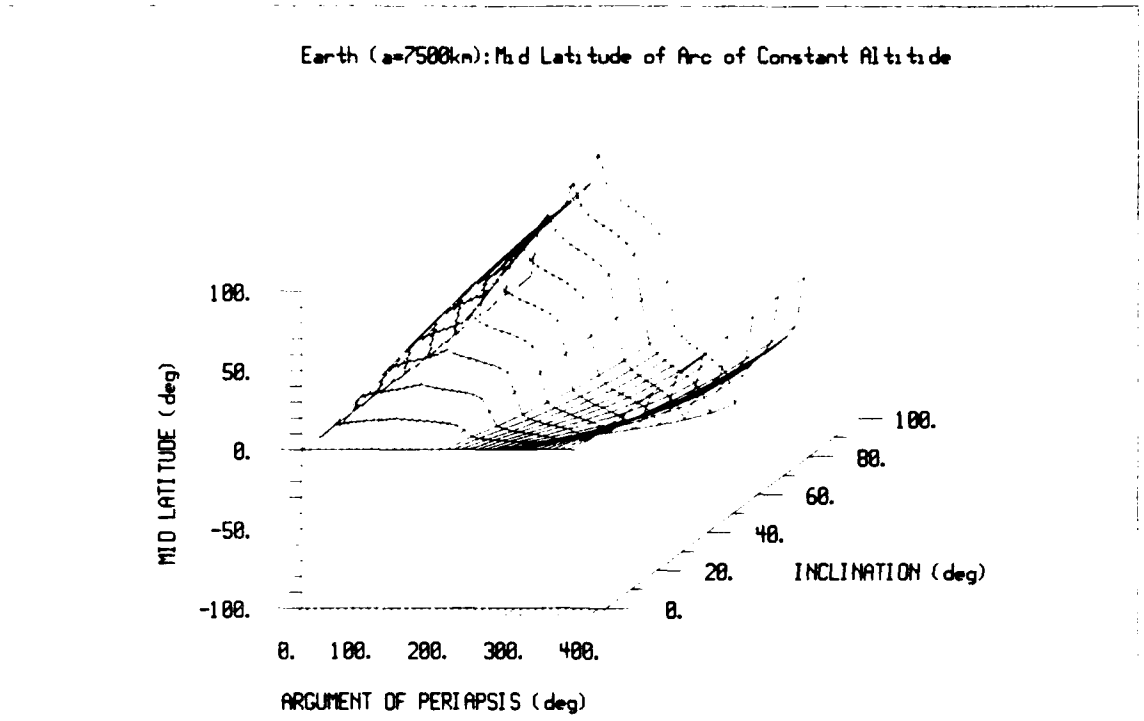

Figure C-7. Earth (a=7500 km): Mid-Latitude of Arc

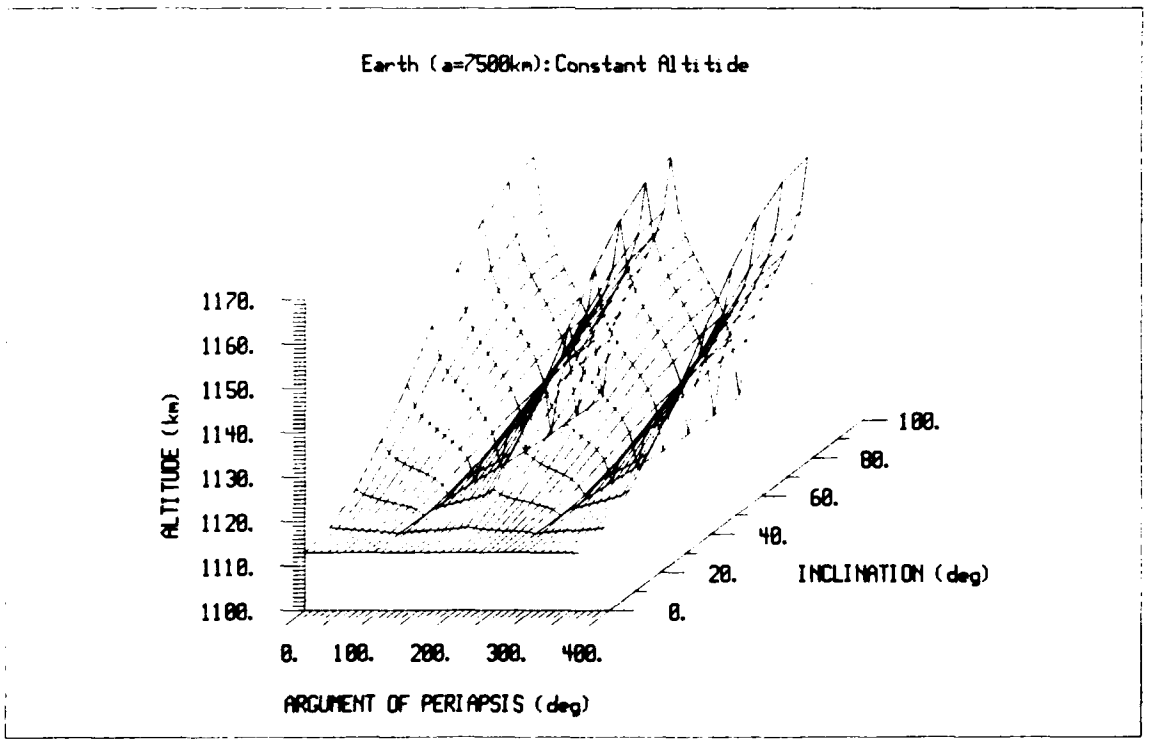

Figure C-8. Earth (a=7500 km): Altitude of Arc

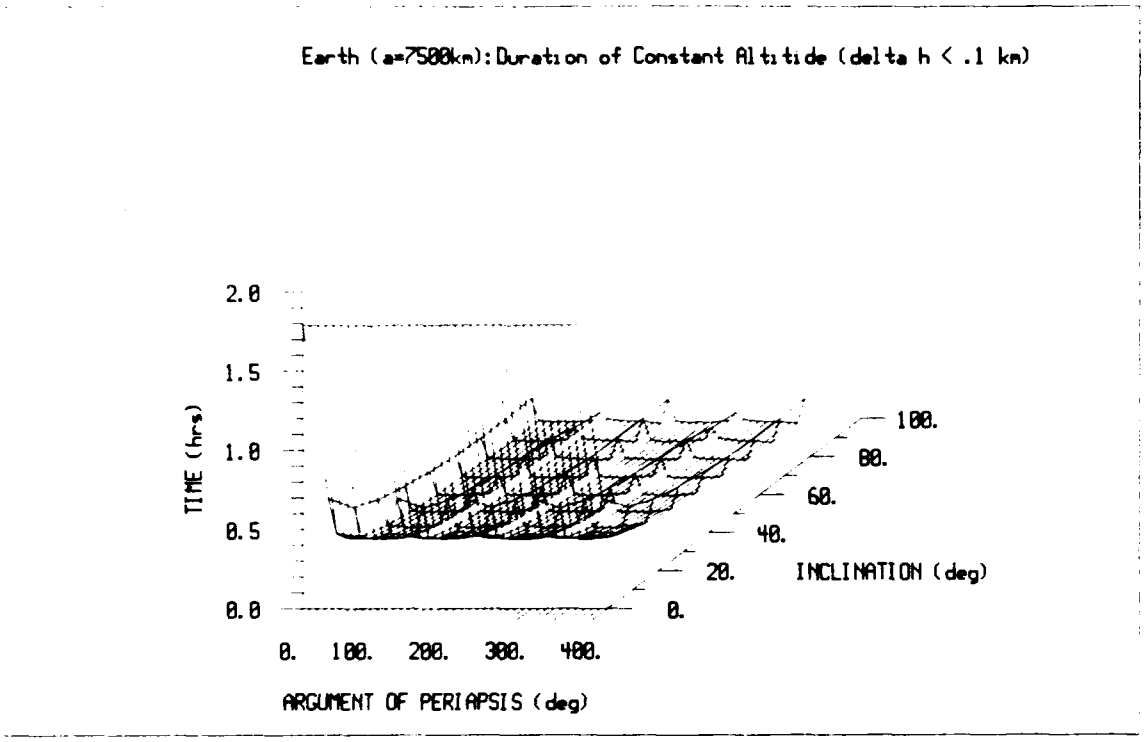

Figure C-9. Earth (a=7500 km): Duration of Arc $\Delta h < .1$ km

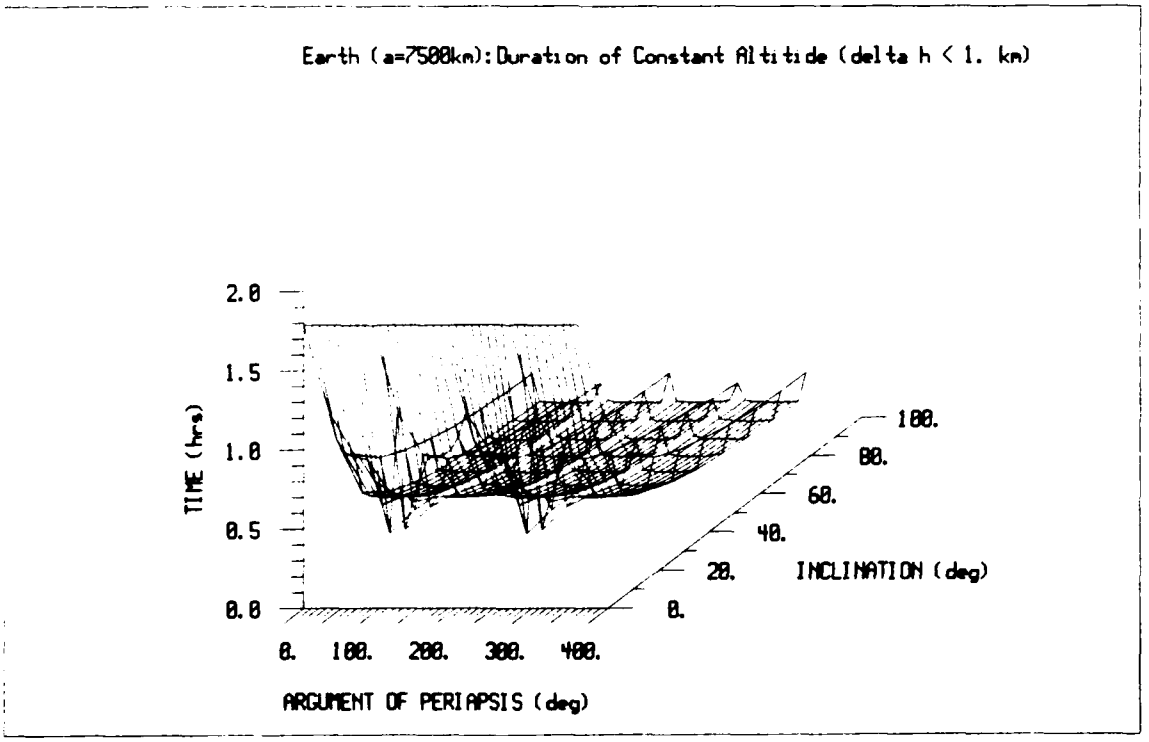

Figure C-10. Earth (a=7500 km): Duration of Arc $\Delta h < 1$km

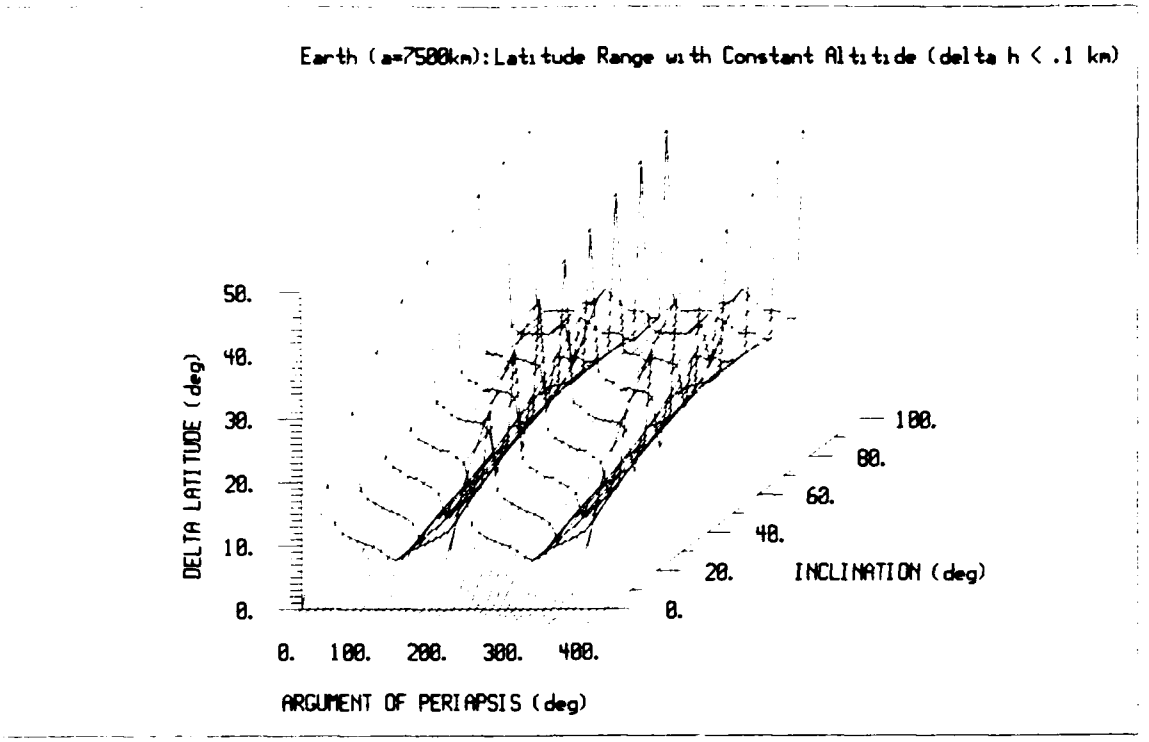

Figure C-11. Earth (a=7500 km): Latitude Range of Arc $\Delta h < .1$ km

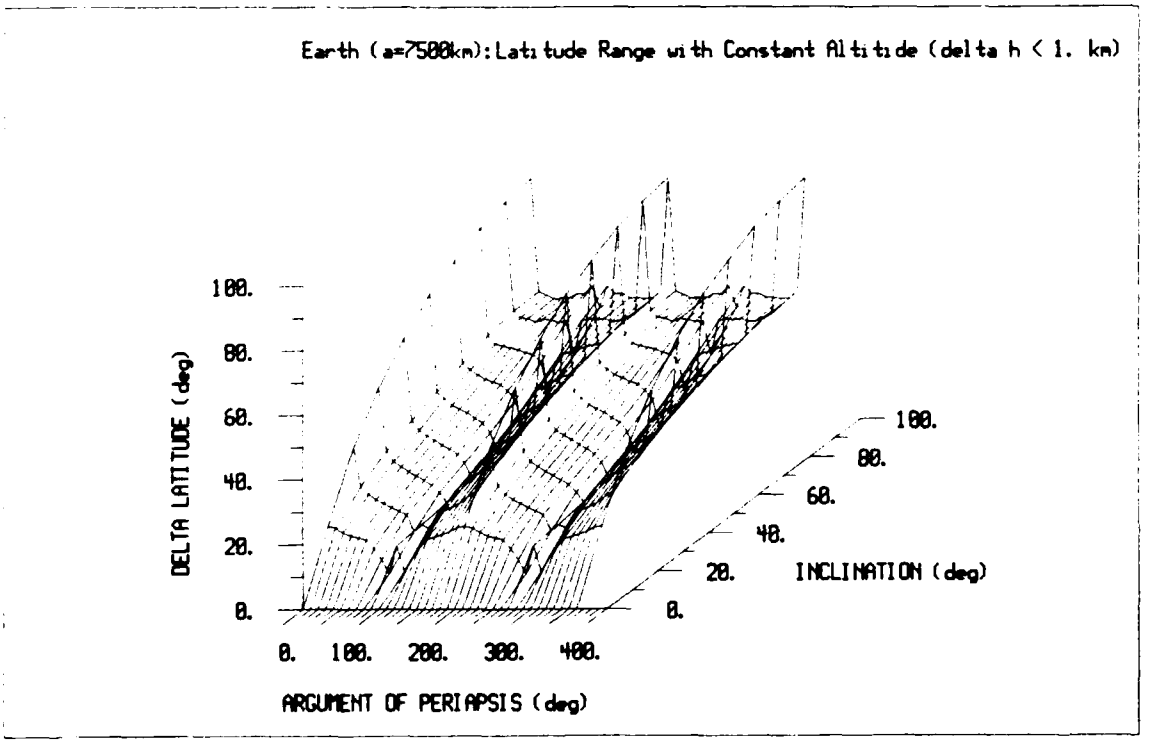

Figure C-12. Earth (a=7500 km): Latitude Range of Arc $\Delta h < 1$km

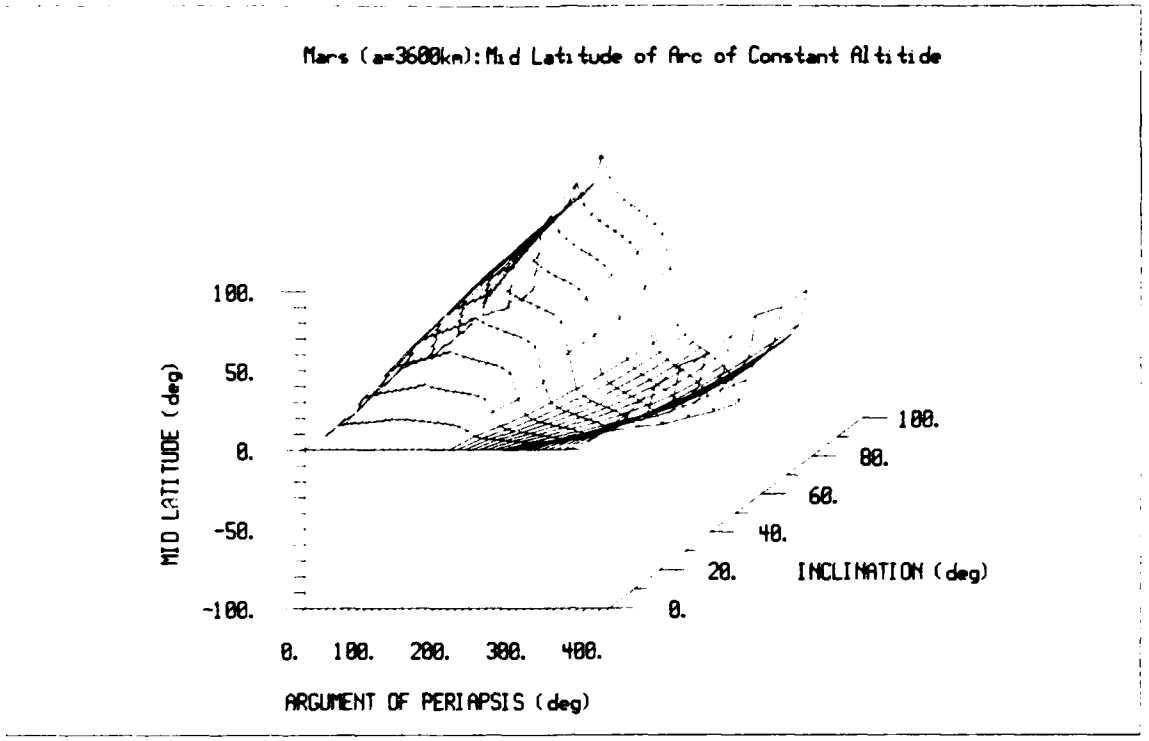

Figure C-13. Mars (a=3600 km): Mid-Latitude of Arc

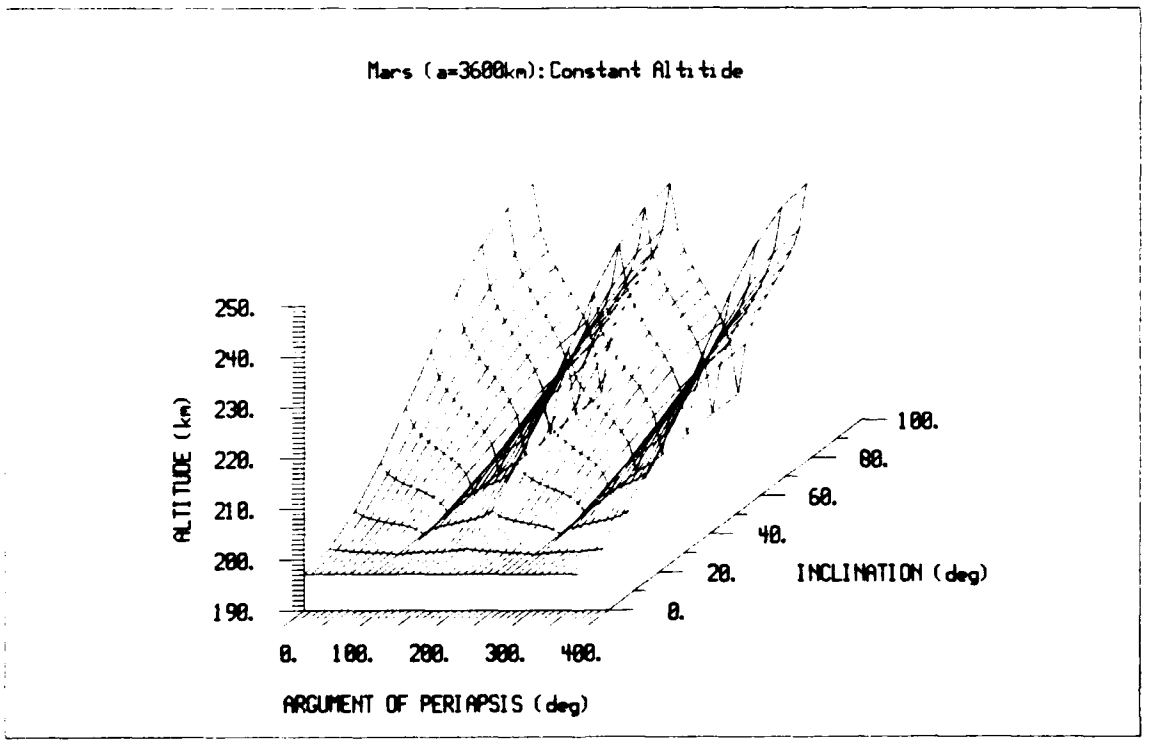

Figure C-14. Mars (a=3600 km): Altitude of Arc

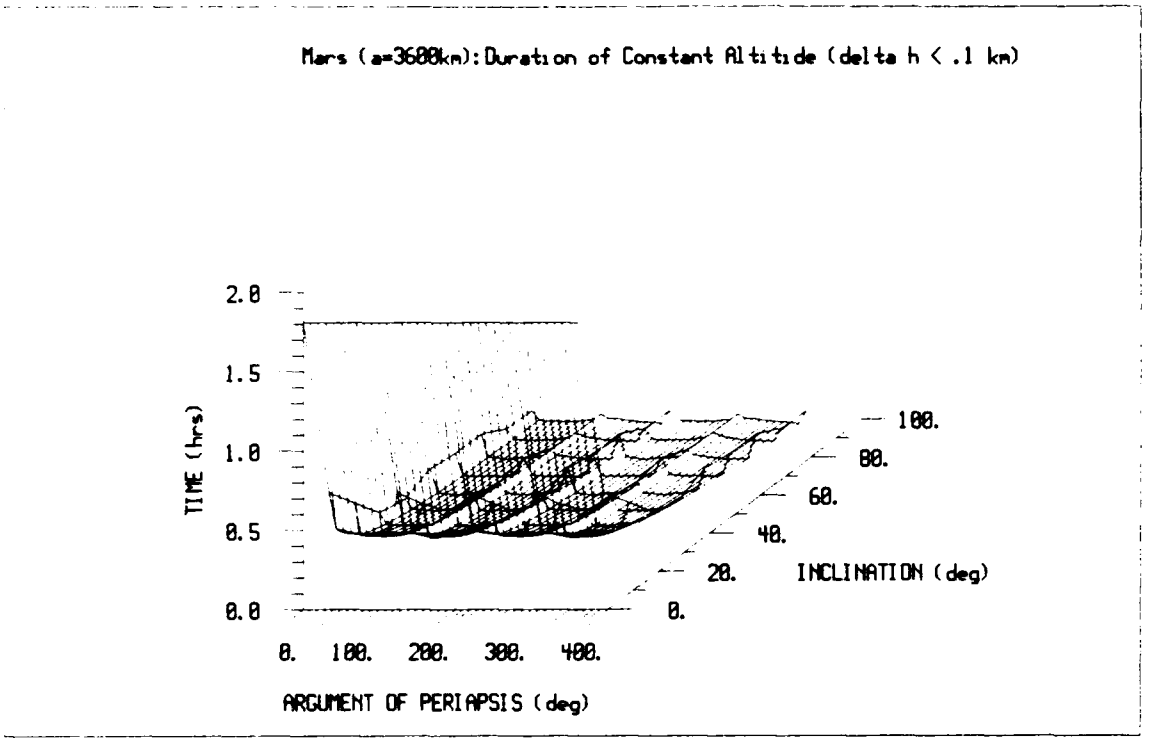

Figure C-15. Mars (a=3600 km): Duration of Arc $\Delta h < .1$ km

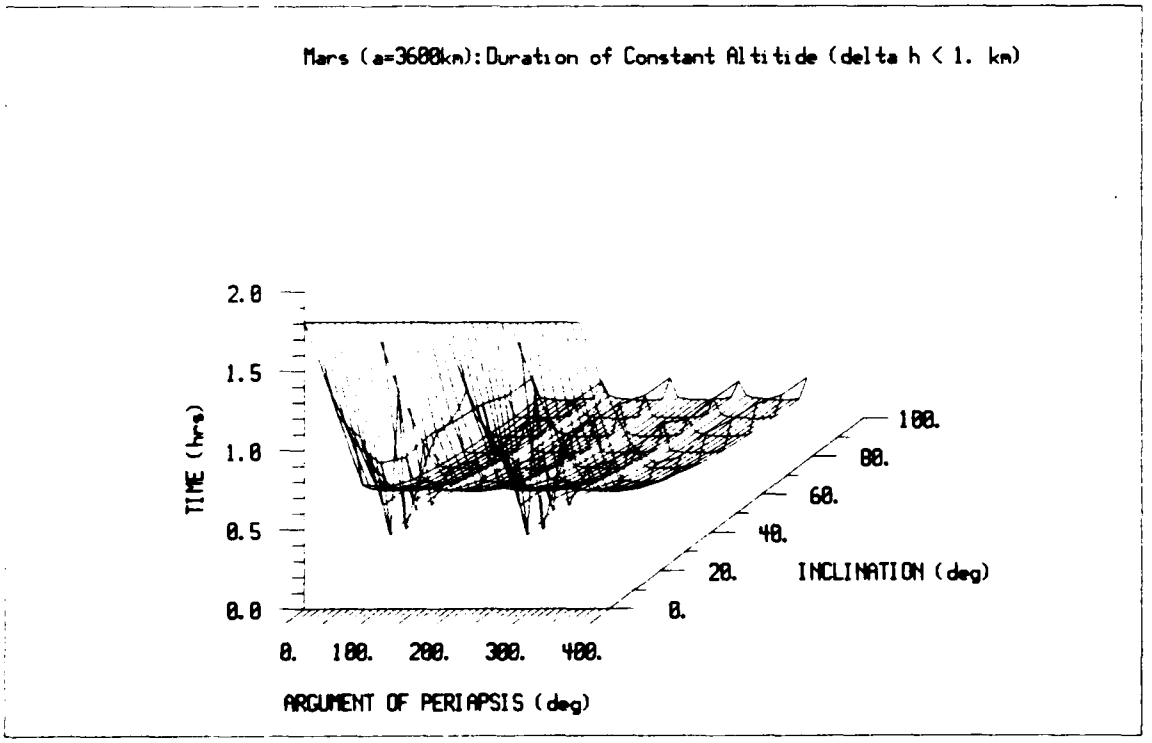

Figure C-16. Mars (a=3600 km): Duration of Arc $\Delta h < 1$km

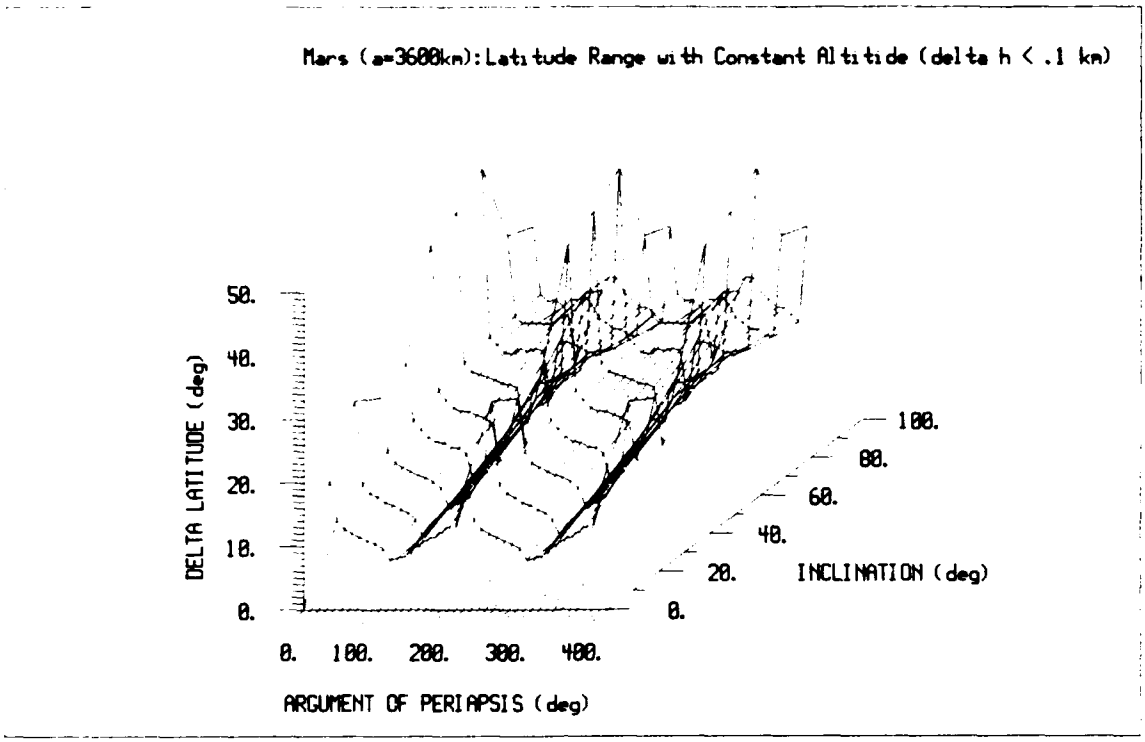

Figure C-17. Mars (a=3600 km): Latitude Range of Arc $\Delta h < .1$ km

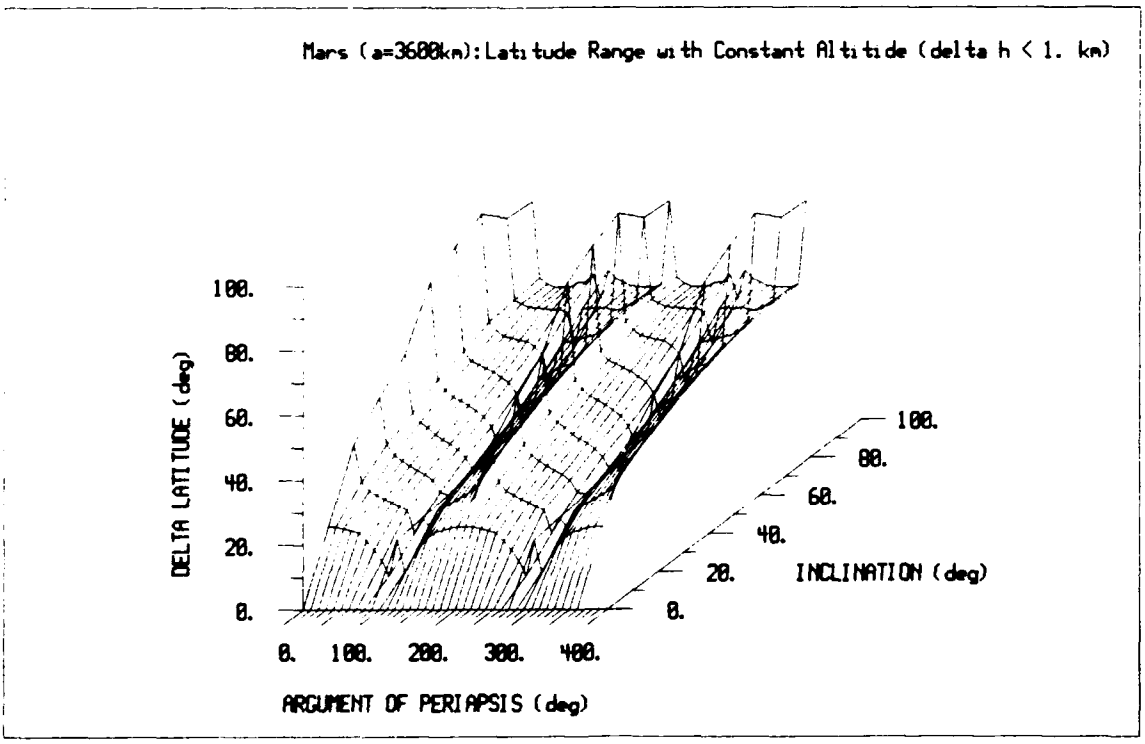

Figure C-18. Mars (a=3600 km): Latitude Range of Arc $\Delta h < 1$km

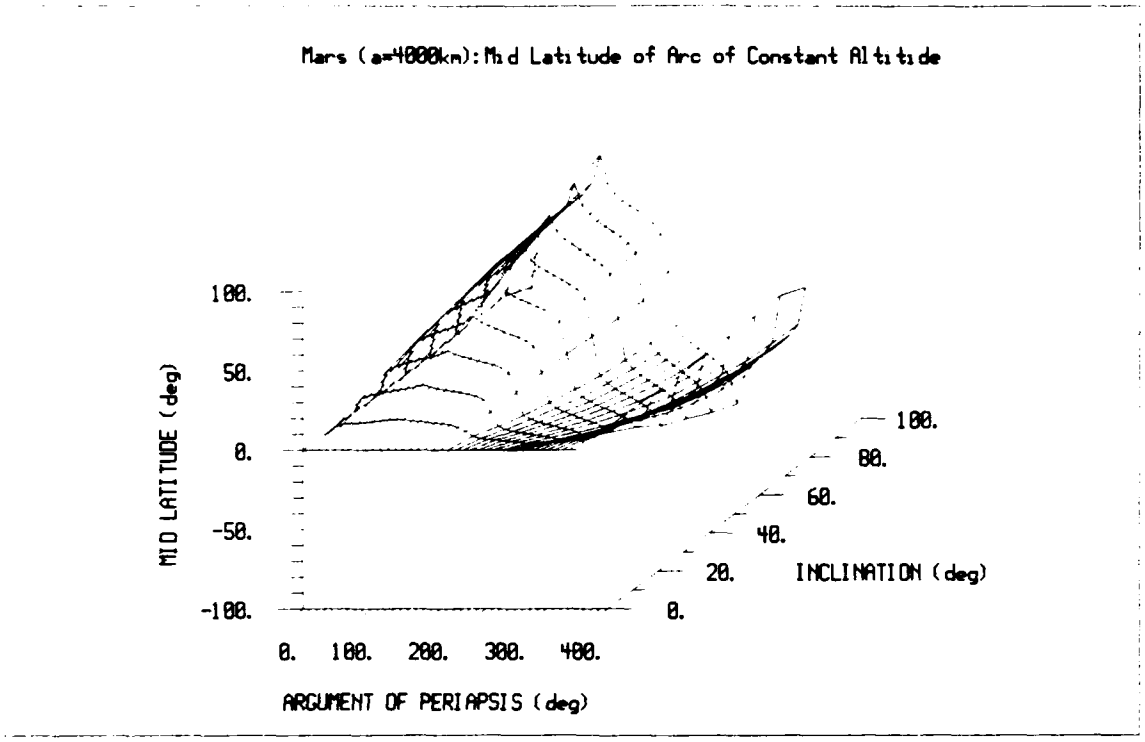

Figure C-19. Mars (a=4000 km): Mid-Latitude of Arc

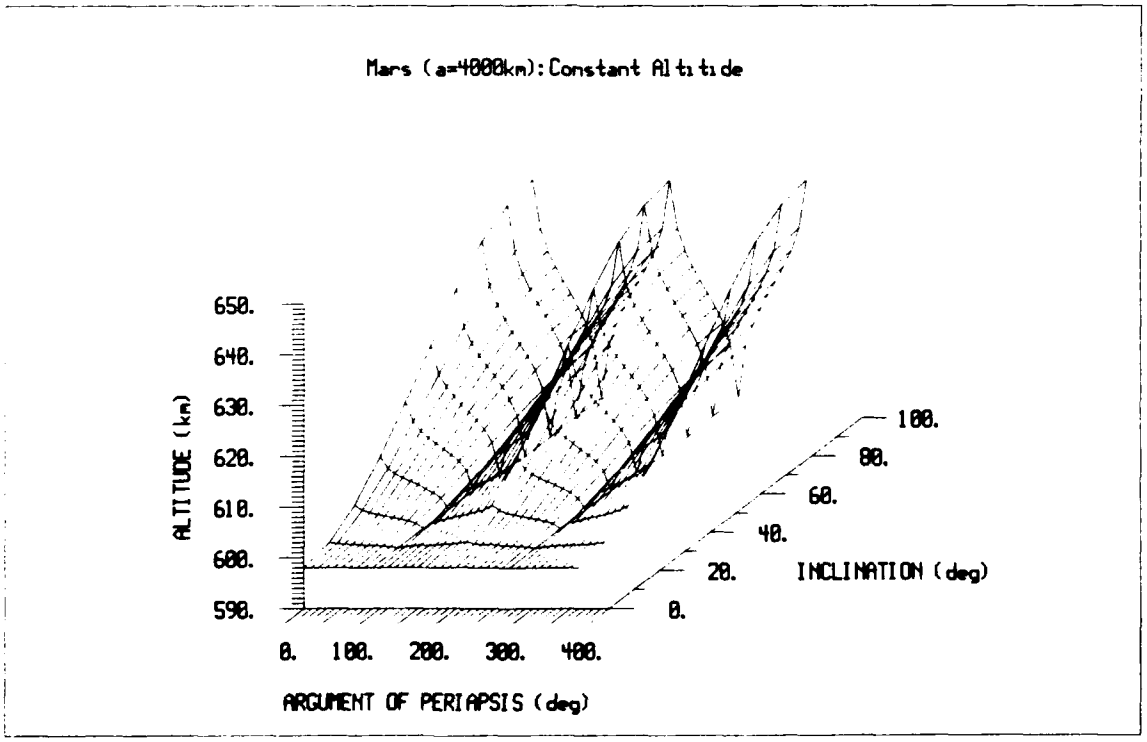

Figure C-20. Mars (a=4000 km): Altitude of Arc

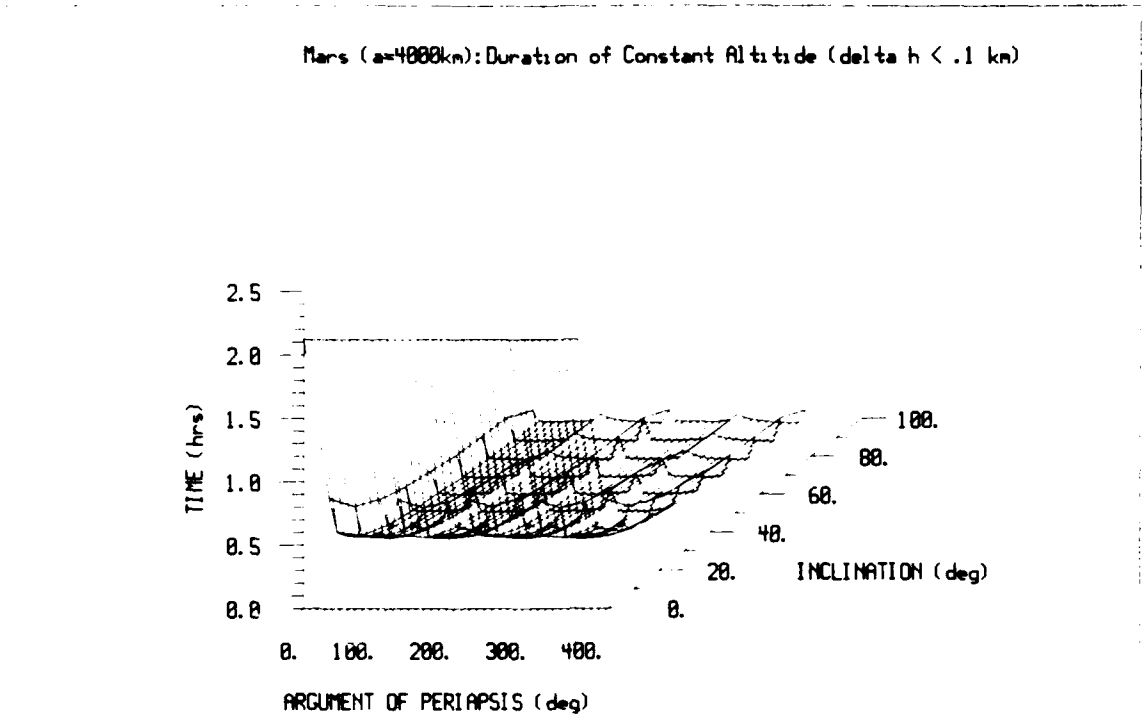

Figure C-21. Mars (a=4000 km): Duration of Arc $\Delta h < .1$ km

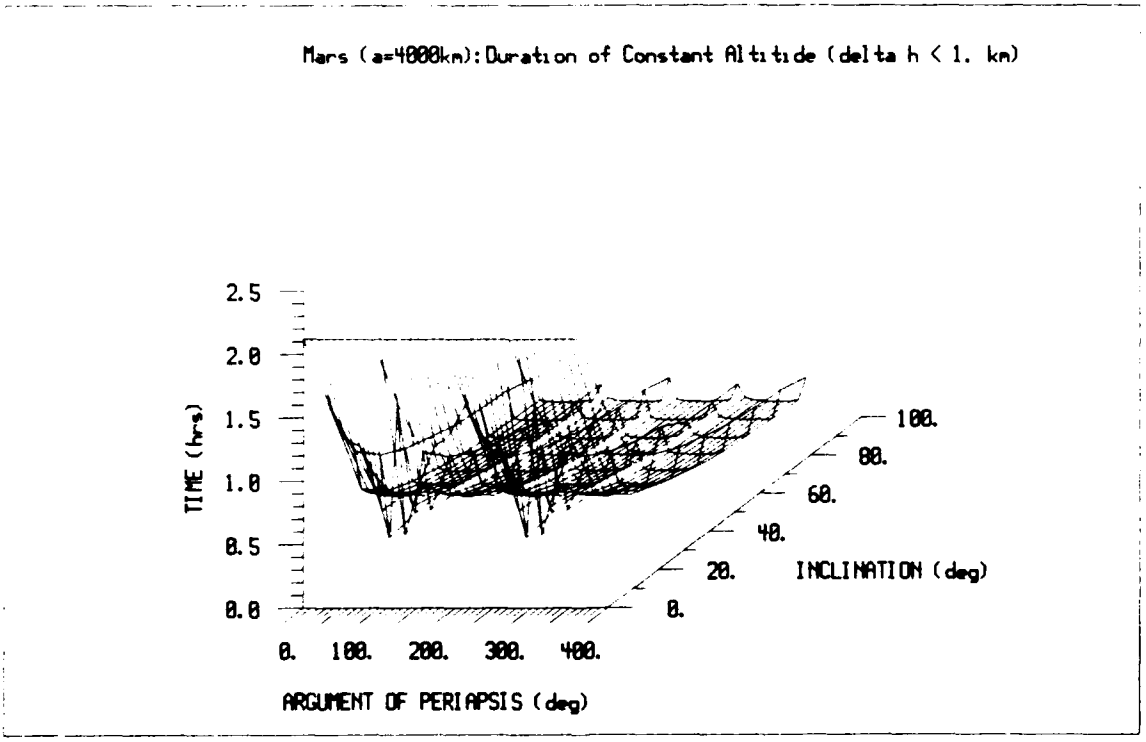

Figure C-22. Mars (a=4000 km): Duration of Arc $\Delta h < 1$km

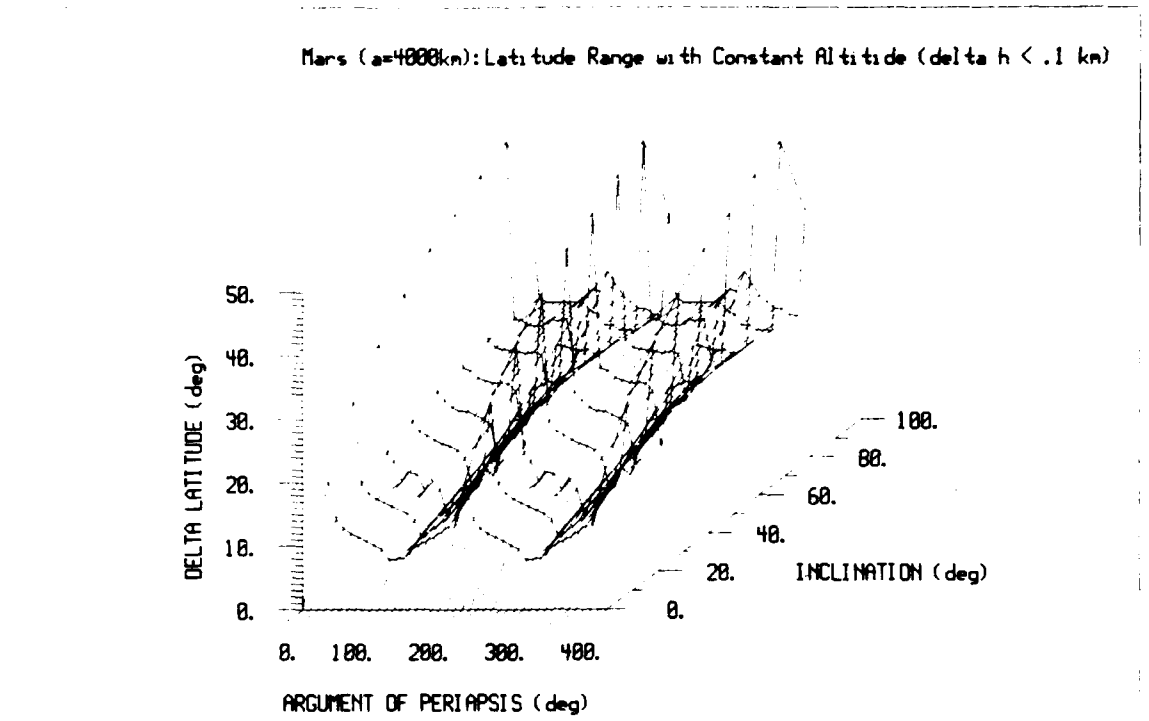

Figure C-23. Mars (a=4000 km): Latitude Range of Arc $\Delta h < .1$ km

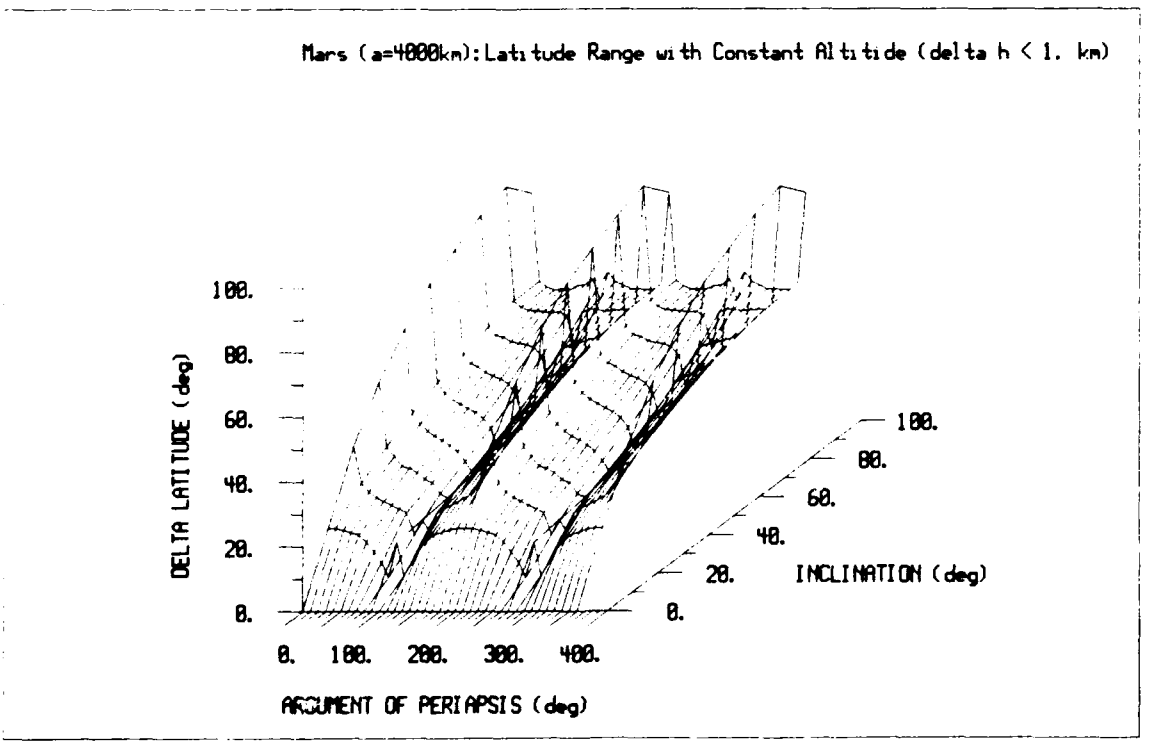

Figure C-24. Mars (a=4000 km): Latitude Range of Arc $\Delta h < 1$km

Appendix D

Secular Changes in Mean Orbital Elements

Figures D-1 through D-30 present the secular changes in semi-major axis (D-1:D-6), inclination (D-7:D-12), argument of periapsis (D-13:D-18), eccentricity (D-19:D-24), and longitude of the ascending node (D-25:D-30). For each orbital element, the first two figures present results for Earth (a = 6700 km) with ballistic coefficients of $.01 \times 10^{-6}$ km^2/kg and $.04 \times 10^{-6}$ km^2/kg. The third and fourth figures present results for Mars (a = 3600 km) with ballistic coefficients of $.01 \times 10^{-6}$ km^2/kg and $.04 \times 10^{-6}$ km^2/kg. The final two figures present results for Earth (a = 7500 km) and Mars (a = 4500 km) with a ballistic coefficient of $.04 \times 10^{-6}$ km^2/kg.

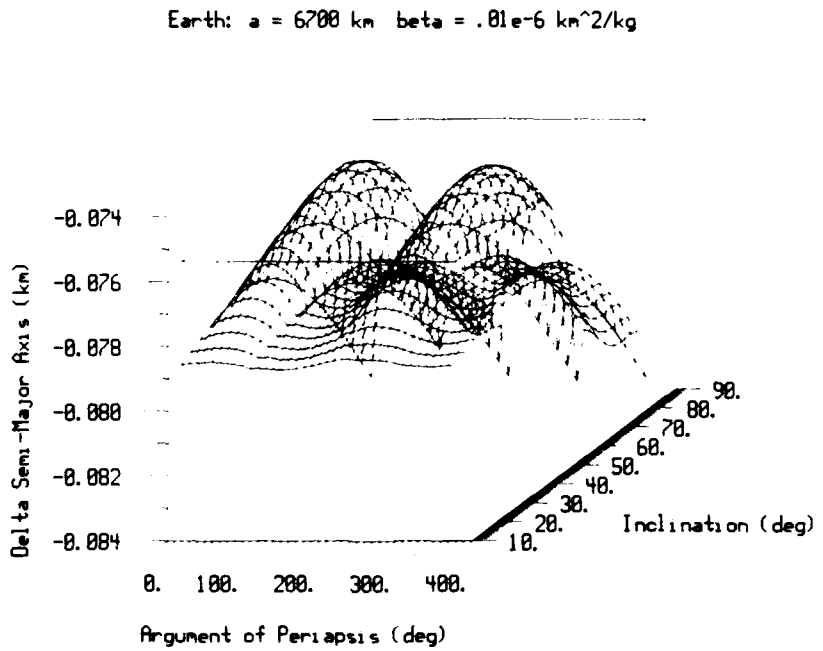

Figure D-1. Earth(a=6700km, β=.01e-6 km^2/kg): Semi-major Axis Change

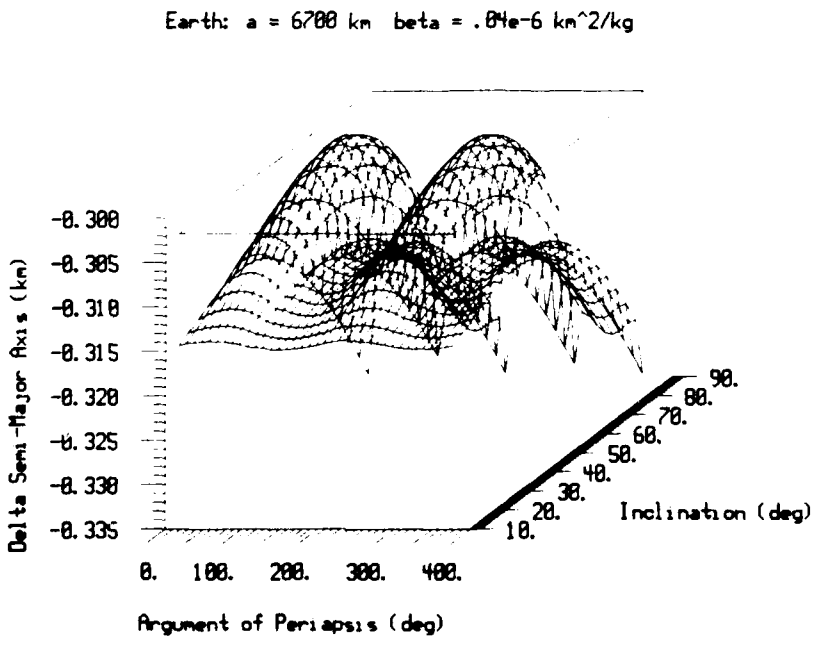

Figure D-2. Earth(a=6700km, β=.04e-6 km^2/kg): Semi-major Axis Change

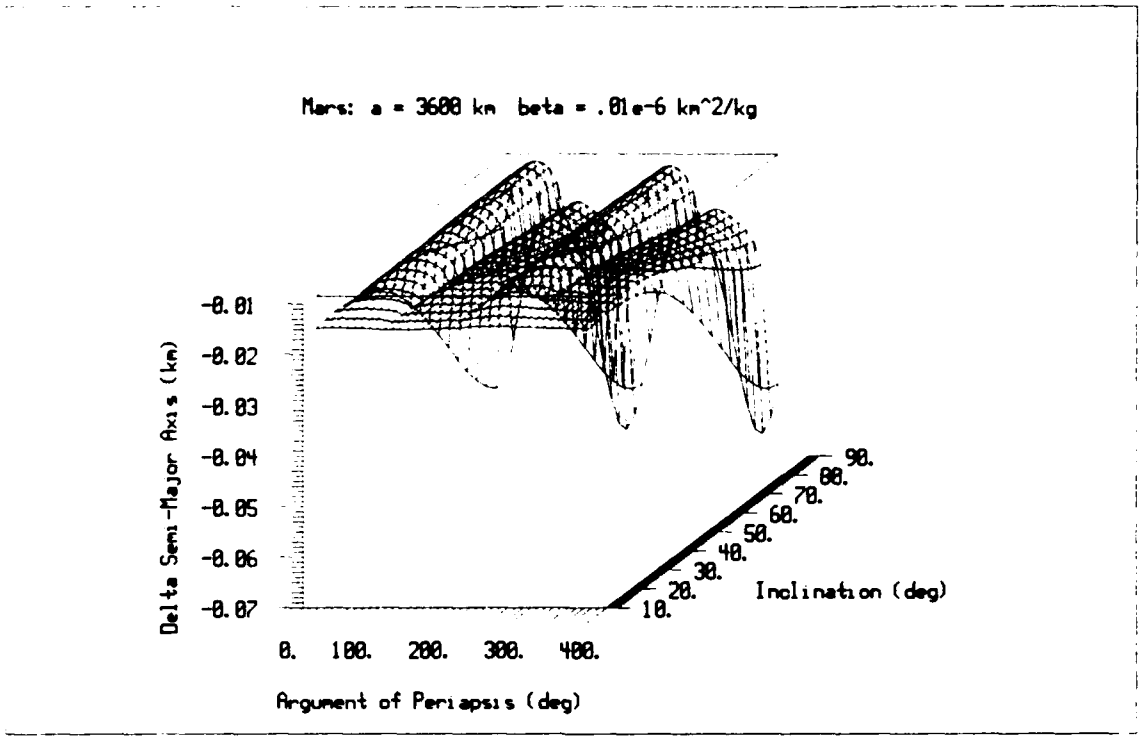

Figure D-3. Mars(a=3600km, β=.01e-6 km^2/kg): Semi-major Axis Change

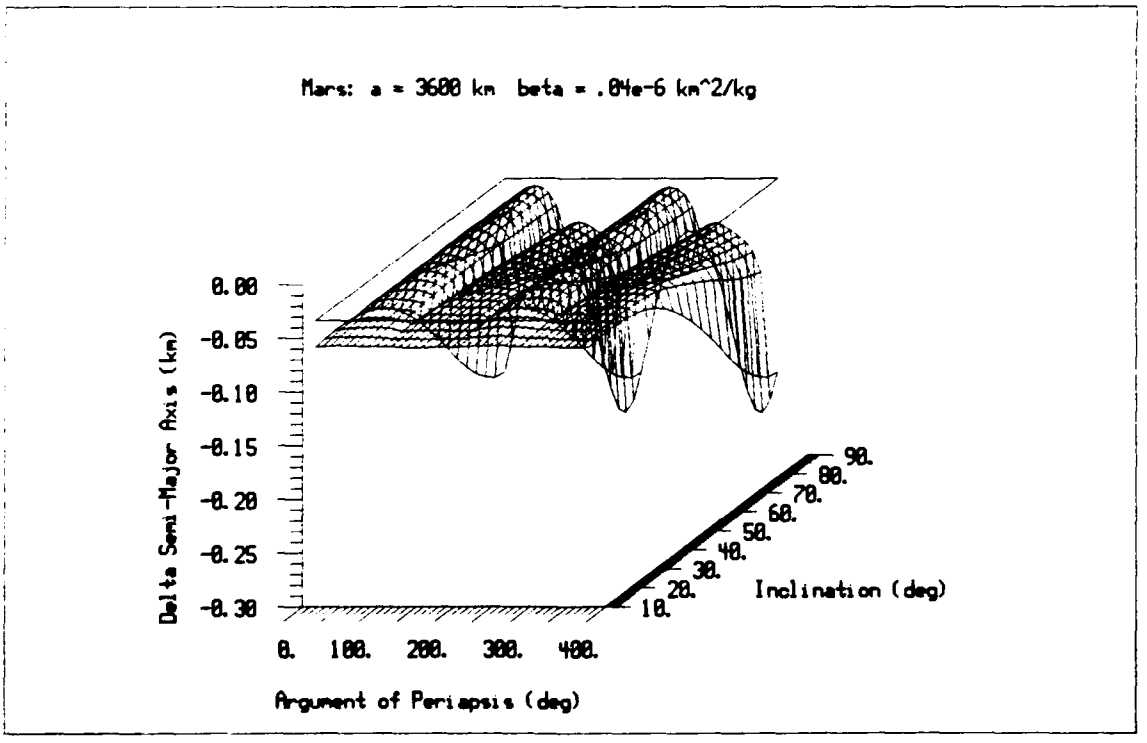

Figure D-4. Mars(a=3600km, β=.04e-6 km^2/kg): Semi-major Axis Change

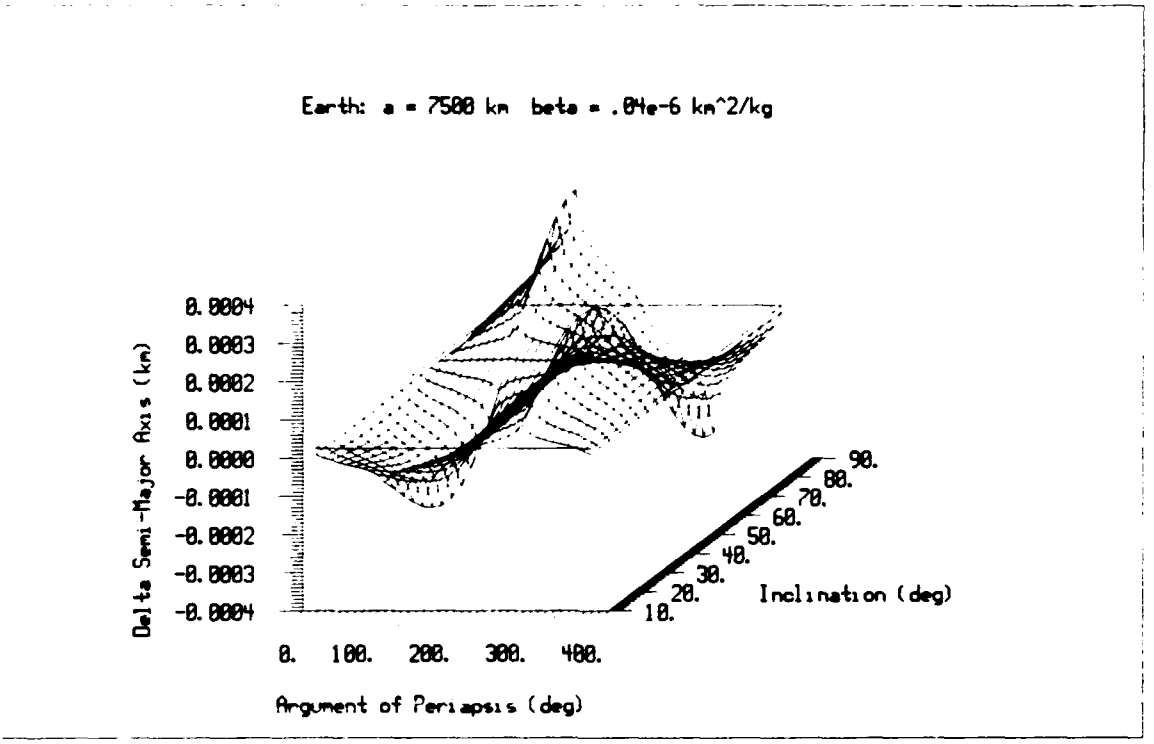

Figure D-5. Earth(a=7500km, β=.04e-6 km^2/kg): Semi-major Axis Change

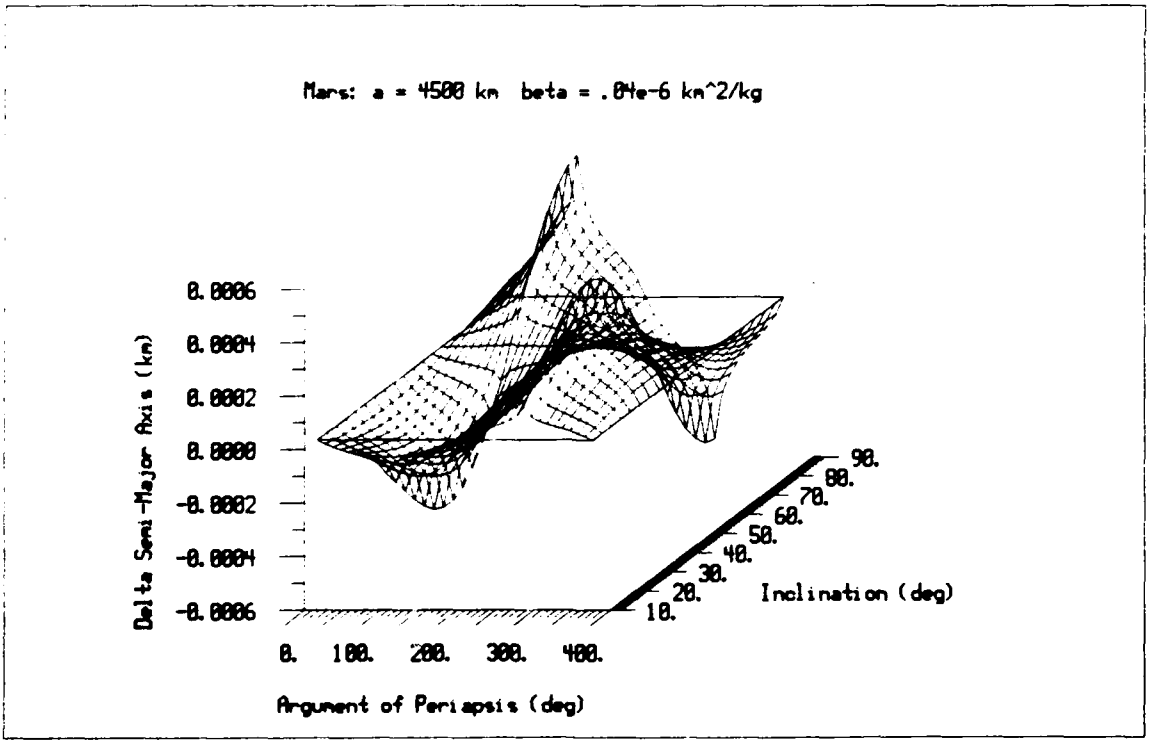

Figure D-6. Mars(a=4500km, β=.04e-6 km^2/kg): Semi-major Axis Change

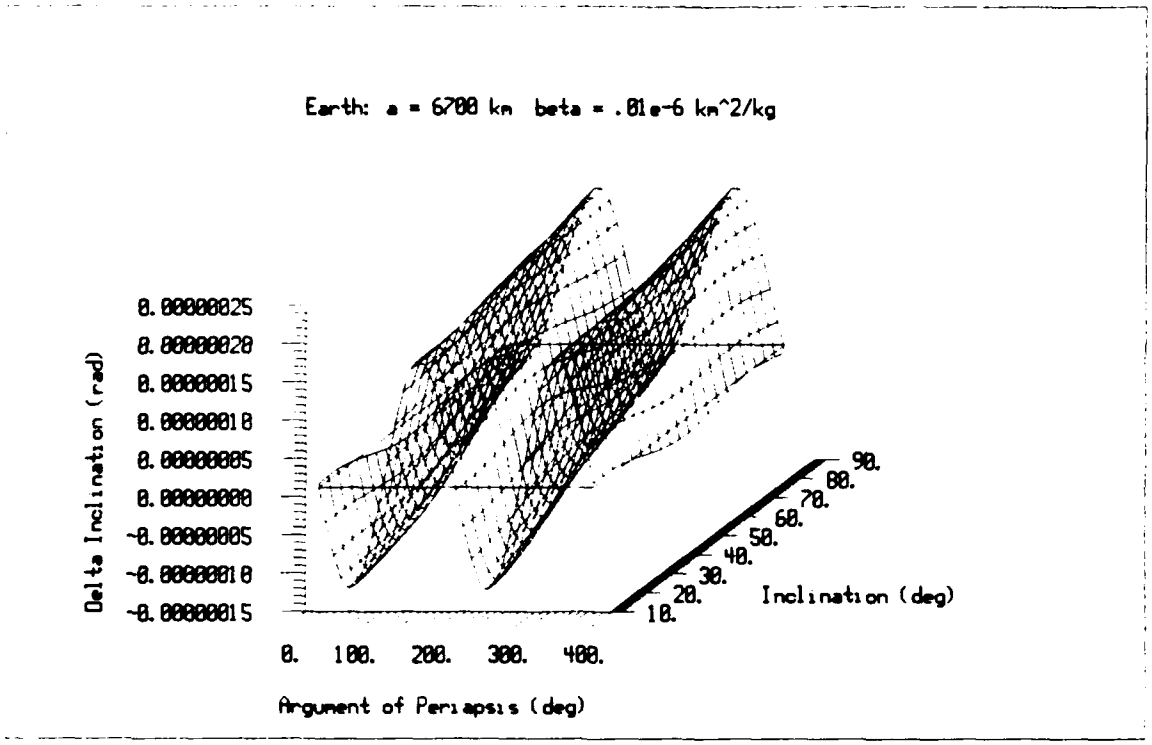

Figure D-7. Earth(a=6700km, β=.01e-6 km^2/kg): Inclination Change

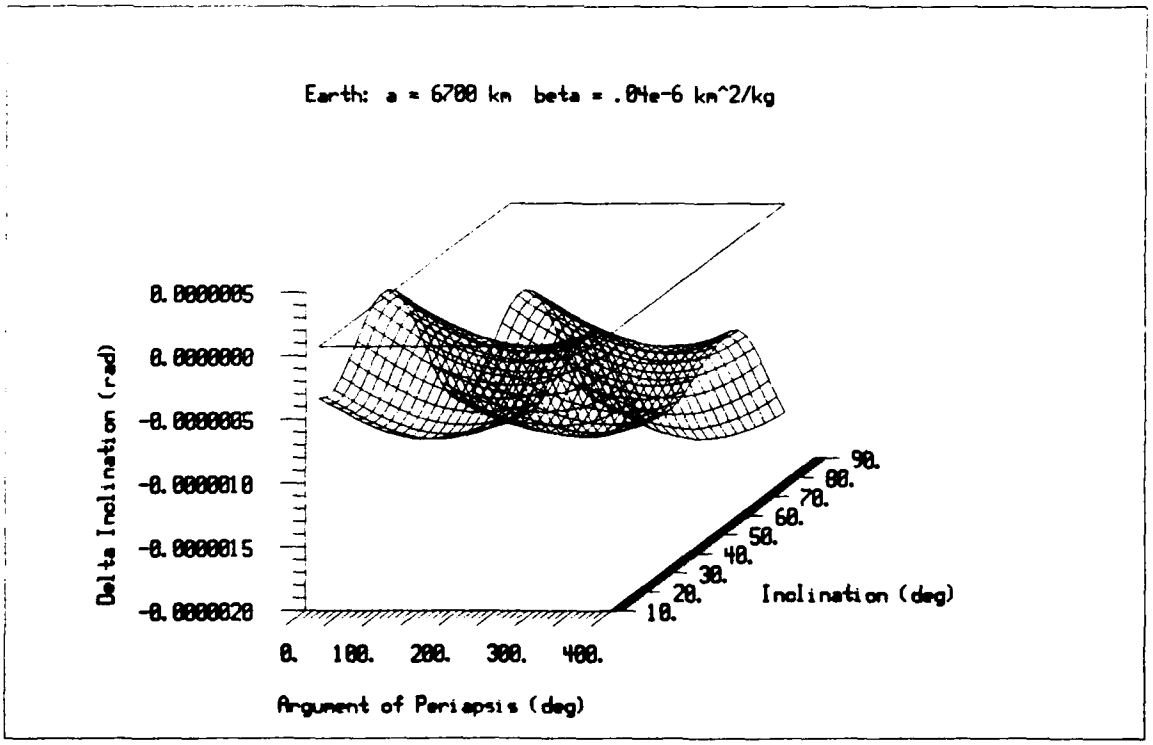

Figure D-8. Earth(a=6700km, β=.04e-6 km^2/kg): Inclination Change

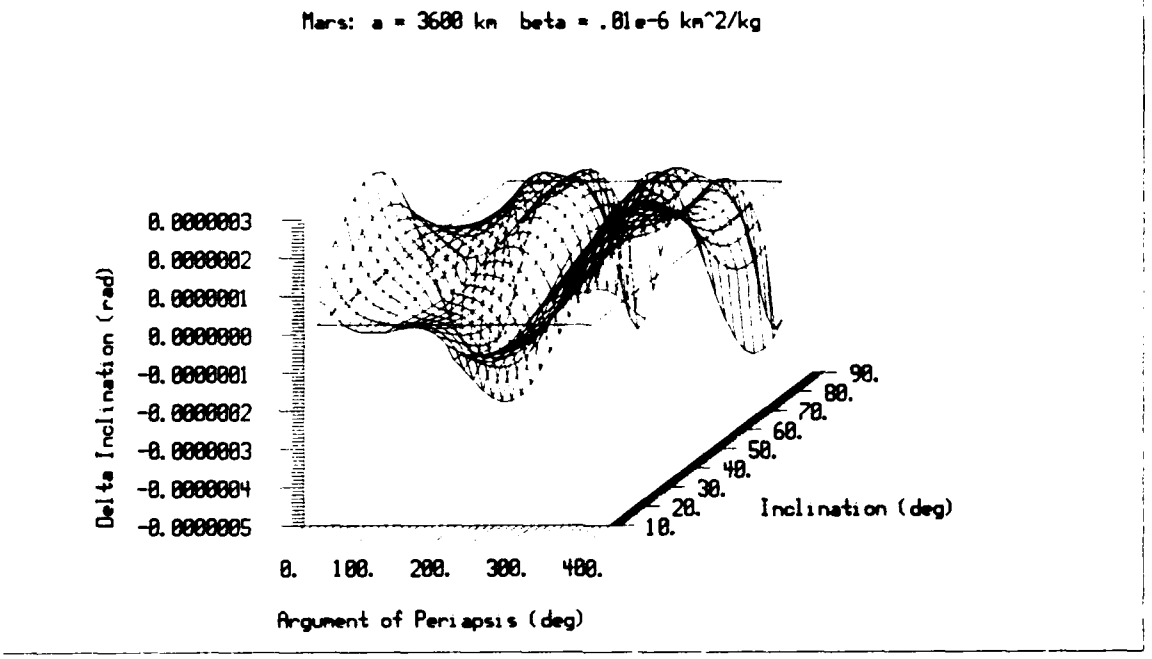

Figure D-9. Mars(a=3600km, β=.01e-6 km^2/kg): Inclination Change

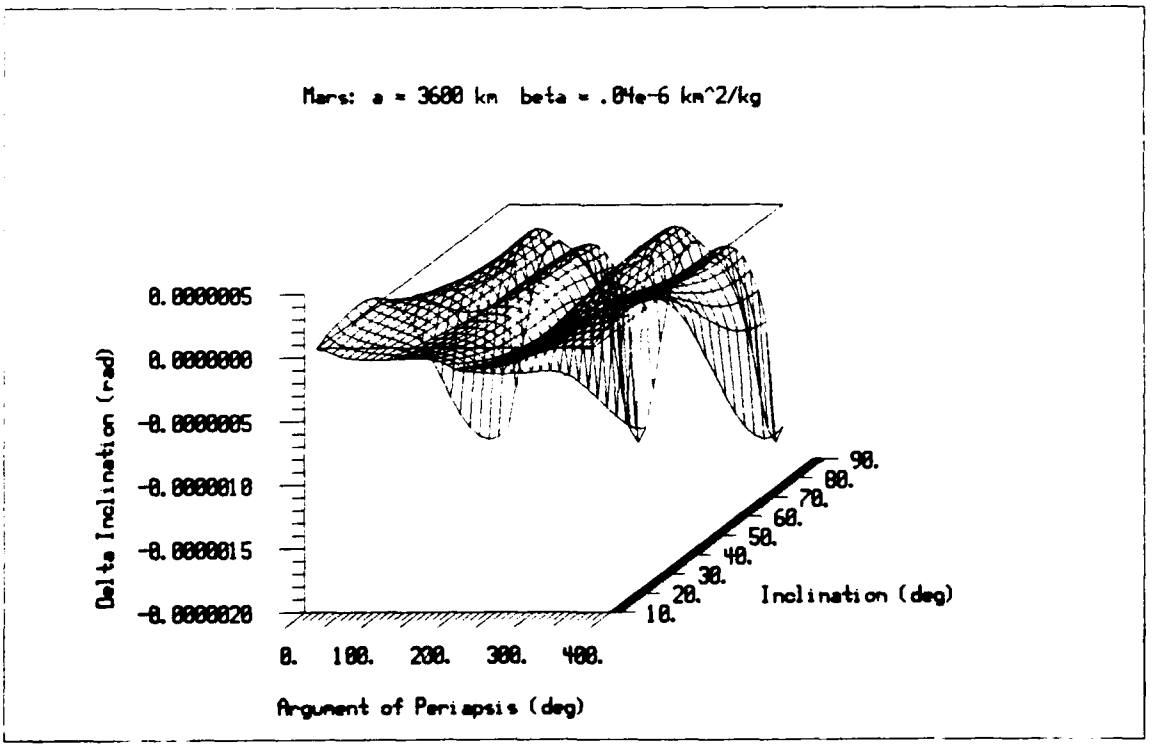

Figure D-10. Mars(a=3600km, β=.04e-6 km^2/kg): Inclination Change

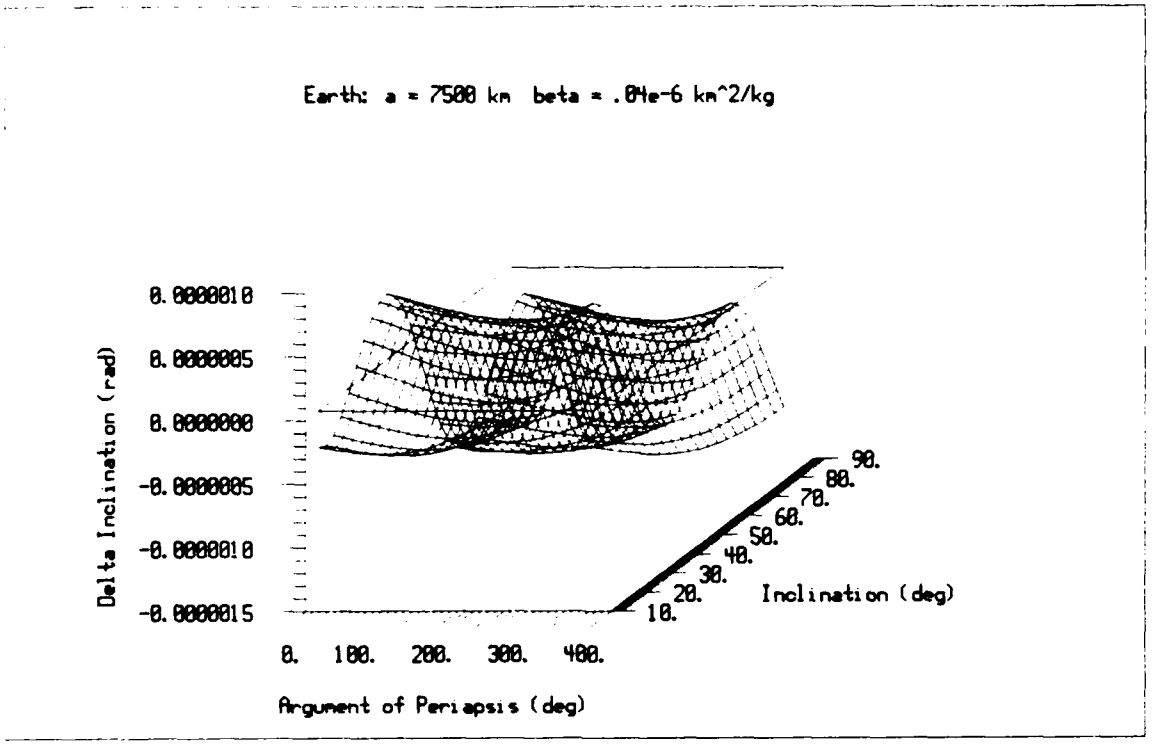

Figure D-11. Earth(a=7500km, β=.04e-6 km^2/kg): Inclination Change

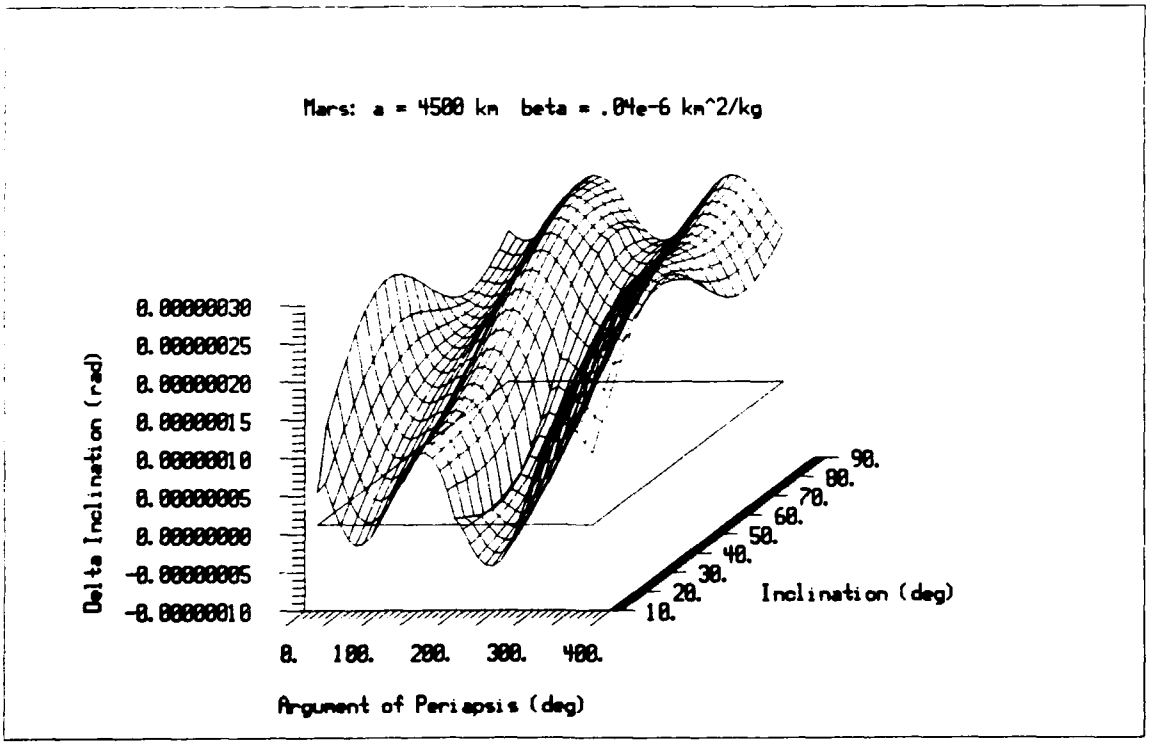

Figure D-12. Mars(a=4500km, β=.04e-6 km^2/kg): Inclination Change

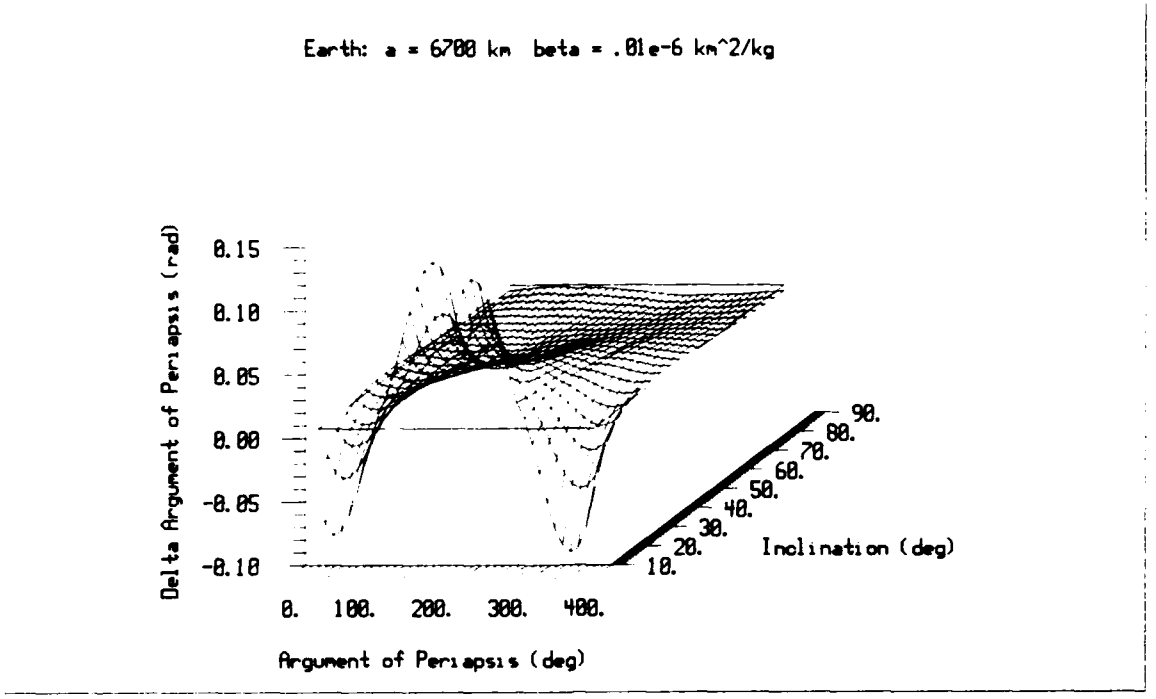

Figure D-13. Earth(a=6700km, β=.01e-6 km^2/kg): Arg of Periapsis Change

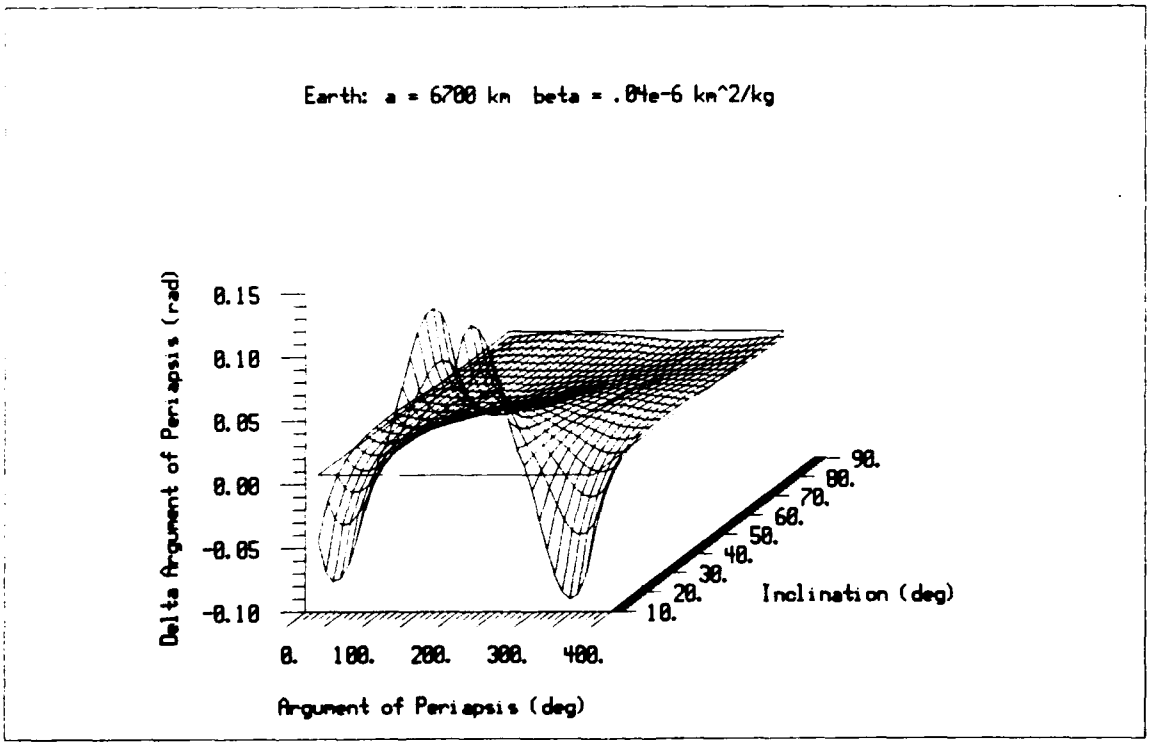

Figure D-14. Earth(a=6700km, β=.04e-6 km^2/kg): Arg of Periapsis Change

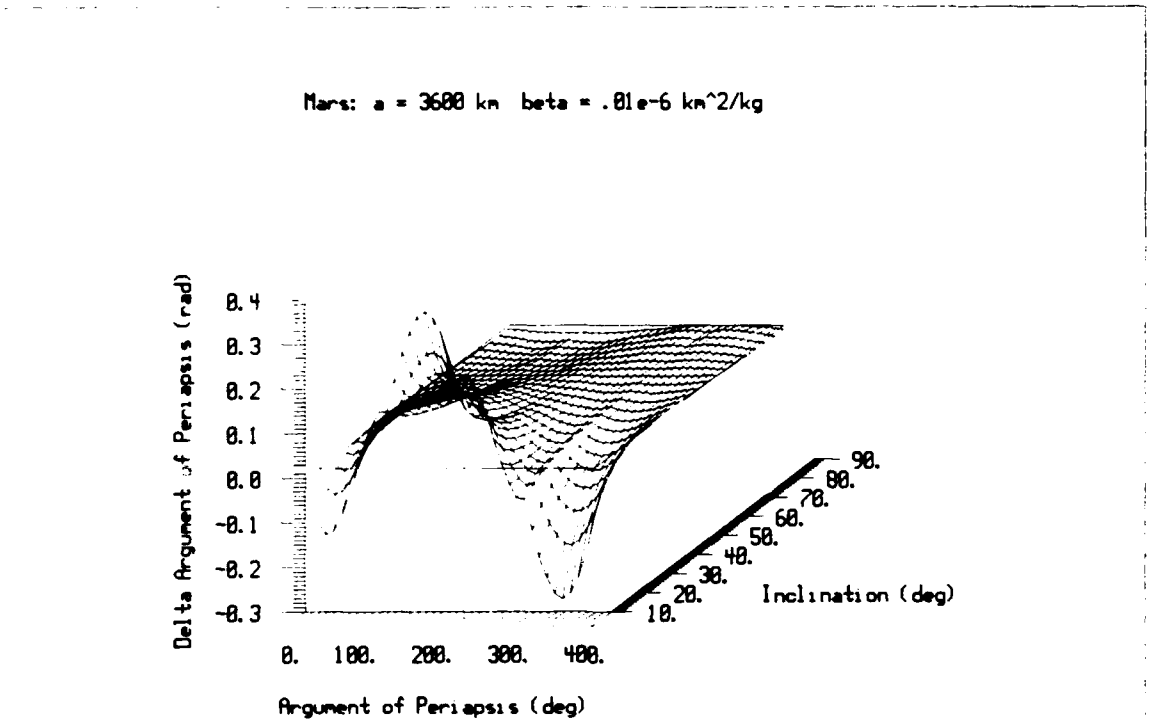

Figure D-15. Mars(a=3600km, β=.01e-6 km^2/kg): Arg of Periapsis Change

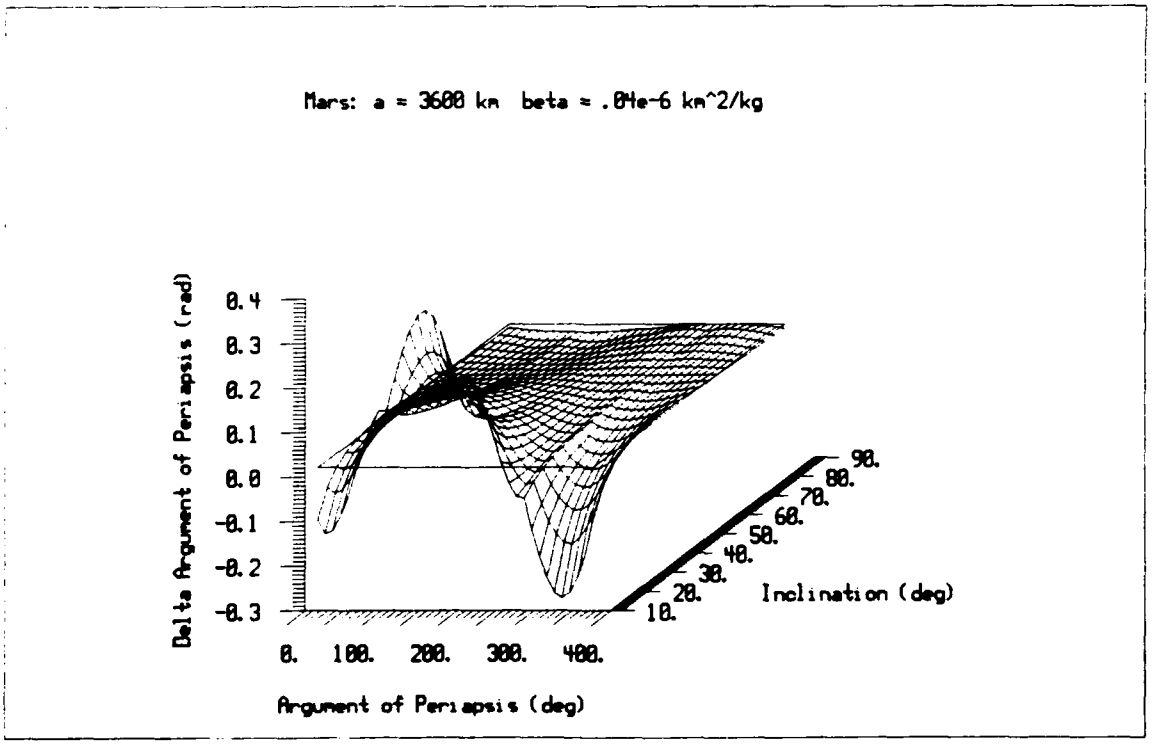

Figure D-16. Mars(a=3600km, β=.04e-6 km^2/kg): Arg of Periapsis Change

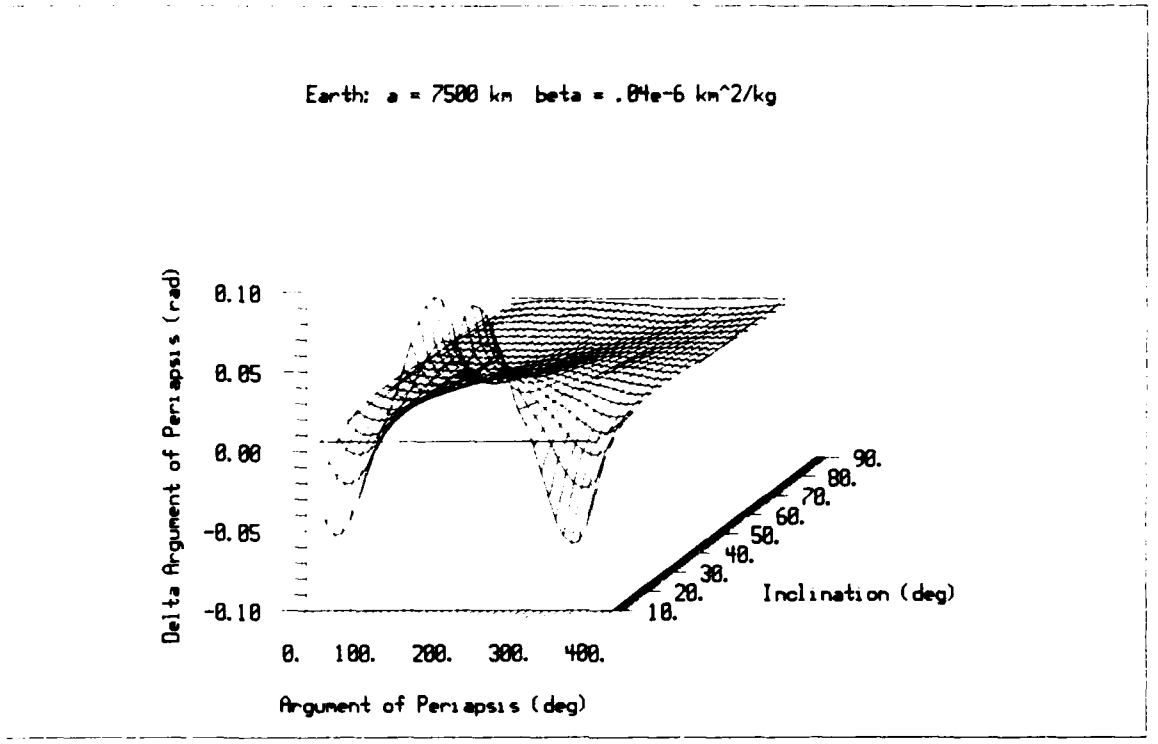

Figure D-17. Earth(a=7500km, β=.04e-6 km^2/kg): Arg of Periapsis Change

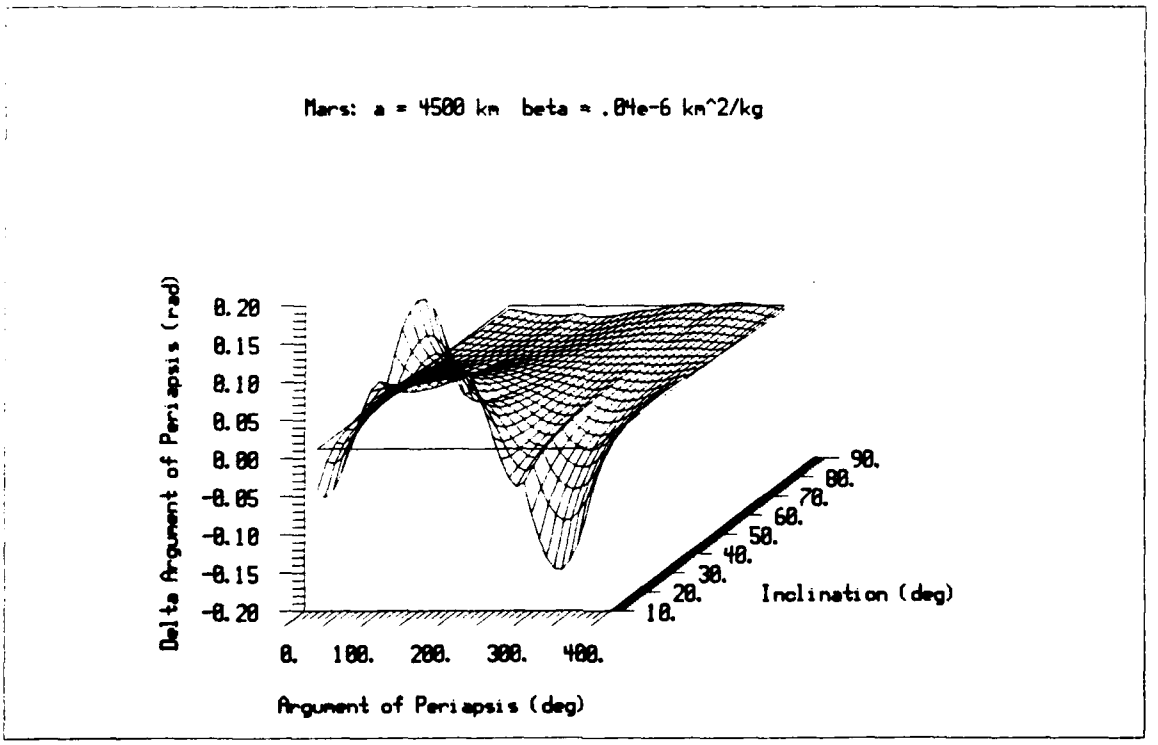

Figure D-18. Mars(a=4500km, β=.04e-6 km^2/kg): Arg of Periapsis Change

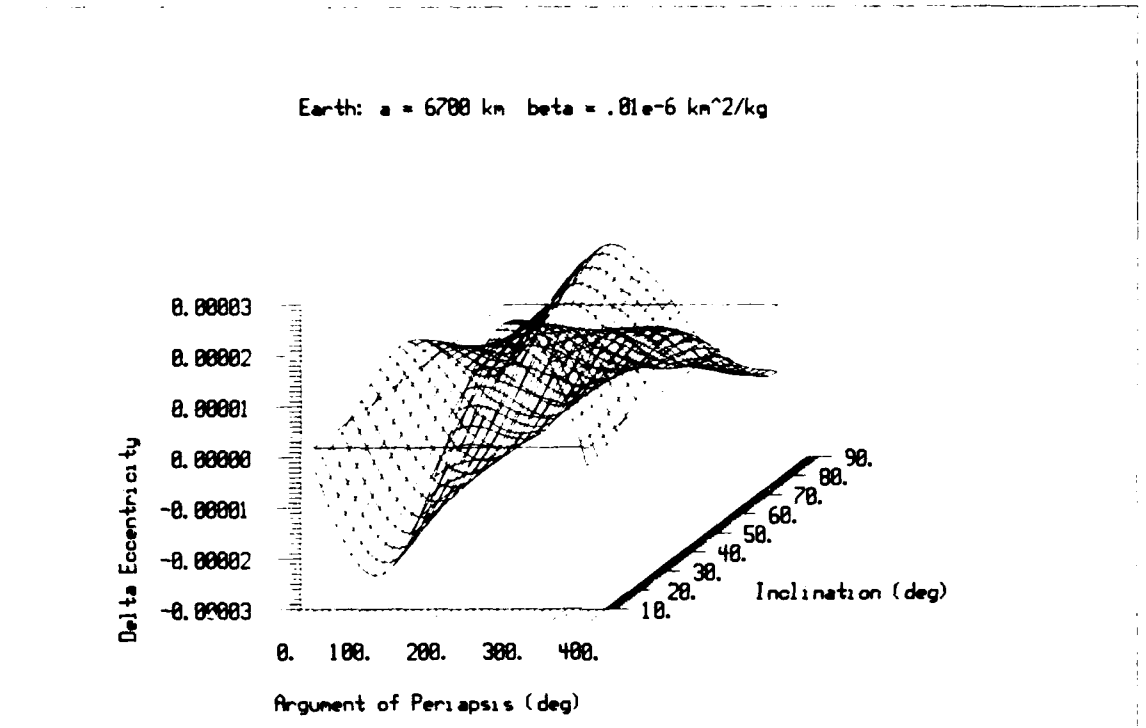

Figure D-19. Earth(a=6700km, β=.01e-6 km^2/kg): Eccentricity Change

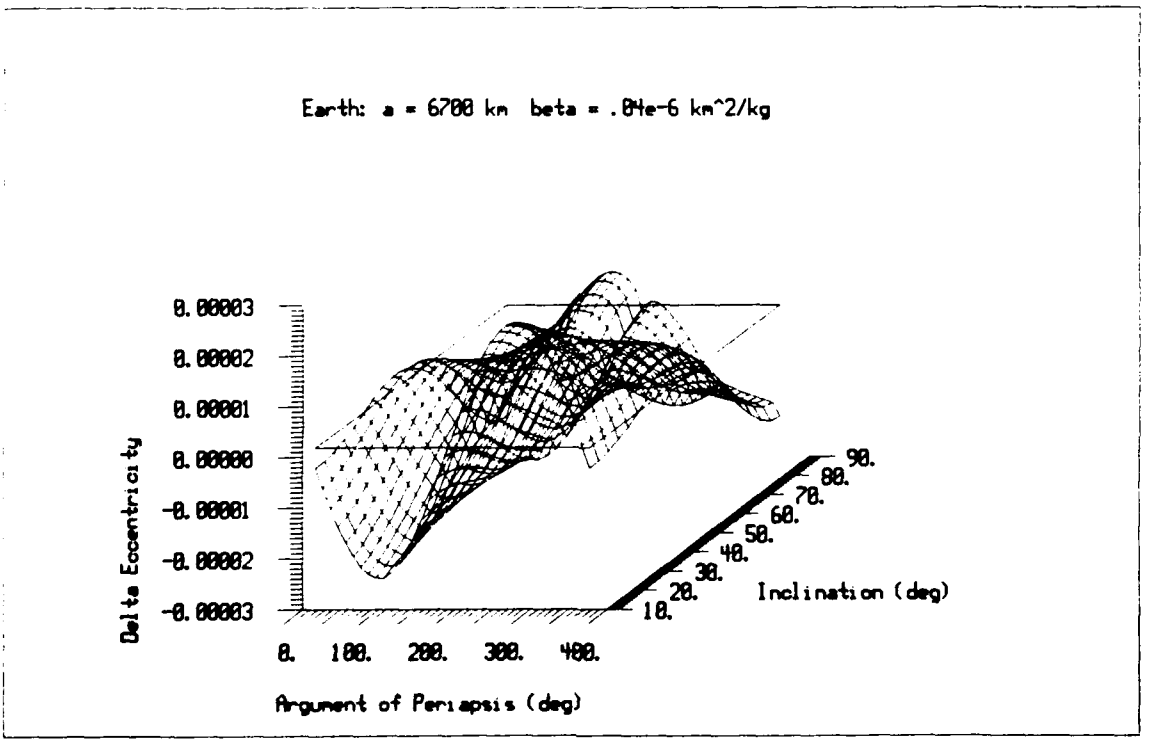

Figure D-20. Earth(a=6700km, β=.04e-6 km^2/kg): Eccentricity Change

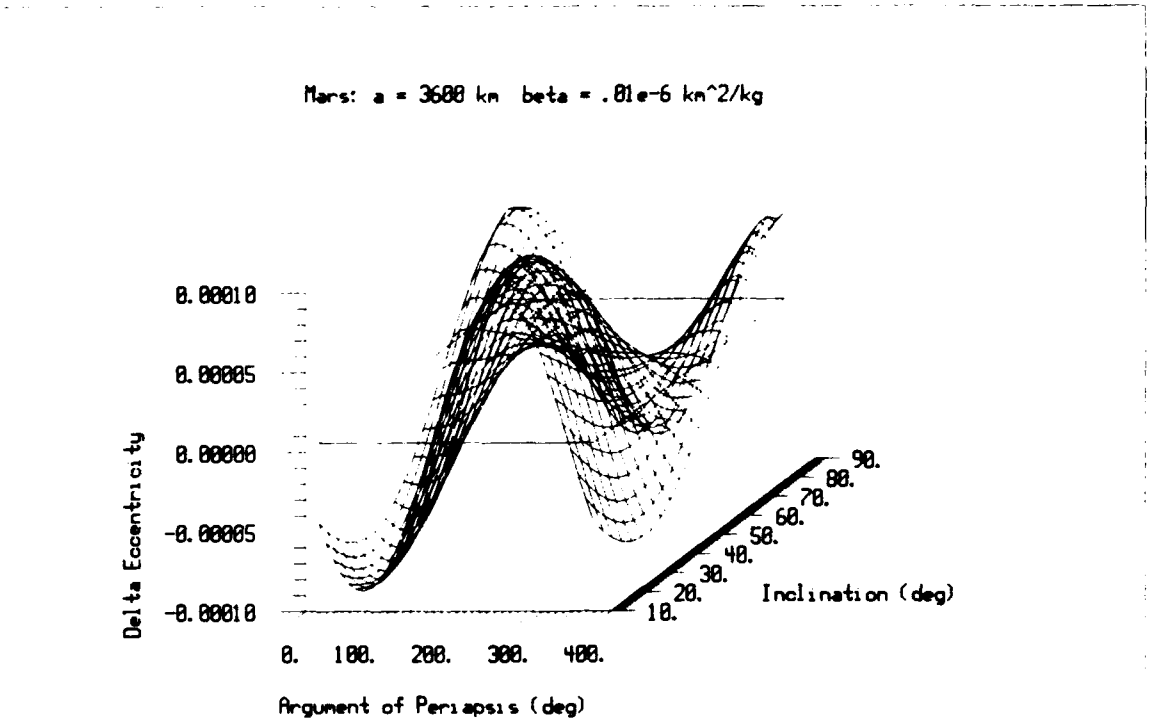

Figure D-21. Mars(a=3600km, β=.01e-6 km^2/kg): Eccentricity Change

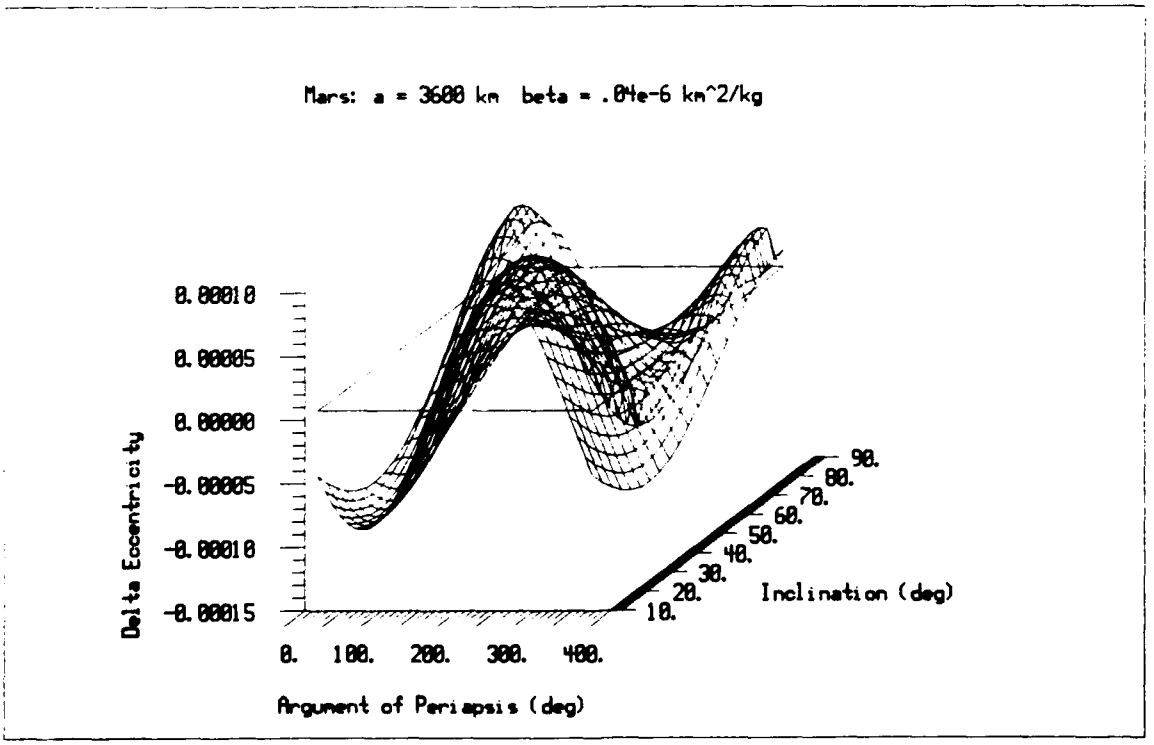

Figure D-22. Mars(a=3600km, β=.04e-6 km^2/kg): Eccentricity Change

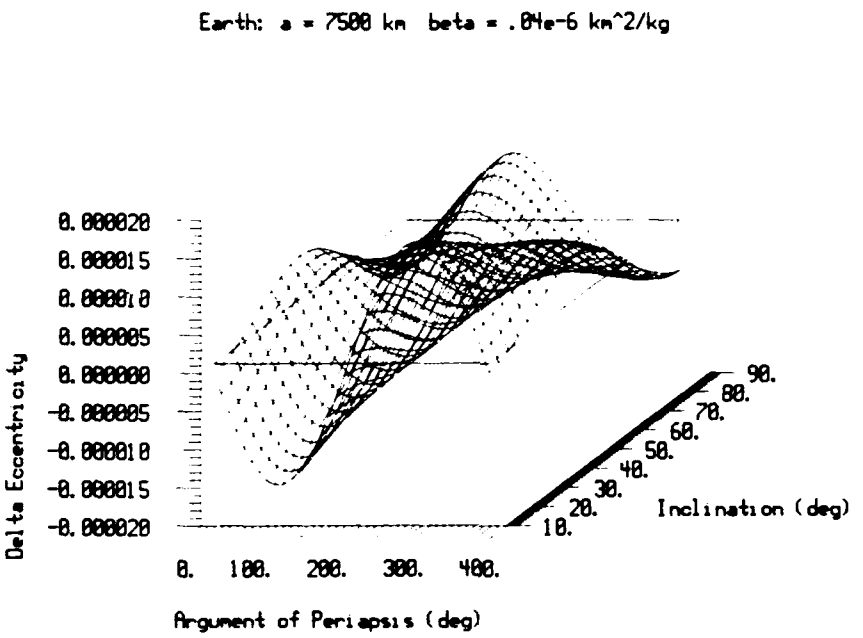

Figure D-23. Earth(a=7500km, β=.04e-6 km^2/kg): Eccentricity Change

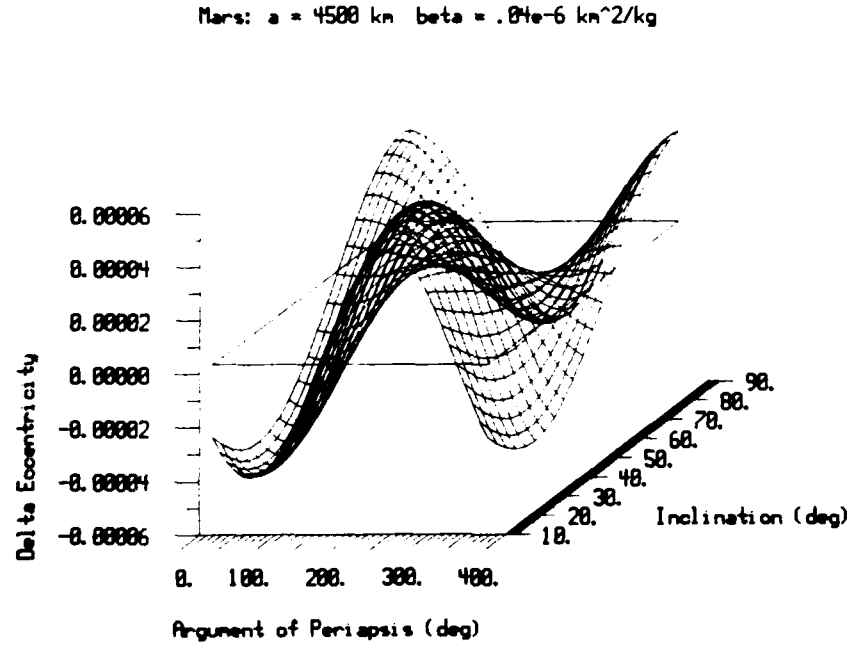

Figure D-24. Mars(a=4500km, β=.04e-6 km^2/kg): Eccentricity Change

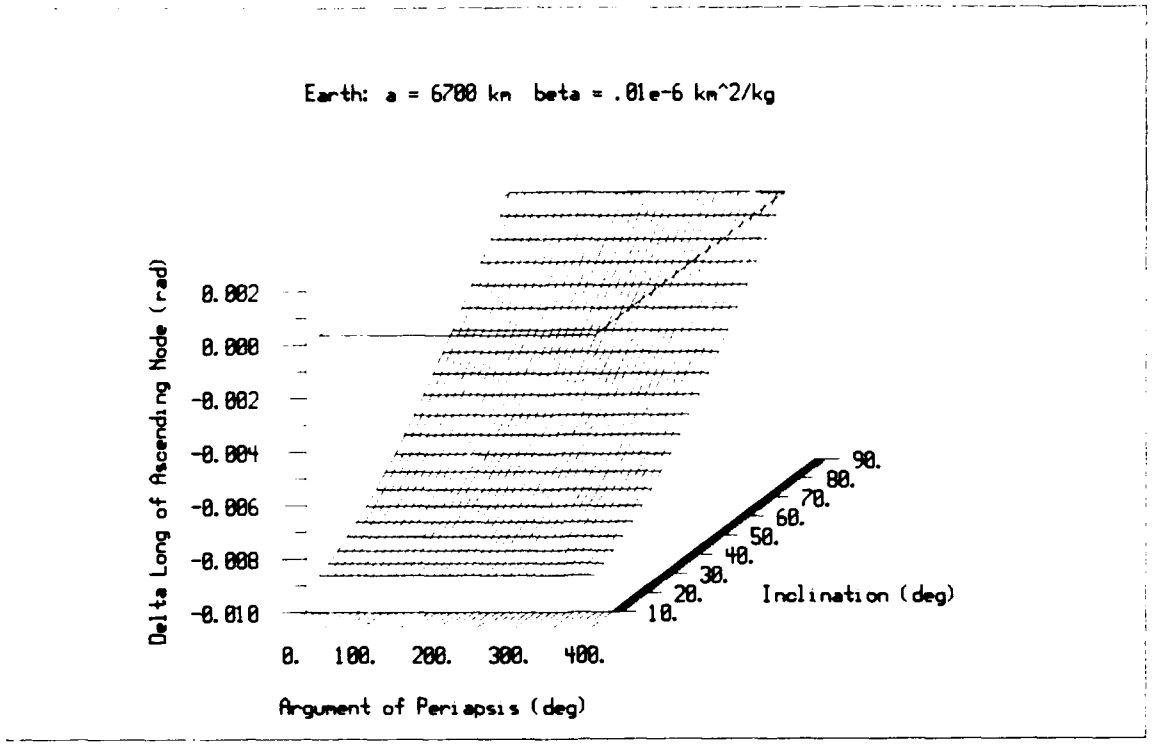

Figure D-25. Earth(a=6700km, β=.01e-6 km^2/kg): Long of Asc Node Change

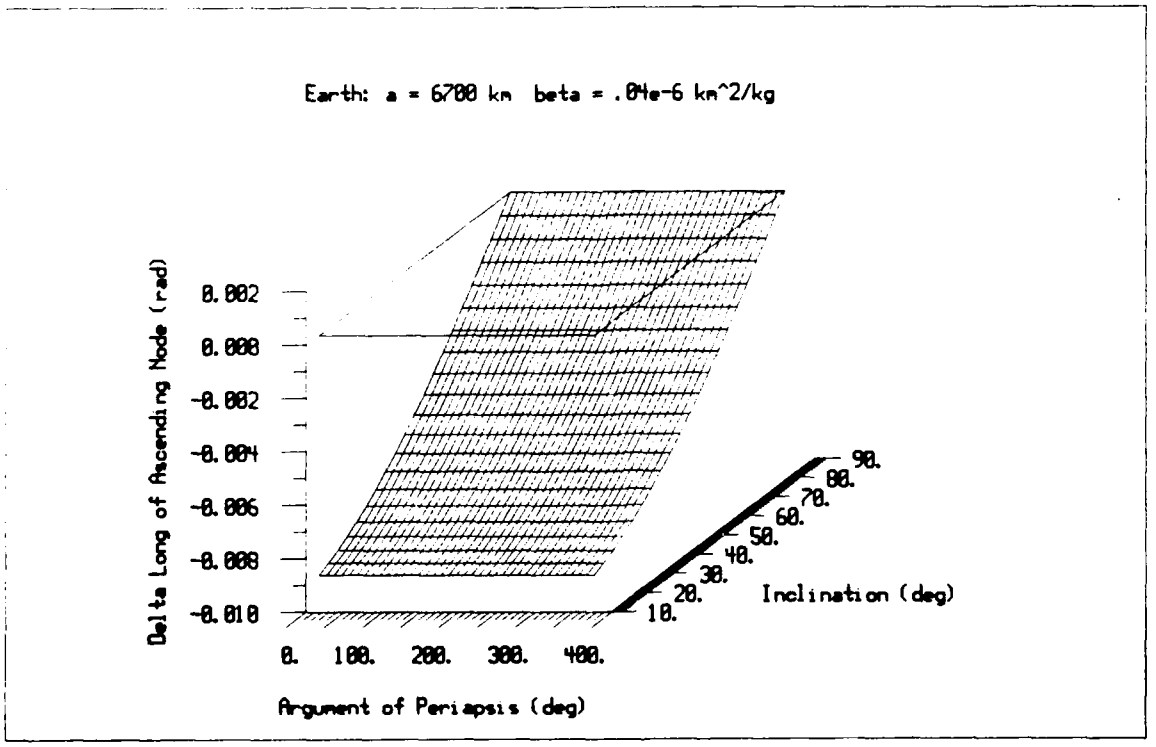

Figure D-26. Earth(a=6700km, β=.04e-6 km^2/kg): Long of Asc Node Change

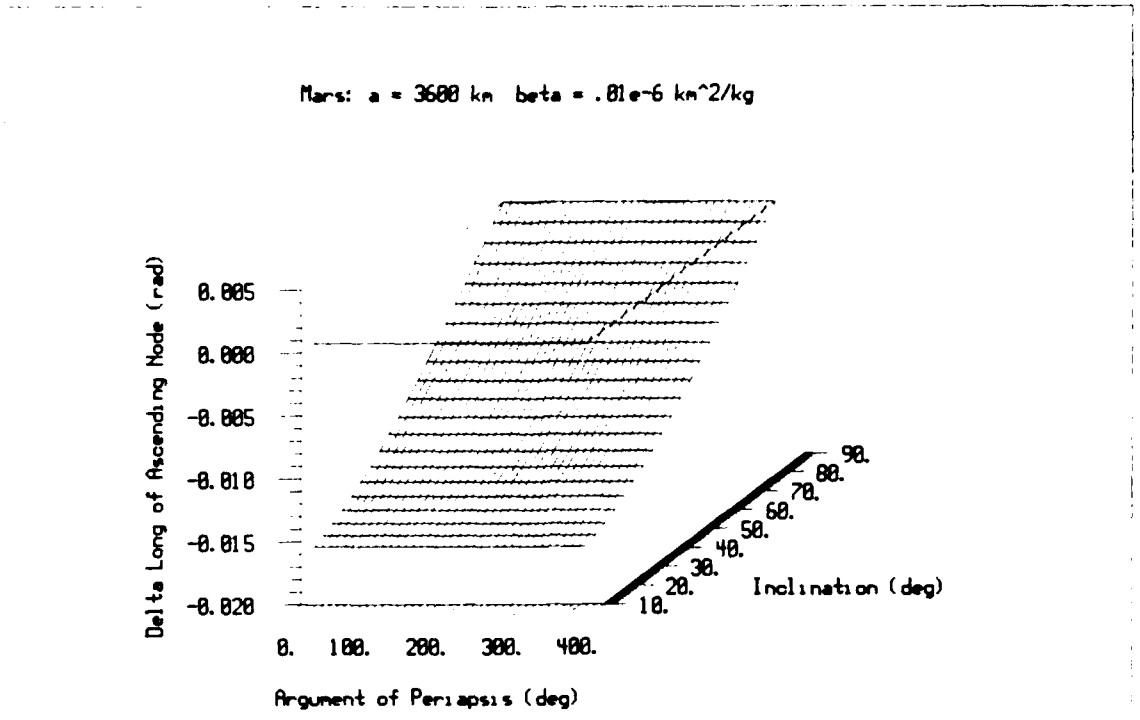

Figure D-27. Mars(a=3600km, β=.01e-6 km^2/kg): Long of Asc Node Change

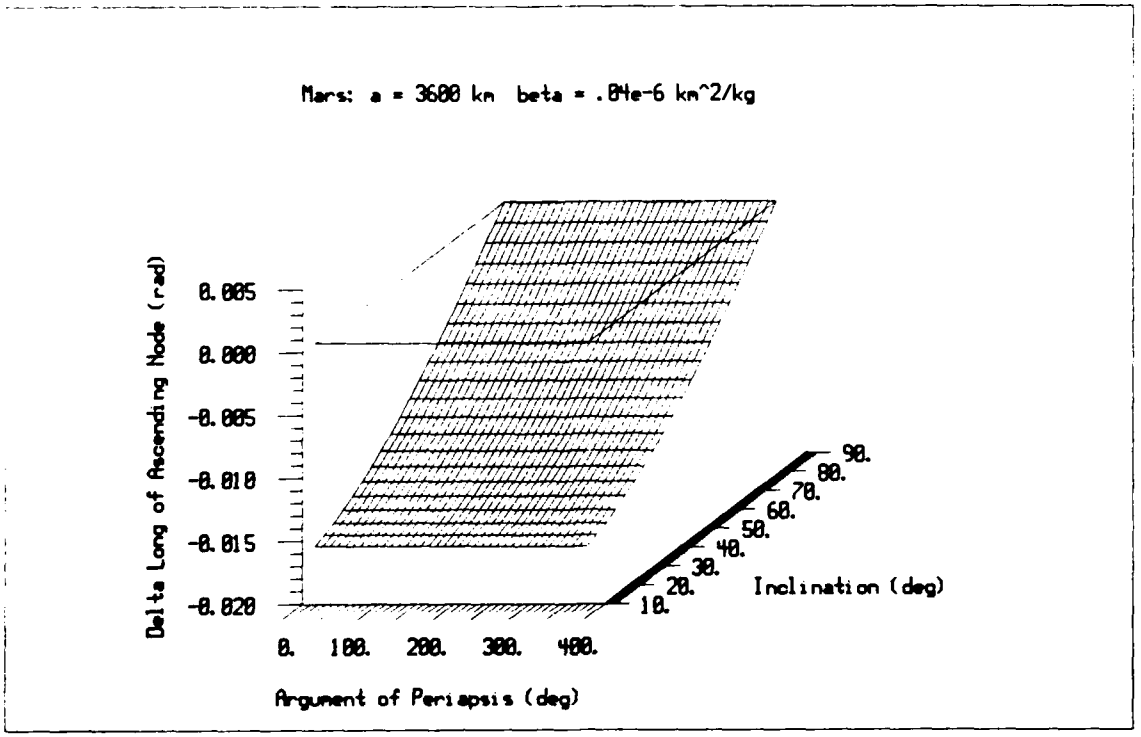

Figure D-28. Mars(a=3600km, β=.04e-6 km^2/kg): Long of Asc Node Change

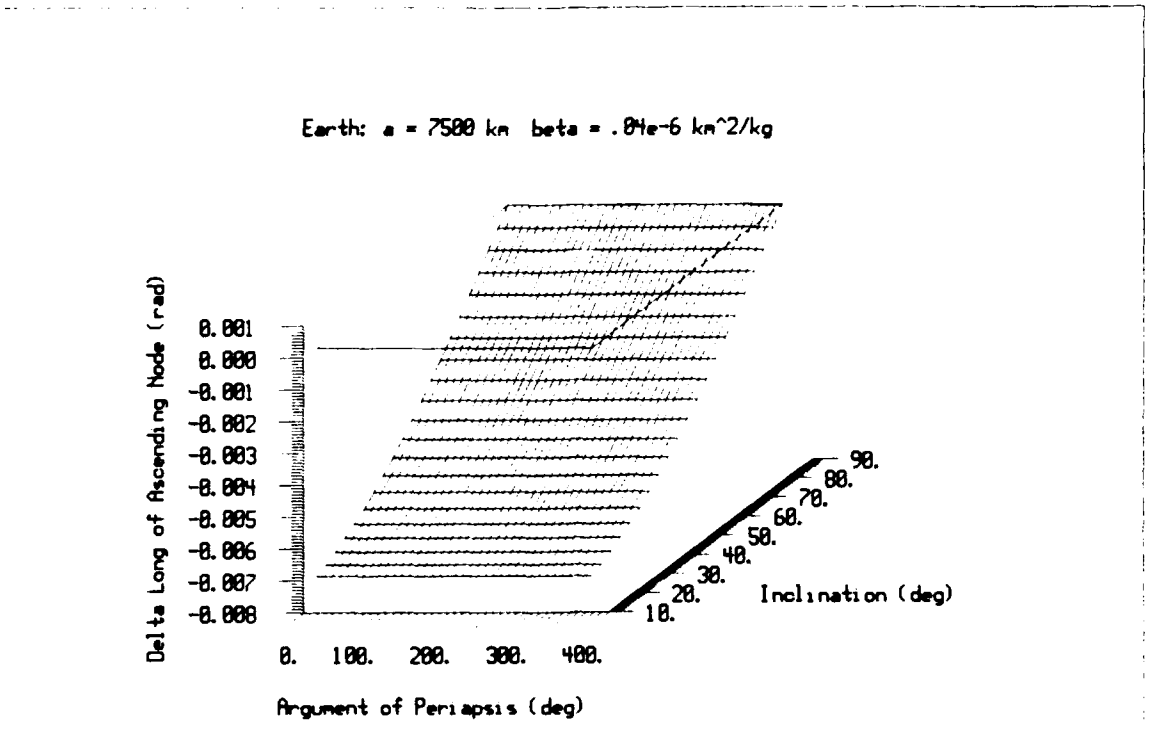

Figure D-29. Earth(a=7500km, β=.04e-6 km^2/kg): Long of Asc Node Change

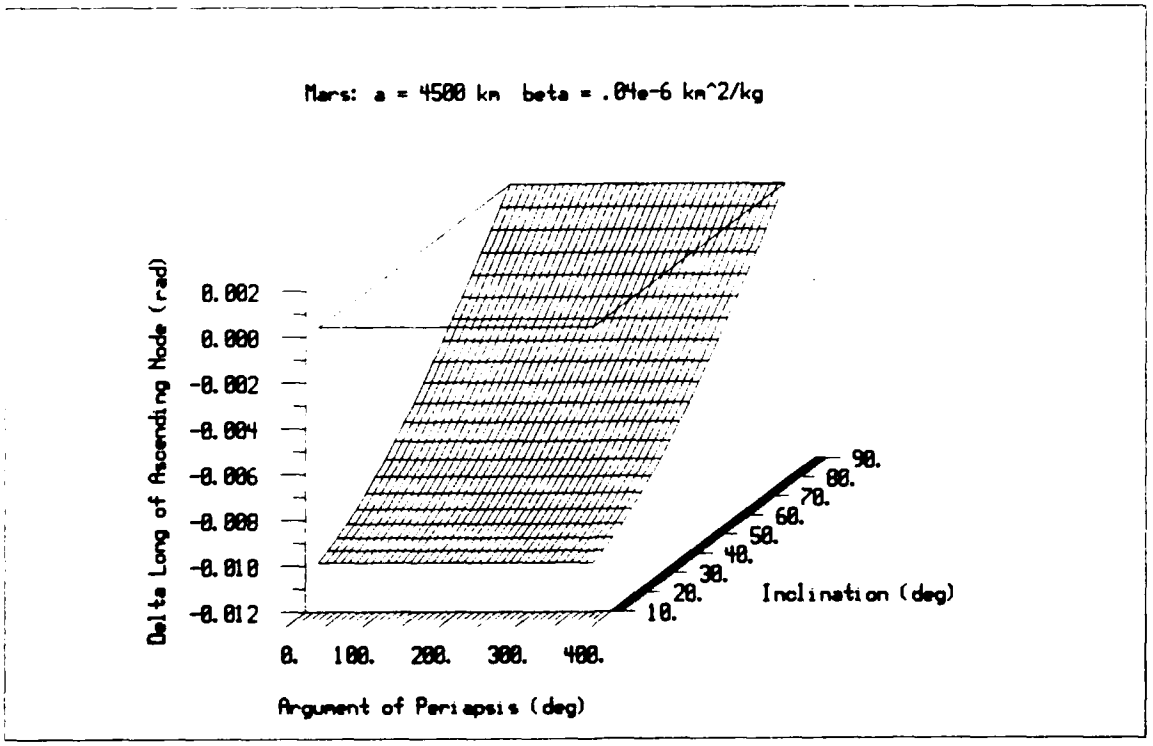

Figure D-30. Mars(a=4500km, β=.04e-6 km^2/kg): Long of Asc Node Change

Appendix E

Velocity Impulse Needed to Maintain Desired Orbit

Figures E-1 through E-6 present the velocity impulse required to maintain a given orbit which contains a constant altitude arc. The figures are presented in the same order as the cases in Appendix D.

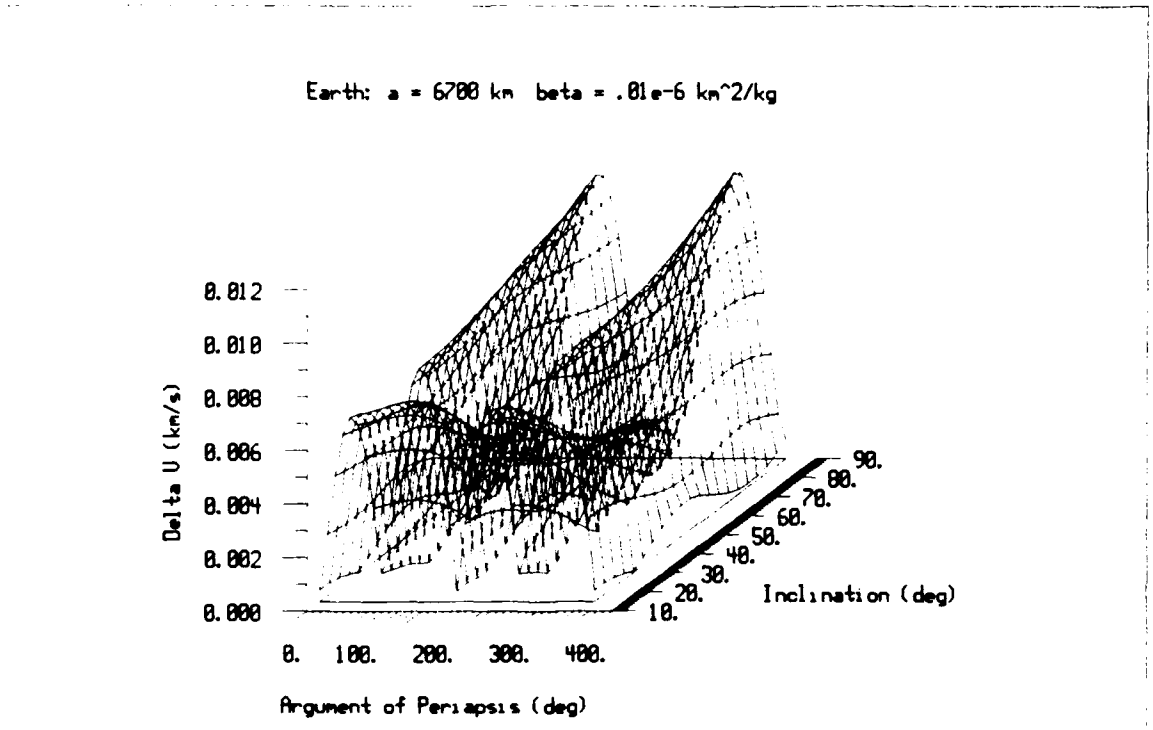

Figure E-1. Earth(a=6700km, β=.01e-6 km^2/kg): Velocity Impulse

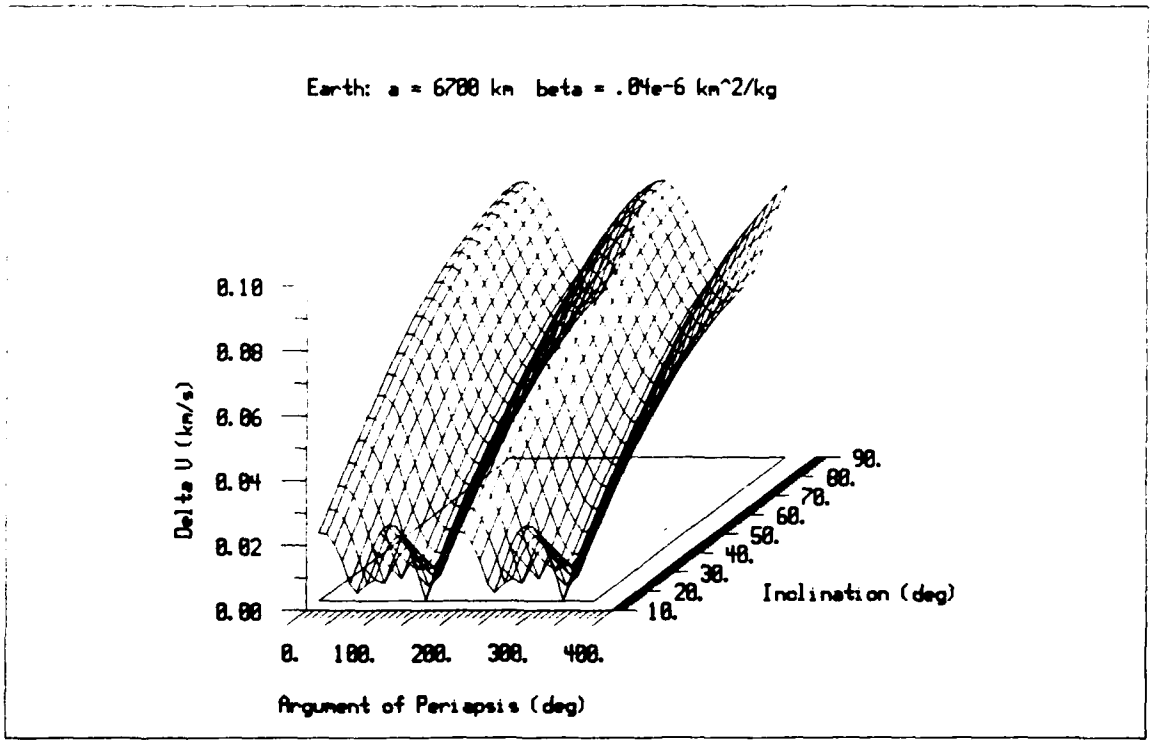

Figure E-2. Earth(a=6700km, β=.04e-6 km^2/kg): Velocity Impulse

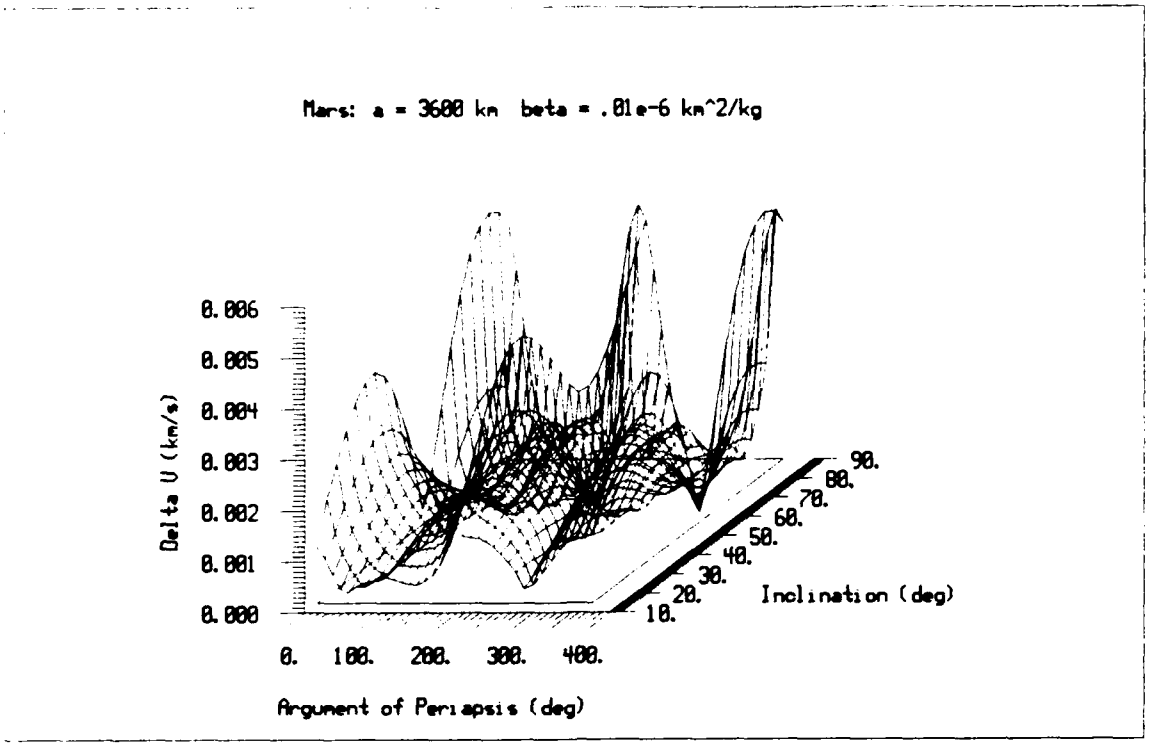

Figure E-3. Mars(a=3600km, β=.01e-6 km^2/kg): Velocity Impulse

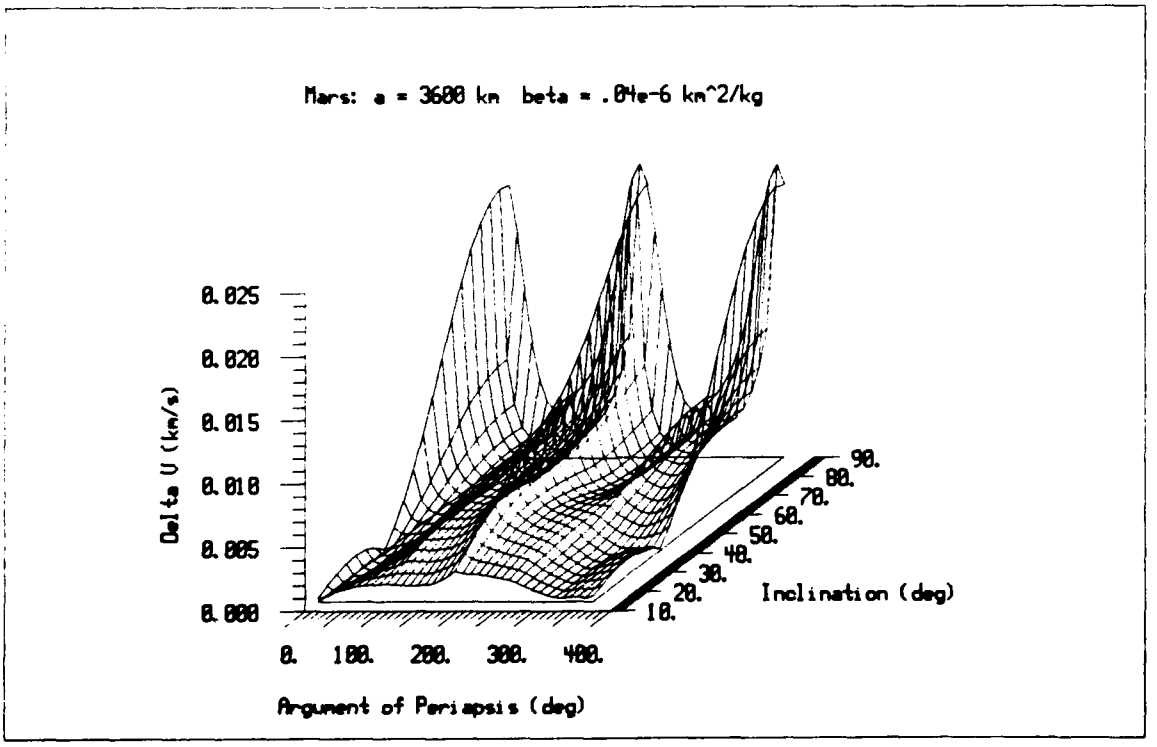

Figure E-4. Mars(a=3600km, β=.04e-6 km^2/kg): Velocity Impulse

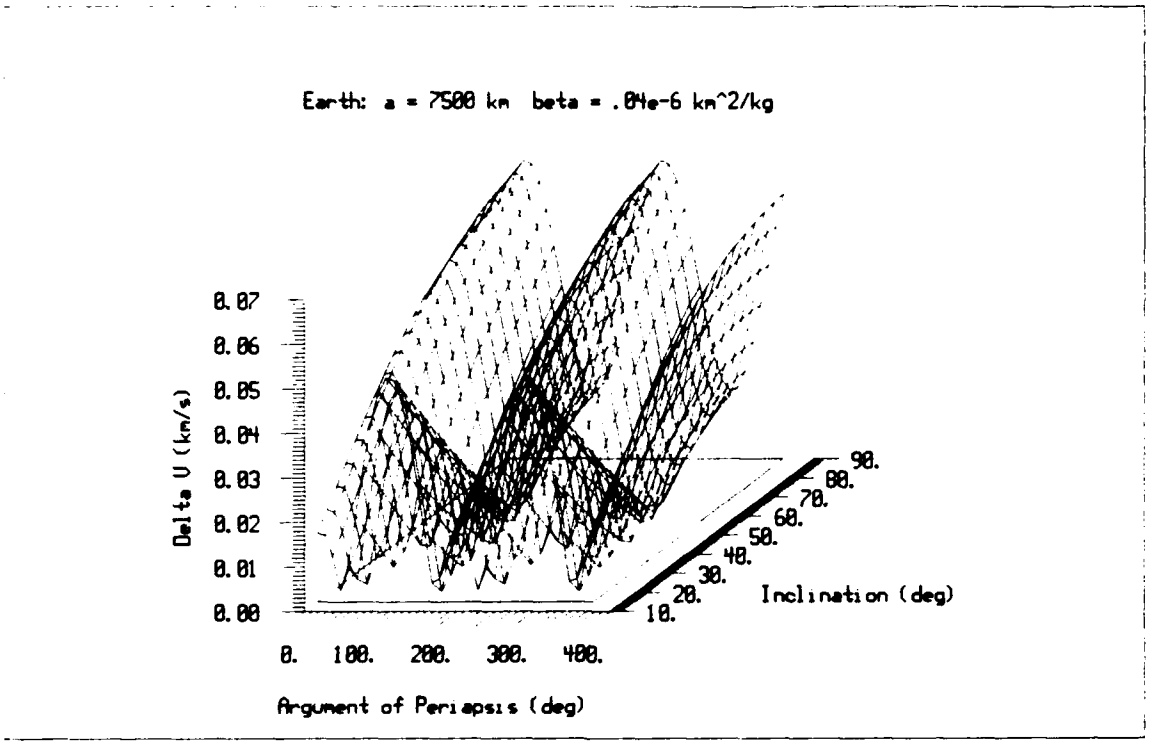

Figure E-5. Earth(a=7500km, β=.04e-6 km^2/kg): Velocity Impulse

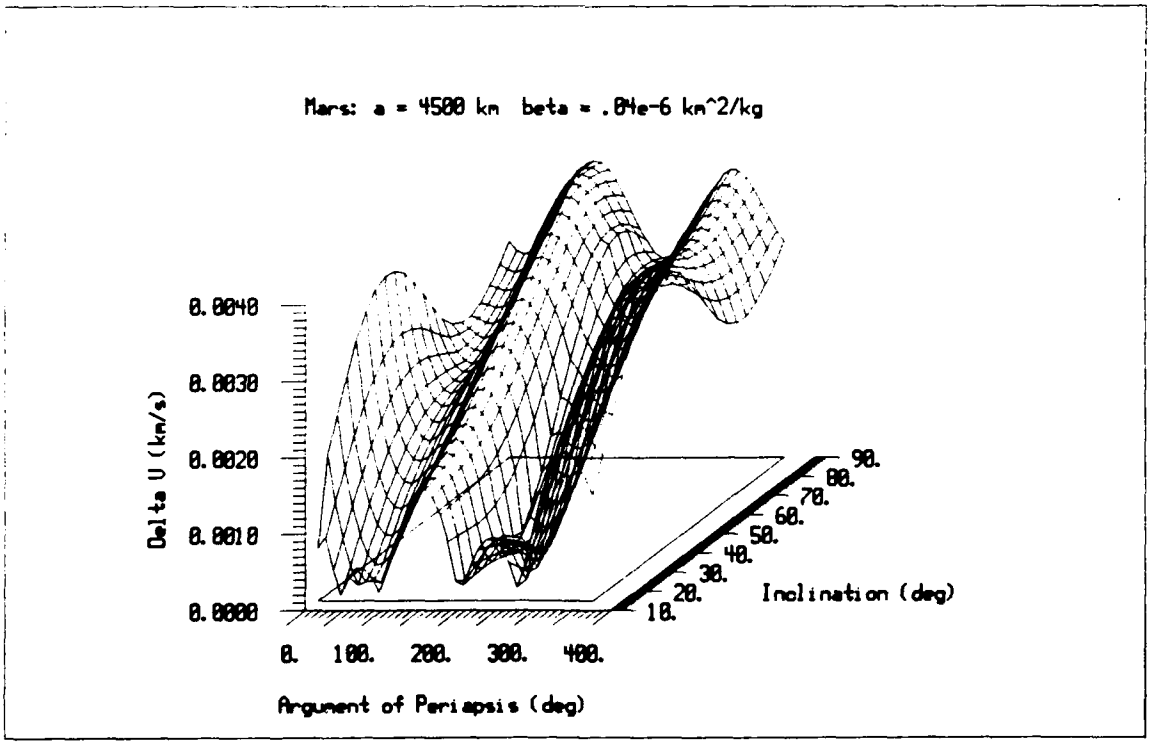

Figure E-6. Mars(a=4500km, β=.04e-6 km^2/kg): Velocity Impulse

Appendix F

Comparison of Curve Fit with Data

Earth: a = 6700 km

ω	i	e (data)	e (fit)	ω	i	e (data)	e (fit)
0.0	10.0	.000157	.000157	0.0	30.0	.001295	.001291
10.0	10.0	.000112	.000112	10.0	30.0	.000919	.000913
20.0	10.0	.000096	.000096	20.0	30.0	.000779	.000781
30.0	10.0	.000088	.000088	30.0	30.0	.000713	.000717
40.0	10.0	.000085	.000085	40.0	30.0	.000684	.000687
50.0	10.0	.000085	.000085	50.0	30.0	.000684	.000687
60.0	10.0	.000088	.000088	60.0	30.0	.000713	.000717
70.0	10.0	.000096	.000096	70.0	30.0	.000779	.000780
80.0	10.0	.000112	.000112	80.0	30.0	.000919	.000913
90.0	10.0	.000157	.000157	90.0	30.0	.001302	.001299
100.0	10.0	.000112	.000112	100.0	30.0	.000919	.000913
110.0	10.0	.000096	.000096	110.0	30.0	.000779	.000780
120.0	10.0	.000088	.000088	120.0	30.0	.000713	.000717
130.0	10.0	.000085	.000085	130.0	30.0	.000684	.000687
140.0	10.0	.000085	.000085	140.0	30.0	.000684	.000687
150.0	10.0	.000088	.000088	150.0	30.0	.000713	.000717
160.0	10.0	.000096	.000096	160.0	30.0	.000779	.000781
170.0	10.0	.000112	.000112	170.0	30.0	.000919	.000913
180.0	10.0	.000157	.000157	180.0	30.0	.001295	.001291
0.0	50.0	.003090	.003081	0.0	70.0	.004682	.004650
10.0	50.0	.002135	.002137	10.0	70.0	.003228	.003218
20.0	50.0	.001821	.001822	20.0	70.0	.002733	.002739
30.0	50.0	.001665	.001667	30.0	70.0	.002503	.002502
40.0	50.0	.001598	.001599	40.0	70.0	.002397	.002401
50.0	50.0	.001598	.001598	50.0	70.0	.002397	.002400
60.0	50.0	.001665	.001667	60.0	70.0	.002503	.002503
70.0	50.0	.001821	.001824	70.0	70.0	.002733	.002738
80.0	50.0	.002135	.002137	80.0	70.0	.003228	.003218
90.0	50.0	.003128	.003118	90.0	70.0	.004771	.004737
100.0	50.0	.002135	.002137	100.0	70.0	.003228	.003218
110.0	50.0	.001821	.001824	110.0	70.0	.002733	.002738
120.0	50.0	.001665	.001667	120.0	70.0	.002503	.002503
130.0	50.0	.001598	.001598	130.0	70.0	.002397	.002400
140.0	50.0	.001598	.001599	140.0	70.0	.002397	.002401
150.0	50.0	.001665	.001667	150.0	70.0	.002503	.002502
160.0	50.0	.001821	.001822	160.0	70.0	.002733	.002739
170.0	50.0	.002135	.002137	170.0	70.0	.003228	.003218
180.0	50.0	.003090	.003081	180.0	70.0	.004682	.004650
0.0	90.0	.005231	.005265	100.0	90.0	.003663	.003644
10.0	90.0	.003663	.003644	110.0	90.0	.003108	.003099
20.0	90.0	.003108	.003100	120.0	90.0	.002834	.002833
30.0	90.0	.002834	.002833	130.0	90.0	.002713	.002717
40.0	90.0	.002713	.002717	140.0	90.0	.002713	.002717
50.0	90.0	.002713	.002717	150.0	90.0	.002834	.002833
60.0	90.0	.002834	.002833	160.0	90.0	.003108	.003100
70.0	90.0	.003108	.003099	170.0	90.0	.003663	.003644
80.0	90.0	.003663	.003644	180.0	90.0	.005231	.005265
90.0	90.0	.005342	.005378				

Earth: a = 7500 km

ω	i	e (data)	e (fit)	ω	i	e (data)	e (fit)
0.0	10.0	.000143	.000145	0.0	30.0	.001185	.001178
10.0	10.0	.000101	.000102	10.0	30.0	.000830	.000832
20.0	10.0	.000087	.000087	20.0	30.0	.000708	.000711
30.0	10.0	.000079	.000080	30.0	30.0	.000648	.000654
40.0	10.0	.000076	.000077	40.0	30.0	.000622	.000626
50.0	10.0	.000076	.000077	50.0	30.0	.000622	.000626
60.0	10.0	.000079	.000080	60.0	30.0	.000648	.000654
70.0	10.0	.000087	.000088	70.0	30.0	.000708	.000711
80.0	10.0	.000101	.000102	80.0	30.0	.000830	.000832
90.0	10.0	.000143	.000145	90.0	30.0	.001191	.001184
100.0	10.0	.000101	.000102	100.0	30.0	.000830	.000832
110.0	10.0	.000087	.000088	110.0	30.0	.000708	.000711
120.0	10.0	.000079	.000080	120.0	30.0	.000648	.000654
130.0	10.0	.000076	.000077	130.0	30.0	.000622	.000626
140.0	10.0	.000076	.000077	140.0	30.0	.000622	.000626
150.0	10.0	.000079	.000080	150.0	30.0	.000648	.000654
160.0	10.0	.000087	.000087	160.0	30.0	.000708	.000711
170.0	10.0	.000101	.000102	170.0	30.0	.000830	.000832
180.0	10.0	.000143	.000145	180.0	30.0	.001185	.001178
0.0	50.0	.002823	.002802	0.0	70.0	.004270	.004234
10.0	50.0	.001945	.001944	10.0	70.0	.002924	.002925
20.0	50.0	.001658	.001659	20.0	70.0	.002490	.002493
30.0	50.0	.001516	.001520	30.0	70.0	.002275	.002279
40.0	50.0	.001455	.001458	40.0	70.0	.002183	.002188
50.0	50.0	.001455	.001457	50.0	70.0	.002183	.002187
60.0	50.0	.001516	.001520	60.0	70.0	.002275	.002280
70.0	50.0	.001658	.001661	70.0	70.0	.002490	.002494
80.0	50.0	.001945	.001944	80.0	70.0	.002924	.002925
90.0	50.0	.002855	.002835	90.0	70.0	.004344	.004309
100.0	50.0	.001945	.001944	100.0	70.0	.002924	.002925
110.0	50.0	.001658	.001661	110.0	70.0	.002490	.002494
120.0	50.0	.001516	.001520	120.0	70.0	.002275	.002280
130.0	50.0	.001455	.001457	130.0	70.0	.002183	.002187
140.0	50.0	.001455	.001458	140.0	70.0	.002183	.002188
150.0	50.0	.001516	.001520	150.0	70.0	.002275	.002279
160.0	50.0	.001658	.001659	160.0	70.0	.002490	.002493
170.0	50.0	.001945	.001944	170.0	70.0	.002924	.002925
180.0	50.0	.002823	.002802	180.0	70.0	.004270	.004234
0.0	90.0	.004784	.004797	100.0	90.0	.003310	.003313
10.0	90.0	.003310	.003313	110.0	90.0	.002817	.002823
20.0	90.0	.002817	.002822	120.0	90.0	.002572	.002580
30.0	90.0	.002572	.002580	130.0	90.0	.002469	.002475
40.0	90.0	.002469	.002476	140.0	90.0	.002469	.002476
50.0	90.0	.002469	.002475	150.0	90.0	.002572	.002580
60.0	90.0	.002572	.002580	160.0	90.0	.002817	.002822
70.0	90.0	.002817	.002823	170.0	90.0	.003310	.003313
80.0	90.0	.003310	.003313	180.0	90.0	.004784	.004797
90.0	90.0	.004876	.004893				

Mars; a = 3600 km

ω	i	e (data)	e (fit)	ω	i	e (data)	e (fit)
0.0	10.0	.000232	.000228	0.0	30.0	.001895	.001935
10.0	10.0	.000170	.000167	10.0	30.0	.001357	.001356
20.0	10.0	.000147	.000143	20.0	30.0	.001163	.001157
30.0	10.0	.000135	.000131	30.0	30.0	.001065	.001061
40.0	10.0	.000130	.000126	40.0	30.0	.001024	.001017
50.0	10.0	.000130	.000126	50.0	30.0	.001024	.001017
60.0	10.0	.000135	.000131	60.0	30.0	.001065	.001061
70.0	10.0	.000147	.000142	70.0	30.0	.001163	.001159
80.0	10.0	.000170	.000167	80.0	30.0	.001357	.001356
90.0	10.0	.000232	.000228	90.0	30.0	.001909	.001948
100.0	10.0	.000170	.000167	100.0	30.0	.001357	.001356
110.0	10.0	.000147	.000142	110.0	30.0	.001163	.001159
120.0	10.0	.000135	.000131	120.0	30.0	.001065	.001061
130.0	10.0	.000130	.000126	130.0	30.0	.001024	.001017
140.0	10.0	.000130	.000126	140.0	30.0	.001024	.001017
150.0	10.0	.000135	.000131	150.0	30.0	.001065	.001061
160.0	10.0	.000147	.000143	160.0	30.0	.001163	.001157
170.0	10.0	.000170	.000167	170.0	30.0	.001357	.001356
180.0	10.0	.000232	.000228	180.0	30.0	.001895	.001935
0.0	50.0	.004547	.004594	0.0	70.0	.006904	.006856
10.0	50.0	.003174	.003188	10.0	70.0	.004771	.004769
20.0	50.0	.002710	.002710	20.0	70.0	.004062	.004060
30.0	50.0	.002479	.002474	30.0	70.0	.003712	.003709
40.0	50.0	.002381	.002372	40.0	70.0	.003562	.003559
50.0	50.0	.002381	.002372	50.0	70.0	.003562	.003558
60.0	50.0	.002479	.002474	60.0	70.0	.003712	.003710
70.0	50.0	.002710	.002708	70.0	70.0	.004062	.004061
80.0	50.0	.003174	.003188	80.0	70.0	.004771	.004769
90.0	50.0	.004630	.004672	90.0	70.0	.007097	.007042
100.0	50.0	.003174	.003188	100.0	70.0	.004771	.004769
110.0	50.0	.002710	.002708	110.0	70.0	.004062	.004061
120.0	50.0	.002479	.002474	120.0	70.0	.003712	.003710
130.0	50.0	.002381	.002372	130.0	70.0	.003562	.003558
140.0	50.0	.002381	.002372	140.0	70.0	.003562	.003559
150.0	50.0	.002479	.002474	150.0	70.0	.003712	.003709
160.0	50.0	.002710	.002710	160.0	70.0	.004062	.004060
170.0	50.0	.003174	.003188	170.0	70.0	.004771	.004769
180.0	50.0	.004547	.004594	180.0	70.0	.006904	.006856
0.0	90.0	.007663	.007668	100.0	90.0	.005402	.005404
10.0	90.0	.005402	.005404	110.0	90.0	.004594	.004595
20.0	90.0	.004594	.004596	120.0	90.0	.004196	.004198
30.0	90.0	.004196	.004197	130.0	90.0	.004025	.004025
40.0	90.0	.004025	.004027	140.0	90.0	.004025	.004027
50.0	90.0	.004025	.004025	150.0	90.0	.004196	.004197
60.0	90.0	.004196	.004198	160.0	90.0	.004594	.004596
70.0	90.0	.004594	.004595	170.0	90.0	.005402	.005404
80.0	90.0	.005402	.005404	180.0	90.0	.007663	.007668
90.0	90.0	.007902	.007908				

Mars: a = 4000 km

ω	i	e (data)	e (fit)	ω	i	e (data)	e (fit)
0.0	10.0	.000214	.000212	0.0	30.0	.001755	.001777
10.0	10.0	.000155	.000153	10.0	30.0	.001248	.001246
20.0	10.0	.000133	.000131	20.0	30.0	.001068	.001065
30.0	10.0	.000122	.000120	30.0	30.0	.001000	.000977
40.0	10.0	.000118	.000116	40.0	30.0	.000940	.000936
50.0	10.0	.000118	.000116	50.0	30.0	.000940	.000936
60.0	10.0	.000122	.000120	60.0	30.0	.001000	.000977
70.0	10.0	.000133	.000131	70.0	30.0	.001068	.001066
80.0	10.0	.000155	.000153	80.0	30.0	.001248	.001246
90.0	10.0	.000214	.000212	90.0	30.0	.001767	.001789
100.0	10.0	.000155	.000153	100.0	30.0	.001248	.001246
110.0	10.0	.000133	.000131	110.0	30.0	.001068	.001066
120.0	10.0	.000122	.000120	120.0	30.0	.001000	.000977
130.0	10.0	.000118	.000116	130.0	30.0	.000940	.000936
140.0	10.0	.000118	.000116	140.0	30.0	.000940	.000936
150.0	10.0	.000122	.000120	150.0	30.0	.001000	.000977
160.0	10.0	.000133	.000131	160.0	30.0	.001068	.001065
170.0	10.0	.000155	.000153	170.0	30.0	.001248	.001246
180.0	10.0	.000214	.000212	180.0	30.0	.001755	.001777
0.0	50.0	.004201	.004225	0.0	70.0	.006373	.006346
10.0	50.0	.002921	.002926	10.0	70.0	.004389	.004393
20.0	50.0	.002492	.002491	20.0	70.0	.003737	.003739
30.0	50.0	.002280	.002275	30.0	70.0	.003415	.003417
40.0	50.0	.002188	.002183	40.0	70.0	.003277	.003278
50.0	50.0	.002188	.002182	50.0	70.0	.003277	.003277
60.0	50.0	.002280	.002276	60.0	70.0	.003415	.003417
70.0	50.0	.002492	.002491	70.0	70.0	.003737	.003738
80.0	50.0	.002921	.002926	80.0	70.0	.004389	.004394
90.0	50.0	.004272	.004295	90.0	70.0	.006538	.006511
100.0	50.0	.002921	.002926	100.0	70.0	.004389	.004394
110.0	50.0	.002492	.002491	110.0	70.0	.003737	.003738
120.0	50.0	.002280	.002276	120.0	70.0	.003415	.003417
130.0	50.0	.002188	.002182	130.0	70.0	.003277	.003277
140.0	50.0	.002188	.002183	140.0	70.0	.003277	.003278
150.0	50.0	.002280	.002275	150.0	70.0	.003415	.003417
160.0	50.0	.002492	.002491	160.0	70.0	.003737	.003739
170.0	50.0	.002921	.002926	170.0	70.0	.004389	.004393
180.0	50.0	.004201	.004225	180.0	70.0	.006373	.006346
0.0	90.0	.007092	.007166	100.0	90.0	.004969	.004964
10.0	90.0	.004969	.004964	110.0	90.0	.004227	.004228
20.0	90.0	.004227	.004228	120.0	90.0	.003861	.003865
30.0	90.0	.003861	.003864	130.0	90.0	.003704	.003708
40.0	90.0	.003704	.003709	140.0	90.0	.003704	.003709
50.0	90.0	.003704	.003708	150.0	90.0	.003861	.003864
60.0	90.0	.003861	.003865	160.0	90.0	.004227	.004228
70.0	90.0	.004227	.004228	170.0	90.0	.004969	.004964
80.0	90.0	.004969	.004964	180.0	90.0	.007092	.007166
90.0	90.0	.007296	.007379				

Bibliography

1. Bain, Rodney D. Lecture notes prepared for Advanced Astrodynamics II. School of Engineering, Air Force Institute of Technology (AU), Wright-Patterson AFB OH, 1988.

2. Brouwer, Dirk. "Solution of the Problem of Artificial Satellite Theory Without Drag," The Astronomical Journal, Vol. 64, p. 378, November 1959.

3. Escobal, Pedro R. Methods of Astrodynamics. New York: Robert E. Krieger Publishing Company, 1979.

4. Foister, Capt James W. Frozen Orbit Analysis in the Martian System. MS thesis, AFIT/GSO/AA/87D-2. School of Engineering, Air Force Institute of Technology (AU), Wright-Patterson AFB OH, December 1987 (AD-A189574).

5. H. M. Nautical Almanac Office, Explanatory Supplement to the Astronomical Ephemeris and the American Ephemeris and Nautical Almanac. London: Her Majesty's Stationery Office, 1961.

6. Kalil, Ford. "Minimum Altitude Variation Orbits about an Oblate Planet," AIAA Journal, Vol. 1, No. 7, p. 1655, 1963.

7. Kaufman, Bernard. "Variation of Parameters and the Long-Term Behavior of Planetary Orbiters," AIAA Paper No 70-1055, AAS/AIAA Astronautics Conference, 1-3 August 1970.

8. Kaula, William K. Theory of Satellite Geodesy. Waltham, Mass: Blaisdell Publishing Company, 1966.

9. King-Hele, Desmond. Theory of Satellite Orbits in an Atmosphere. London: Butterworths, 1964.

10. Kliore, A 'ed). The Mars Reference Atmosphere. Innsbruck: JPL, 1978.

11. Kwok, Johnny H. The Artificial Satellite Analysis Program (ASAP). Jet Propulsion Laboratory, 1 April 1985.

12. Merson, R. H. "The Motion of a Satellite in an Axi-Symmetric Gravitational Field," Geophys. Journal, Vol. 4, p. 17, 1961.

13. O'Keefe, John A., Ann Eckels, and R. Kenneth Squires. "The Gravitational Field of the Earth," The Astronomical Journal, Vol. 64, p.245, September 1959.

14. Roy, Archie E. The Foundations of Astrodynamics. New York: The Macmillan Company, 1965.

15. Smart, William M. Celestial Mechanics. London: Longmans, Green and Co, 1953.

16. Sterne, Theodore E. "Effect of the Rotation of a Planetary Atmosphere Upon the Orbit of a Close Satellite," ARS Journal, Vol. 29, No. 10, p. 777, 1959.

17. -----. "The Gravitational Orbit of a Satellite of an Oblate Planet," The Astronomical Journal, Vol. 63, p. 28, January 1958.

18. Tang, Charles C. II. "An Accurate and Efficient Satellite Long-Term Orbit Predictor Employing 'Fictitious' Mean Orbital Elements," AIAA Paper 88-4243, 1988.

19. Vinh, Nguyen X., Adolf Busemann, and Robert D. Culp. Hypersonic and Planetary Entry Flight Mechanics. Ann Arbor: The University of Michigan Press, 1980.

20. Zendell, Alan, Richard D. Brown, and Samir Vincent. NASA Space Vehicle Design Criteria (Environment): Gravity Fields of the Solar System. NASA SP-8117, April 1975.

Vita

Captain Christina L. Cain joined the Air Force in 1977, and after training was assigned to the 401st (Torrejon AB, SP) and 347th (Moody AFB, GA) Tactical Fighter Wings as an aerospace ground equipment mechanic. In 1981 she was assigned to the University of Arizona under the Airman Education and Commissioning Program. In 1984 after graduating with a Bachelor of Science in Aerospace Engineering and completing OTS, she was assigned to the Flight Dynamics Laboratory of the Air Force Wright Aeronautical Laboratories at Wright-Patterson AFB, OH. In addition to her duties as a project engineer for a wide variety of research efforts involving cryogenics and spacecraft thermal management, she has been attending AFIT part-time since 1985.

UNCLASSIFIED

SECURITY CLASSIFICATION OF THIS PAGE

REPORT DOCUMENTATION PAGE

Form Approved
OMB No. 0704-0188

1a. REPORT SECURITY CLASSIFICATION Unclassified	1b. RESTRICTIVE MARKINGS
2a. SECURITY CLASSIFICATION AUTHORITY	3. DISTRIBUTION/AVAILABILITY OF REPORT Approved for public release; distibution unlimited.
2b. DECLASSIFICATION/DOWNGRADING SCHEDULE	
4. PERFORMING ORGANIZATION REPORT NUMBER(S) AFIT/GA/ENY/89J-1	5. MONITORING ORGANIZATION REPORT NUMBER(S)
6a. NAME OF PERFORMING ORGANIZATION School of Engineering 6b. OFFICE SYMBOL (If applicable) AFIT/ENY	7a. NAME OF MONITORING ORGANIZATION
6c. ADDRESS (City, State, and ZIP Code) Air Force Institute of Technology (AU) Wright-Patterson AFB, Ohio 45433-6583	7b. ADDRESS (City, State, and ZIP Code)
8a. NAME OF FUNDING/SPONSORING ORGANIZATION 8b. OFFICE SYMBOL (If applicable)	9. PROCUREMENT INSTRUMENT IDENTIFICATION NUMBER
8c. ADDRESS (City, State, and ZIP Code)	10. SOURCE OF FUNDING NUMBERS PROGRAM ELEMENT NO. / PROJECT NO. / TASK NO / WORK UNIT ACCESSION NO.

11. TITLE (Include Security Classification)
ORBITS CONTAINING ARCS OF MINIMUM ALTITUDE VARIATION

12. PERSONAL AUTHOR(S)
Christina L. Cain, Capt, USAF

13a. TYPE OF REPORT	13b. TIME COVERED	14. DATE OF REPORT (Year, Month, Day)	15. PAGE COUNT
MS Thesis	FROM _____ TO _____	1989 June	122

16. SUPPLEMENTARY NOTATION

17. COSATI CODES			18. SUBJECT TERMS (Continue on reverse if necessary and identify by block number)
FIELD	GROUP	SUB-GROUP	Orbits, Earth Orbits, Low Orbit Trajectories
22	01		

19. ABSTRACT (Continue on reverse if necessary and identify by block number)

Thesis Advisor: Capt R D Bain
Assistant Professor of Astronautical Engineering
Department of Aeronautics and Astronautics

20. DISTRIBUTION/AVAILABILITY OF ABSTRACT	21. ABSTRACT SECURITY CLASSIFICATION
☐ UNCLASSIFIED/UNLIMITED ☒ SAME AS RPT. ☐ DTIC USERS	UNCLASSIFIED

22a. NAME OF RESPONSIBLE INDIVIDUAL	22b. TELEPHONE (Include Area Code)	22c. OFFICE SYMBOL
Capt R D Bain, Assistant Prof of Astro Eng	(513) 255 3633	AFIT/ENY

DD Form 1473, JUN 86 *Previous editions are obsolete.* SECURITY CLASSIFICATION OF THIS PAGE

UNCLASSIFIED

This thesis identifies the mean orbital elements which produce arcs of minimum altitude variation over an oblate planet with an axi-symmetric gravitational field. Such orbits are useful for surveillance or scientific study missions using optics with fixed focal lengths.

Both Earth and Mars are considered and the optimum eccentricity is found as a function of argument of periapsis and inclination for two values of semi-major axis for each planet. The results are curve fit to develop a single equation which identifies the eccentricity needed to produce an arc of minimum altitude variation given the argument of periapsis, inclination, semi-major axis, ellipticity of the planet, equatorial radius, and the zonal J_2.

Once arcs with minimum altitude variations are identified, the properties of the arcs are considered. The mid-latitude, altitude, duration, and latitude range of the arcs are found as a function of argument of periapsis and inclination for various planet and semi-major axis combinations.

The secular change in mean orbital elements ~~is then considered to~~ determine the most stable orbits. Secular changes in orbital elements due to the geopotential, drag, and third body effects are considered. The velocity impulse needed to return the satellite to the original orbit from the perturbed orbit is found and used to determine stability. Identifying orbits which require minimum station keeping fuel allows planners to select orbits permitting longer useful longer useful operational life.

Theses (GAE)

Keywords: Low Orbit Trajectories